Unmanned Aerial System derived Multi-Spectral Imagery for the Monitoring of Coastal Dune Plant Communities

_____

A thesis

submitted in partial fulfilment

of the requirements for the Degree of

Master of Science

at

Lincoln University

by

Michael Fake

_____

Lincoln University

2019

Abstract of a thesis submitted in partial fulfilment of the
requirements for the Degree of Master of Science.

Abstract

Unmanned Arial System derived Multi-Spectral Imagery for the Monitoring of
Coastal Dune Plant Communities

by

Michael Fake

Plant community monitoring was conducted at Kaitorete Spit Scientific Reserve using UAS based remote sensing and traditional field-based techniques. Multispectral, high resolution UAS imagery was used as the basis for image classification. Different classification methods and data manipulation techniques were evaluated in order to present the most accurate representation of plant communities for comparison against those derived from the field data. Overall image classifcation results were on par with those from similar studies, however their suitability for application to the monitoring of the specific environmental and ecological conditions at Kaitorete Spit remains of low confidence. UAS imagery was able to be used to identify coarse scale ecological features which could then be used to define distinct ecological communities in a simlar but not identical manner to that of the field data. At a finer-scale, UAS imagery could detect some, but not all, key ecological features such as individual species or fine-scale indicators of diverse habitat types.

Keywords: Remote Sensing, UAS, UAV, Drone, Image Classification, Plant Community, Vegetation, Coastal, Sand Dunes, Ordination, TWINSPAN, Clustering.

Acknowledgements

Table of Contents

List of Tables

List of Figures

Chapter 1

Introduction

1.1 Remote Sensing in Ecology

One of the principal objectives in ecology is to measure, comprehend and predict patterns in biodiversity (Holyoak, Leibold, Mouquet, Holt, & Hoopes, 2005). Remote sensing (RS) is the science of collecting information and data using non-contact and remote methods (K. Wang, Franklin, Guo, & Cattet, 2010). Remote sensing has great potential to revolutionise the way that we practice ecology, as it provides both the technology and data sources required to address large-scale issues (Kerr & Ostrovsky, 2003). Some of the more important advantages in the use of RS in ecology are the acquisition of digital information, its repeatability and the cost-benefit of the process compared to traditional ground-based techniques (Hall et al., 2009). Traditional ground-based methods can also be time-consuming and susceptible to observer based error (Turner et al., 2003). In larger studies that employ multiple observers to quantify and characterise vegetation, the ability to accurately differentiate plant species varies substantially between observers, regardless of observer experience (Bergstedt, Westerberg, & Milberg, 2009). The simultaneous and continuous collection of data from remote sensing platforms and subsequent image processing algorithms can help avoid these sources of observer bias (Spanhove, Vanden Borre, Delalieux, Haest, & Paelinckx, 2012). The ability to rapidly resurvey large areas while collecting continuous data can be valuable for when monitoring short-term and real-time changes in ecosystem response (A. Gitelson et al., 1993) (A. Gitelson et al., 1993; Verbesselt, Zeileis, & Herold, 2012; X. Zhang et al., 2003). The ability to monitor environments that are logistically difficult to access (He, Rocchini, Neteler, & Nagendra, 2011; Spanhove et al., 2012), or inherently dangerous (Şerban et al., 2016) is also a significant advantage when compared to field-based methods.

Remote sensing incorporates the use of the reflectance spectra of land-cover elements captured in an image pixel, such as vegetation, soils and other geological materials (Turner et al., 2003). The reflectance of each element depends on a given objects biophysical and structural properties. For instance, for plants, the size, density, and structural layout of the branches and leaves will result in light being preferentially absorbed or scattered in different wavelengths (Underwood, Ustin, & Ramirez, 2007). Natural interspecific variations in biological components, such as chlorophyll and other pigments, water, proteins, starches and structural carbohydrates, will produce characteristic signatures for different species, allowing for the remote identification of species and communities (Carvalho, Schlerf, van der Putten, & Skidmore, 2013; Underwood et al., 2007).

Remote sensing of biodiversity involves two main methodologies; firstly the direct sensing of biodiversity at the individual, population and/or community level conducted via terrestrial (Dassot, Constant, & Fournier, 2011), airborne (Baldeck & Asner, 2013; Bork & Su, 2007; Bradbury et al., 2005; R. A. Hill & Thomson, 2005) or spaceborne sensors (Czerepowicz, Case, & Doscher, 2012; Lisita, Sano, & Durieux, 2013; Mathieu, Aryal, & Chong, 2007). Secondly, the indirect sensing of biodiversity through the use of ecological parameters as environmental and habitat indicators (Almeida-Neto & Ulrich, 2011; Anteau, Wiltermuth, Sherfy, & Shaffer, 2014; Buermann et al., 2008; Julian, Young, Jones, Snyder, & Wright, 2009; Shirley et al., 2013).

Terrestrial remote sensing typically involves studies of ecosystem physical structure using ground-based systems. Ground-based scanners perform better than aerial sensors at smaller scales and for below-canopy forest metrics (Dassot et al., 2011; Nevalainen et al., 2014). The main advantages are its high spatial accuracy and its non-destructive nature compared to traditional measures of forest attributes (Bork & Su, 2007; Hu et al., 2018; Stovall, Anderson-Teixeira, & Shugart, 2018). Ground-based scanners are often used to augment field and aerial remote sensing data in studies of habitat and forest structure (Barbosa et al., 2016; Olsoy et al., 2018; Orwig et al., 2018), and can be employed in studies of entire forests down to the quantification of individual trees (Bayer, Seifert, & Pretzsch, 2013; Pyorala et al., 2018), stem (Henning & Radtke, 2006; Lau et al., 2018), or leaf attributes (Elsherif, Gaulton, & Mills, 2018; Hancock, Gaulton, & Danson, 2017). The main drawback of ground-based scanners however is the high occurrence of data occlusion (spatial structure of the data resulting in larger objects blocking those behind them), high equipment costs and the practicality of collecting data across larger scales (Donager et al., 2018; Heinzel & Huber, 2017; Newnham et al., 2015).

Aerial remote sensing platforms include both manned and unmanned aerial systems. The main advantage of airborne over terrestrial systems is the ability to cover larger areas with a higher degree of repeatability. Manned systems such as planes are limited in comparison to unmanned systems due to the higher skills and costs required to operate, the inherent safety risks of aircraft operation and the fact that their use is mostly restricted to commercial operations (Manfreda et al., 2018). Due to the high-costs of manned systems, small scale studies and those of short revisit-times are typically unfeasible.

Spaceborne sensors have been widely used for decades for larger-scale environmental monitoring. However, despite ongoing development in the capabilities and availability of satellite data, their application to monitoring of finer-scale ecological and environmental processes is still somewhat limited. While direct monitoring of broad vegetation types was possible, early community studies using satellite imagery were limited in their ability to detect low-density levels of vegetation cover

(Westman & Price, 1988) and phenological variation, even with hyperspectral imagery (Okin, Roberts, Murray, & Okin, 2001) The broad range of data types allow for multiple different applications in conservation and ecology; such examples include invasive species monitoring and modelling (Andrew & Ustin, 2009; Becker, Zmijewski, & Crail, 2013; Lantz & Wang, 2013; Young, Abbott, Caldwell, & Schrader, 2013), biophysical modelling of forest structure and resources (Czerepowicz et al., 2012; Dash, Pearse, & Watt, 2018) and ecosystem disturbance response (Karau, Sikkink, Keane, & Dillon, 2014; Pettorelli, Safi, & Turner, 2014; Pettorelli et al., 2005; Rastmanesh, Moore, Kharrati-Kopaei, & Behrouz, 2010; Skole & Tucker, 1993). One of the main advantage of satellite data is the existence of many decades worth of data which allows for long-term monitoring of environmental change (Corbane et al., 2015; Dornhofer & Oppelt, 2016; Karau et al., 2014; Pettorelli et al., 2014; Pettorelli et al., 2005; Platt, 2014; Reif & Theel, 2017; Shumack, Hesse, & Turner, 2017; Skole & Tucker, 1993). Xie, Sha, and Yu (2008) provide an excellent overview of the major satellite sensors and their applications in vegetation mapping up until the time of publication.

1.1.1 Unmanned Aerial Systems

Background

Recent advances in unmanned aerial vehicles (UAVs) including miniaturisation, standardisation and cost-reduction have enabled the collection of data using small, remote-controlled aerial drones (Manfreda et al., 2018). As with any relatively new technology, there still exists some variation in the nomenclature surrounding UAVs. While "UAV" and "drone" are the more widely known names or acronyms, terms such as "Unmanned Arial Systems (UAS)" and "Remotely Piloted Aircraft Systems (RPAS)" are also widely used. In New Zealand, no single formal term has been defined by the Civil Aviation Authority (CAA), yet the term "Unmanned Aircraft" is used widely across CAA guidance material (CAA, 2018). "UAS" has been defined by the International Civil Aviation Organisation as the more up-to-date term rather than "UAV", whereas "RPAS" are defined as "A set of configurable elements consisting of a remotely-piloted aircraft, its associated remote pilot station(s), the required command and control links and any other system elements as may be required, at any point during flight operation." (ICAO, 2012). For the purpose of this study, the term UAS shall be used.

Applications

UAS have massive potential to reduce costs of collecting data as they incur fewer operational costs, including both technology and labour (Anderson & Gaston, 2013; Breckenridge, Dakins, Bunting, Harbour, & Lee, 2012; Dubayah & Drake, 2000; Kerr & Ostrovsky, 2003; Matese et al., 2015; Pajares, 2015; Paneque-Galvez, McCall, Napoletano, Wich, & Koh, 2014). While highly suited to smaller studies, these advantages are lost for studies over 10-20 ha (Manfreda et al., 2018). Another strong advantage of UAS is that they are less susceptible to atmospheric effects due to their lower

operational height, and are not restricted to certain hours of operation or availability, allowing for near-continuous data collection (Manfreda et al., 2018).

UAS have been proven effective for environmental and ecological monitoring. Such applications include the detection and quantification of characteristic rangeland habitat features (Breckenridge et al., 2012; Breckenridge, Dakins, Bunting, Harbour, & White, 2011), mapping canopy-gap metrics relating to floristic biodiversity and forest disturbance and regeneration (Stephan Getzin, Nuske, & Wiegand, 2014; S. Getzin, Wiegand, & Schoning, 2012), post-restoration monitoring of at-risk habitats (Dufour et al., 2013; Knoth, Klein, Prinz, & Kleinebecker, 2013; Reif & Theel, 2017; Zahawi et al., 2015) wildfire risk modelling (Shin, Sankey, Moore, & Thode, 2018) and invasive species monitoring (Chabot, Dillon, Ahmed, & Shemrock, 2017; Chabot, Dillon, Shemrock, Weissflog, & Sager, 2018; Ouyang et al., 2013).

The utility and ease of operation of UAS, as well as their low intrusiveness, make them particularly attractive in wildlife surveys (G. P. Jones, Pearlstine, & Percival, 2006; Koh & Wich, 2012; Watts et al., 2010). UAS have been used in direct monitoring of individual large grazing mammals (Guo et al., 2018), elephants and orang-utans (Koh & Wich, 2012), alligators (Watts et al., 2010), as well as coastal bird species (Barr, Green, DeMaso, & Hardy, 2018; Dulava, Bean, & Richmond, 2015; Sarda-Palomera et al., 2012). By combining population data and time-series imagery, indirect effects of herbivore movement and land management practices have also been studied (Mayr, Malss, Ofner, & Samimi, 2018; Morrison et al., 2018; D. Williams, Thorne, Sumba, Muruthi, & Gregory-Michelman, 2018). By identifying plant species that are important for key wildlife species, UAS have been used in the indirect monitoring of available primate habitat (Alexander et al., 2018)

Current Limitations

Manfreda et al. (2018) provide an excellent summary of the current limitations surrounding the use of UAS for environmental monitoring. Their main conclusions surrounding limitations can be summarised as those based on UAS size, the relative lack of standardised data collection and processing skills and the restrictions placed upon their use via government legislation. Anderson and Gaston (2013), in an earlier review of UAS for spatial ecology, highlighted similar issues in drone size, operational skill and legislation. Duffy et al. (2018) provide a useful breakdown of the challenges faced in UAS operations based on the type of environmental setting in which they can occur.

The limitation of operational range and reduction of cost-effectiveness for larger studies mean that traditional satellite and manned aerial surveys may be more feasible, but only when the high-frequency of data collection via UAS is not considered (Manfreda et al., 2018). The limitations of operational range from small battery size were highlighted by Chen et al. (2018), and the restriction

of range via the distance limitations of radio operated control stations was emphasised by Goncalves and Henriques (2015). The small size of UAS, while enabling data collection below atmospheric conditions that affect other remote sensing systems, leaves them vulnerable to interference from local environmental conditions, such as wind, rain and temperature (Goncalves & Henriques, 2015; Suo, McGovern, & Gilmer, 2018). The small size also restricts the total payload of the drone itself, reducing the capacity to carry larger, more advanced sensors and equipment (Manfreda et al., 2018). Small payload capacity may limit operational efficacy, as an increase in spatial resolution is not as effective as an increase in spectral resolution (Komarek, Kloucek, & Prosek, 2018) The accuracy of the onboard GPS unit and its importance for data accuracy, as well as the issue of UAS payload was a significant barrier to their application for coastal management (B. Chen et al., 2018). The importance of payload in relation to UAS capability was also raised by Colomina and Molina (2014) in a review of UAS for remote sensing and photogrammetry.

The fact that the relatively low costs involved in certain UAS studies make them available to a wide range of organisations contributes to the issue of a lack of standardised methodology and processing of data (Corbane et al., 2015). Manfreda et al. (2018) point out that with smaller studies and study sites comes a fragmentation of the adopted procedures and methodologies. In addition to this, a broad difference in budgets, skill sets and sensor technology contribute to the lack of unified principles and methods, translating to wide variations in recorded accuracies from differing techniques (Andrews, Gares, & Colby, 2002). The rapid access to high spatial and spectral datasets also creates high demand for data storage and processing capacity. Low-budget projects may not have access to adequate data processing power, reducing the effectiveness of their work. For satellite technology the data are often produced to a very high standard by a commercial operation; for UAS based studies, however, the final accuracy of the data is dependent on the skills and available processing power of the end user (Manfreda et al., 2018). Much of the existing and more well-known techniques available for data processing were developed for satellite and manned aerial remote sensing system, whose image pixels sizes were in the meters rather than centimetres (Candiago, Remondino, De Giglio, Dubbini, & Gattelli, 2015). Manfreda et al. (2018) state that there is a clear need for defined procedures in data processing due to the significant effect of error propagation from improper image mosaicking and data processing.

1.2 Vegetation Classification

1.2.1 Methods of Image Classification

Image classification is the primary means by which landscape information can be extracted from remote sensing data (G. M. Foody, 2002; Marceau, Howarth, & Gratton, 1994; K. Wang et al., 2010;

Xie et al., 2008). The classification of vegetation and other land-cover types is a common application of remote sensing in ecological (Dymond & Johnson, 2002; Jeganathan, Dash, & Atkinson, 2014), conservation (Knoth et al., 2013; Ramírez-García, López-Blanco, & Ocaña, 1998) and wildlife management studies (Sarda-Palomera et al., 2012). When classifying vegetation characteristics using imagery there are a multitude of different methodologies and techniques available; choosing the right methods depends on the desired output.

Conventional image analyses are based on pixel orientation classification approaches that rely only on simple spectral (multispectral) or visual Red Blue Green (VRBG) information contained in the pixel data (D. Jones, Pike, Thomas, & Murphy, 2011). Increasing the spatial resolution of imagery results in a greater power of detection of smaller image elements (Aplin, 2005; Mathieu et al., 2007), as at finer resolutions, the sub-pixel variation is reduced and the overall image accuracy is increased. This gain in individual pixel accuracy comes at the cost of increased variation between pixels (Mathieu et al., 2007), which has a detrimental effect of decreased spectral separability of the classes and a subsequent lowering of classification quality (Oloo, 2017; Underwood et al., 2007). Spectral overlap can also be a significant source of error when assessing small scale features, such as individual plant succession stages (Carvalho et al., 2013).

Compared with pixel-based methods, object-based image analysis (OBIA) (also called geographic object image analysis GEOBIA) utilizes other image object features, such as size, shape and position in conjunction with spectral data (Benz, Hofmann, Willhauck, Lingenfelder, & Heynen, 2004; Lisita et al., 2013). The base units of OBIA are image objects which represent significant and typically homogenous groups of pixels in an image (G. Chen, Hay, Carvalho, & Wulder, 2012; P. Zhang, Lv, & Shi, 2013). These can be predefined by the user or derived automatically using algorithmic approaches. Remote sensing and OBIA show a strong utility for the analysis and quantification in invasion biology for both flora (D. Jones et al., 2011; Lantz & Wang, 2013; Smith et al., 2008) and fauna (Navratil & Wilps, 2013), as well as general vegetation and ground cover mapping (G. Chen et al., 2012; Yu et al., 2006)

Classification algorithms can be either "supervised" or "unsupervised", and the classification can either be on a pixel by pixel basis, or done as "image objects". Supervised methods rely on data from a training dataset, which is typically built via the collection of "ground truth" data in the field, or manually built post-image collection of points and polygons that represent target class features (Lu & Weng, 2007). The aim of the training dataset is to create descriptive statistics for each class in the image, which are then used to derive class membership of a given pixel or image object. The quality and accuracy of the dataset used are of fundamental importance to classification outcome (Foody, Mathur, Sanchez-Hernandez, & Boyd, 2006). When the area in question shows high natural

complexity either in structure or land cover, creating a sufficiently representative training sample becomes inherently challenging (Lu & Weng, 2007).

Unsupervised methods differ in that the pixel class is calculated using the statistical similarity of the spectral reflectance of each unit (Xie et al., 2008). The classes are then manually labelled using image interpretation skills. Due to the inherently complicated manner in which remote sensing data is collected, it is not uncommon for what exists as a single vegetation class or cover type to exhibit a wide range in spectral signatures in the remotely sensed images. Unsupervised methods are susceptible to within-class spectral variation, as well as spectral errors from image capture and processing (Xie et al., 2008). Supervised methods are more susceptible to user, rather than inherent, spectral error, as sampling methods can be designed to account for with-in class spectral variation (Foody et al., 2006). For a comprehensive review of classification types, see Lu and Weng (2007).

1.2.2 Spectral and Spatial Resolution in Image Classification

Very high spatial resolution (VHR) images are now becoming available for commercial use, as are hyperspectral sensors. Hyperspectral sensors split the electromagnetic spectrum into more discrete and more accurate spectral bands than multispectral sensors. Multispectral sensors can typically detect only four spectral bands: Red, Blue, Green and (typically, but not always) Near Infra-Red (NIR) (Underwood et al., 2007). Both VHR and hyperspectral imagery greatly enhance the capacity for ecologists to detect individual plant species signatures as well as signatures characteristic of certain plant communities (Andrew & Ustin, 2009; Turner et al., 2003; K. Wang et al., 2010; K. Wang, Franklin, Guo, He, & McDermid, 2009) However, while remote sensing has advanced to the point at which large individuals (usually trees, but see Koh and Wich (2012) and Sarda-Palomera et al. (2012)) can be identified with a good degree of accuracy, the application of remote sensing is currently limited in its ability to differentiate between individual species, such as herbs (Bradley & Fleishman, 2008).

Hyperspectral data has many benefits over multispectral data in terms of its power in vegetation classification. By increasing the complexity of the available data, more precise classification techniques can be applied. Recent applications have included increased accuracies in early detection and tracking of the extent of biological species invasions (Andrew & Ustin, 2009; Ouyang et al., 2013; Underwood et al., 2007; A. P. Williams & Hunt, 2002), analysis of chemical compositions (Carvalho et al., 2013) and discrimination of individual mangrove species in a diversely populated mangrove forest (Koedsin & Vaiphasa, 2013). Multispectral studies are still relevant, however, as the combination of multispectral data with advanced classification techniques, such as object-based image analysis (OBIA) (Laba et al., 2010) as well as careful timing in image acquisition, can yield good levels of classification accuracy (D. Jones et al., 2011; Muellerova, Pergl, & Pysek, 2013).

While identifying species at low densities using low-resolution imagery can be difficult, this process can be greatly enhanced if the species in question has distinct phenological states that significantly differ from those species in its surroundings (Andrew & Ustin, 2009; He et al., 2011; M. L. Lu, Huang, Chung, & Huang, 2013; Ustin & Gamon, 2010). Phenological changes in vegetation can create distinct spectral patterns that can be readily detected with remote sensing, particularly so with hyperspectral sensors (Ouyang et al., 2013). There are two general categories in phenological studies: Short-term studies that take advantage of the detectable phenological differences between species for species identification (Ouyang et al., 2013) and longer-term studies that focus on monitoring the temporal fluctuations a given regions vegetation phenology over time (Knox et al., 2013; Muellerova et al., 2013). Detecting changes in phenology requires data with high temporal resolution (Knox et al., 2013), including both in terms of spectral and field data (Nagendra et al., 2013).

1.3   Community Analyses with Remote Sensing

One main remote sensing application of particular interest to this study is that of plant community analyses via the classification of UAS derived imagery. Community ecology is the study of the organisation of ecological communities based on species and or environmental variables (Leibold et al., 2004). The classification of images derived via remote sensing allows for the delineation and identification of different ground cover types including individual plant and animal species. The concept of scale in ecology heavily influences the application of different remote sensing techniques and methodologies. Coarse-scale factors such as broadly defined community composition and habitat modelling are relatively common applications for remote sensing, however, the direct detection of fine-scale ecological phenomena has only recently been feasible due to the limited availability of the advanced technology required (Klosterman et al., 2018).

In a quasi-ecological-arms-race, the pursuit of higher spatial and spectral sensors for ecological monitoring, the use of UAS for community analyses is a rapidly growing field. Baena, Moat, Whaley, and Boyd (2017) used multispectral (RGB + Red-Edge), very-high-resolution UAS derived imagery and OBIA to identify and quantify keystone tree species across wide heterogeneous equatorial dry forest landscapes in Northern Peru. Zweig, Burgess, Percival, and Kitchens (2015) investigated the feasibility of UAS for mapping multi-species wetland communities using multi-scale, high-resolution, true-colour multiband (RGB) imagery. Klosterman et al. (2018) conducted forest species community analysis of species and non-species specific communities using high-resolution multiband (RGB) imagery to investigate the relationship between species assemblages and spatial variations in plant phenology.

While the benefits of UAS and very high-resolution data are clear, the suitability of its wide application to ecological studies remains uncertain. The issue of appropriate scale in remote sensing relates to the importance of proper experimental design. Just as the design of field-based observational studies need to relate to the ecological phenomena in focus (Eberhardt & Thomas, 1991), so too does the type and degree of remote sensing technologies being applied. Zweig et al. (2015) state that "An important consideration when using this new data source is to let the scientific question define the data specifications and not let the technology define the scientific question". In their recent study, the very high-resolution imagery acquired via UAS was too fine for the specific communities and their inherent spatial and spectral characteristics. The authors state that had the test of such imagery not been the focus of their study, the high costs involved would have yielded data with limited scientific value.

1.4   Remote Sensing of Sand Dune Environments

Remote sensing of coastal dune environments has been carried out for multiple decades. Hugenholtz, Levin, Barchyn, and Baddock (2012) provide a comprehensive review of the progression in the application of RS for analysis of sand dune environments over the past forty to fifty years. In the time since the review was published, the research continues to advance. The structural and spatial characteristics of dunes, such as size, shape, movement and extent of the dunes have been widely studied using satellite (Kaliraj, Chandrasekar, Ramachandran, Srinivas, & Saravanan, 2017), aerial (Brownett & Mills, 2017; Charbonneau, Wootton, Wnek, Langley, & Posner, 2017) and terrestrial (Conlin, Cohn, & Ruggiero, 2018; Corbi, Riquelme, Megias-Banos, & Abellan, 2018) remote sensing platforms. Structural data typically comes from the use of LiDAR, which historically was restricted to satellite and aerial platforms. LiDAR sensors deployed on UAS are becoming more common thanks to increased payloads and miniaturisation of sensor technologies.

Structure From Motion (SFM) is an advanced technique of 3-dimensional monitoring and allows the creation of a three-dimensional "point-clouds" from overlapping imagery, using scene geometry as well as sensor position and orientation (Westoby, Brasington, Glasser, Hambrey, & Reynolds, 2012). SFM is of particular interest in UAS studies as it can be derived from relative simple imagery (Conlin et al., 2018), however, references to its application in coastal monitoring are limited (Goncalves & Henriques, 2015). Recent advances in SFM technology and methodologies have resulted in spatial accuracies and data densities that were once only available via LiDAR (Goncalves & Henriques, 2015). While SFM presents a valuable tool for monitoring coastal environments, Conlin et al. (2018) found UAS based SFM platforms only produced similar vertical positioning errors to traditional structural assessments on un-vegetated dune systems. SFM returns a point cloud of surface heights, which includes that of any vegetation present. To correct for this, the average height of the vegetation can

be measured and then subtracted from the surface models via classification and broad processing of vegetated areas. Conlin et al. (2018) found when using average vegetation heights however that the relatively simplistic approach negatively influenced the final accuracies when mapping diverse and heavily vegetated dune environments.

Existing satellite and aerial imagery are often used in conjunction with UAS imagery to monitor environmental change over time. Albuquerque, Alves, Espinoza, Oliveira, and Simoes (2018) combined historic satellite imagery with current UAS data to investigate the changes to dune structure and shoreline position in response to extra-tropical cyclone activity. Baughman et al. (2018) investigated dune movement in Alaskan sub-Arctic sand dunes using existing satellite imagery and aerial LiDAR data. Brownett and Mills (2017) provide a meta-analysis of the combined use of aerial imagery, LiDAR and terrestrial remote sensing for monitoring multiple coastal sand dune habitats on the British coast.

The use of UAS for the analysis of dune ecological communities is still relatively uncommon. Goncalves and Henriques (2015) used a lightweight "flying wing" UAS to collect multiband, high resolution (<5cm) imagery of coastal dunes in Portugal. The authors were able to map the physical and vegetation structure of the dunes using SFM photogrammetry with accuracies that were equal to or greater than that derived from manned aerial surveys. Suo et al. (2018) used a multi-rotor UAS to capture high resolution (2.5cm), multispectral (RGB + Red Edge + NIR) imagery of the Brittas-Buckroney dune complex on the coast of Ireland. In this study, a combination of photogrammetry and image classification was used to map dune vegetation and ground cover. The accuracies of classifications based on different combinations of spectral bands were tested, with those containing NIR and Red Edge image bands performing better than those with just RGB. Bastos et al. (2018) classified dune environments to aid in the creation of photogrammetric surface models. Vegetation was separated from open ground and classified by height, which was then used to remove the vegetation height from the surface model, creating a digital terrain model. Using this technique they were able to create a DTM using UAS with similar accuracies to that of a DTM derived from ground-based GPS methods. Suo et al. (2018) were able to accurately classify discrete beach zones from high resolution (10cm), multiband (RGB) imagery. The study compared four different types of image classification, finding similar accuracies for SVM, MLC and Random Forest, an ensemble learning method for supervised classifications. The authors were also able to show that for site-specific studies with frequent data capture events, training data from independent capture events can be used to generate acceptable classification accuracies.

1.5 The rationale for the study

The Department of Conservation (DOC) has expressed interest in the application of aerial drone survey technologies for conservation efforts. In particular, they are interested in the potential for aerial drone survey data to provide such information as vegetation classifications, particularly for the monitoring of species both invasive and threatened; the detection of non-target species impacts from spraying operation, and the characterisation of species' habitats within the dune system. Dune systems have been highlighted as being of good potential for the testing of this technology as they appear to exhibit simple topography with clear zonation in vegetation.

Sand dune plant communities are defined as being 'dominated by herbaceous plants and low shrubs occurring on recent, unstable dune sands' (Newsome, 1987). Active dunes typically have low plant diversity in comparison to more stable dune systems and are dominated by species that are able to adapt to or tolerate the harsh environmental conditions found there (M. Hilton, Harvey, Hart, James, & Arbuckle, 2006). New Zealand's sand dunes have been detrimentally affected by human activities, including agriculture, forestry and recreation, as well as the introduction of a number of invasive plant and animal species (M. Hilton et al., 2006; M. J. Hilton, 2006; Partridge, 1992; Pegman & Rapson, 2005).

Invasive plant species pose a significant threat to dynamic landscapes that are negatively affected by intensive human modification (Millennium Ecosystem Assessment 2005). Such species not only seriously threaten current states of biodiversity and ecosystem functioning (Pysek & Richardson, 2010), but also can lead to drastic long-term changes in the characteristics of key landscapes (Chytry et al., 2012). The exotic sand-stabilising marram grass (*Ammophila arenaria* (L.) Link) is a significant invasive species found at most of the remaining dune systems in New Zealand (Gadgil, 2002). The widespread intentional establishment of *A. arenaria* populations as a method of sand stabilisation began in the early 1900s and continued until around the passing of the 1991 Resource Management Act; the new Act brought about a change in thinking towards the preservation and restoration of the natural character of ecosystems (Gadgil, 2002). The ability of *A. arenaria* to displace native dune species and change the environmental characteristics of sand dune communities in New Zealand is well known (Dixon, Hilton, & Bannister, 2004; Hesp, 2002; M. Hilton et al., 2006; Norton, 1991; Wardle, 1991). Some native species, such as *Spinifex secriceus* (R. Br.), are more effective in stabilising fore-dunes than *A. arenaria*; however, *A. arenaria* effectively dominates the stabilisation of the rear-dunes due to a lack of a dominant ecologically equivalent native species (Esler, 1970). Tree Lupin (*L. arboreus* Sims) is another prominent invasive species present in many coastal environments. The intentional planting of Lupin has been conducted for much of the previous century to aid in the stabilisation and reclamation of dunes for agriculture and forestry due to the

n-fixing ability of the legume (Berg & Smithies, 1973; Dick, 1994; Gadgil & Ede, 1998). Lupin is a threat to natural coastal ecosystems because not only does it directly compete with most native dune species (Molloy, Partridge, & Thomas, 1991) but the fixation of nitrogen can significantly alter the surrounding environment (Pickart, 2004), facilitating weed invasions (Maron & Connors, 1996).

1.5.1 Aims and objectives

Aims

The aim of this study is to assess the use of high resolution, multispectral imagery for monitoring coastal plant communities. Traditional field-based community analysis methods will be conducted to serve as a baseline for the GIS-derived community data to be compared against.

Objectives

1. Conduct plant community analysis surveys of the site to establish a standard ecological model of the sand dune plant communities.

2. Using UAS based remote sensing, collect high spatial resolution, multispectral imagery at Kaitorete Spit.

3. Using GIS, carry out image classification on the imagery with the aim of digitally recreating the field based datasets.

4. Use ordination and clustering techniques to classify the different vegetation communities at Kaitorete Spit using both field and GIS data.

5. Compare the results of the GIS analysis to that obtained from field data

1.5.2 Thesis structure

This thesis is structured as follows:

Chapter 1 presents an overview of the use of remote sensing in ecology with specificity towards the use of UAS based ecological community analysis.

Chapter 2 provides the general research design and the development and refinement of the methodologies used to extract biologically relevant community data from the UAS imagery.

Chapter 3 presents the results of image processing and analysis as well as the comparison of the field community data to that derived via UAS and how variations in image resolution may affect these results.

Chapter 4 includes a discussion of main results of this study and further discusses their suitability and relevance for the particular ecological phenomena and their inherent monitoring requirements at Kaitorete Spit.

Chapter 5 brings together the main conclusions of this study and provides recommendations for future studies and the continued ecological monitoring of Kaitorete Spit.

Chapter 2

Methodology

2.1 Site Description

More accurately called a barrier beach complex (Soons, Shulmeister, & Holt, 1997), Kaitorete Spit (Kaitorete) is a depositional barrier bar of mixed sand and gravels, originating at Taumutu, near the mouth of the Rakaia River, and extending for approximately 28 km towards the volcanic cliffs at the edge of Banks Peninsula (Figure 1). The spit itself has existed for around 8,000 years, with the barrier arm having progressed over two millennia from the Taumutu end until finally reaching Banks Peninsula, subsequently forming a barrier beach and enclosing two fresh to brackish water lakes; Te Waihora/Lake Ellesmere and Wairewa/Lake Forsyth. (Soons et al., 1997). The width of the barrier complex ranges from 250 m at its westernmost point to up to 5 km at its widest. Dune heights are 3 – 5 m on average, with the highest dune heights approaching 15 m (Johnson, 1992).

The study site for Kaitorete Spit is restricted to a smaller area of the greater spit (Figure 2), encompassing the majority of the dunes within and surrounding the DOC Kaitorete Spit Science Area and Conservation Reserve. This legal classification allows for more effective habitat management and protection compared to Kaitorete Spit as a whole. The natural heritage and conservation values of Kaitorete Spit have been identified as being nationally significant (Davis, 2002; Lettink, 2008; Partridge, 1992; Patrick, 1994; Peace, 1975; Pudji, 1997). Kaitorete Spit is the largest unmodified dune system in the Canterbury region (Johnson, 1992). Characterised by the uninterrupted sand and gravel beach that runs for the entire length, the site is also home to distinct, active, fore and rear-dune ecosystems (Davis, 2002; Hooson, 2015). Kaitorete is home to the largest dune population of the indigenous and at-risk sand-binding sedge, pīngao (*Ficinia spiralis* A. Rich (=*Desmoschoenus spiralis*) (golden sand sedge)) (Johnson, 1992; Partridge, 1992). Other notable plants at the site are the threatened and locally endemic species *Carmichaelia appressa* G. Simpson (prostrate broom), *Muehlenbeckia astonii* Petrie (shrubby tororaro, wiggywig, mingimingi) and *Craspedia "Kaitorete"*, a currently undescribed species endemic to Kaitorete Spit. The active fore-dune native vegetation is characterised pīngao, sand sedge (*Carrex pumila* Murray), shore bindweed (*Calystegia soldanella* (L.) R.Br. ex Roem. & Schult.) and sand tussock (*Poa billardierei* (Spreng.) St.-Yves).

Within the bounds of the reserve pest species are actively controlled, creating an environment in which a more-natural coastal dune ecosystem can function. The dune vegetation is at risk from a number of introduced species, including marram grass, broom (*Cytisus scoparius* (L.) Link), gorse (*Ulex europaeus* L.) and tree lupin (*L. arboreus* Sims). Domestic stock and grazing pests, such as

European rabbits (*Oryctolagus cuniculus* (L., 1758)) and European hares (*Lepus europaeus* (Pallas, 1778)), also threaten the dunes (DOC, unpublished report). Although a serious threat to the dune system, the local population of *L. arboreus* has, in the past, been naturally all but eradicated by the combined efforts of the root fungus *Colletotrichum gloeosporioides* (Penz) and the native Kowhai Moth (*Uresiphita polygonalis maorialis* (Felder & Rogenhofer))(Molloy et al., 1991). While anecdotal reports suggest that the fungus still periodically lowers *L. arboreus* population levels, the activity of the Kowhai Moth has not been studied. The moth has been associated with a few non-native species and its presence at Kaitorete may, in fact, rely on the populations of these exotics, as Peace (1975) noted a vast reduction in the natural range of its native host species, the Small-Leaved Kowhai (*Sophora microphylla* (Aiton)

Kaitorete Spit has a long history of human activity. The site was used extensively by Maori in pre-European times for food-gathering and was viewed as an important strategic location between rival Iwi (Holmes, 1998). Post-European arrival, much of the land has been and continues to be used for farming, including arable cropping and sheep and beef grazing. A small community called Birdling's Flat sits at the eastern-most point of Kaitorete Spit. This community's name comes from William Birdling who in around 1850 acquired 5000 acres of land and developed it for farming purposes (Peace, 1975). Extensive gravel and sand mining operations were carried out up until the '90s, with a large sand pit being located in and around what is now the Kaitorete Scientific reserve. At this site alone, an estimated 274,384 m^2 of material was removed over the length of its operation (Holmes, 1998). Mining occurred across the entire dune system which resulted in the loss of rear, mid and fore-dunes in some areas. A study of the recovery of the vegetation post-mining was carried out in the nineties and showed that in many cases the mining has likely had irreversible effects on the vegetation of the site (Partridge, 1992).

Kaitorete also has a history of military activity. Between 1950 and 1958, the RNZA used an area to the west of Birdling's Flat for artillery practice. Towards the middle of the spit, an area near the junction of Baileys Road and what was then known as Habgood's Quarry Road (the last turn-off to the beach as you head west on Bailey's Rd, was used by the RNZAF as a practice bombing range between 1940 and 1958. The impact of this activity was reportedly limited to a few small craters and the occasional fire (Peace, 1975). As of 1997, the area was used for parachuting practice (Pudji, 1997).
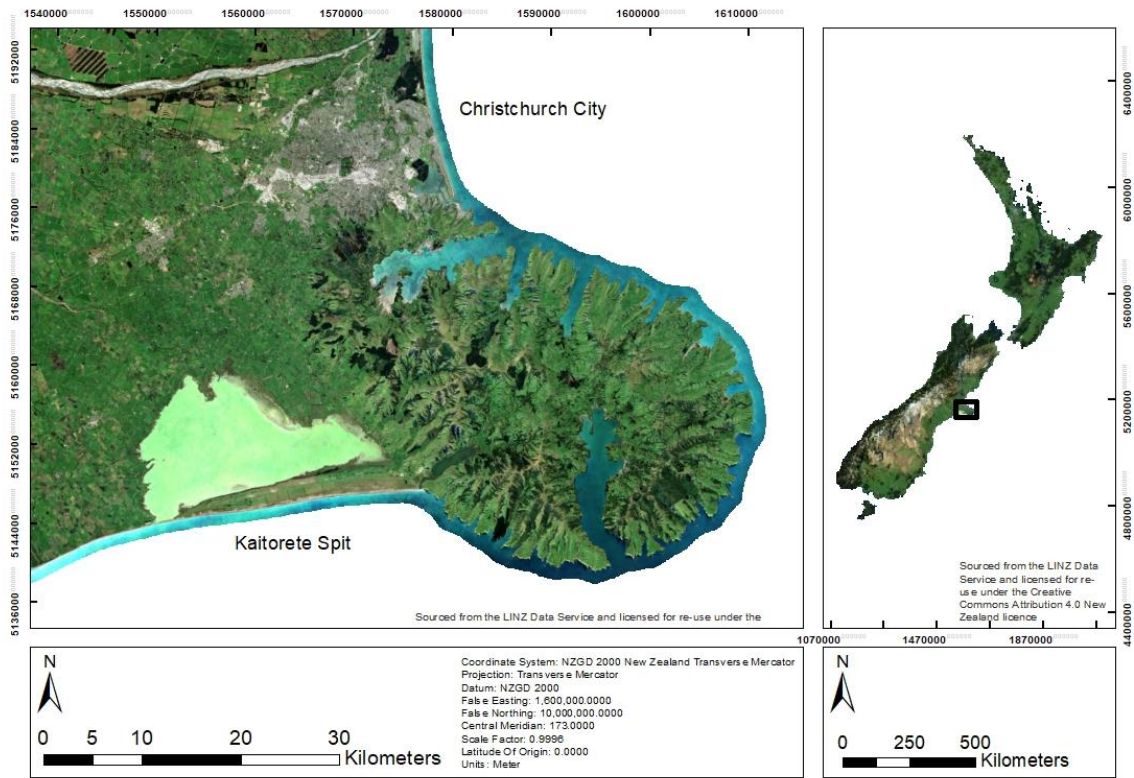
Figure 1. Location of the study site at Kaitorete Spit, in Canterbury, New Zealand.
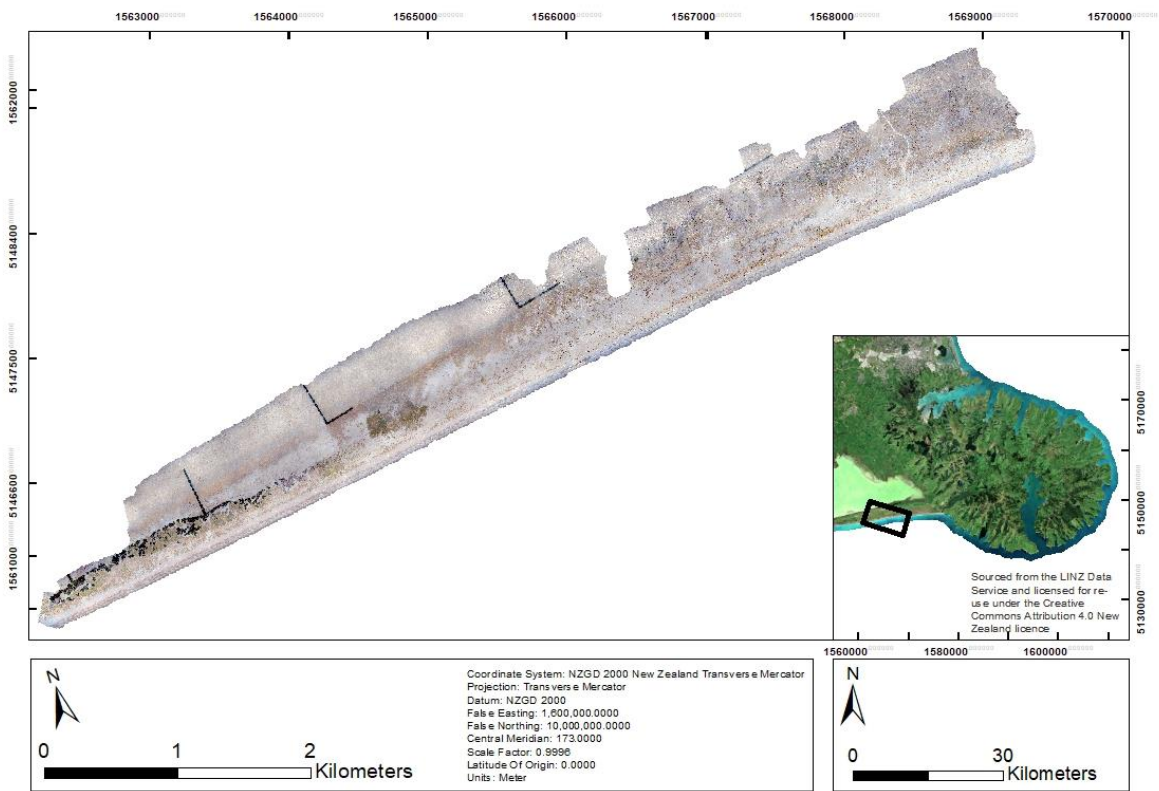
Figure 2. Study extent and location in relation to Banks Peninsula, Canterbury, New Zealand.

2.2 Data collection

2.2.1 Vegetation Surveys

Vegetation surveys were conducted late 2013 at Kaitorete Spit. Transects were established perpendicular to the high tide mark at every 300 m in additional distance from an established reference point inside the image boundary, with plots laid down every 10 m along the transect until reaching the inland maximal extent of the dune. Plots were 6 m x 6 m, divided into nine 2 m x 2 m quadrats. For the vegetation within each quadrat, the estimated per cent cover (to the nearest 5%) was recorded for each species of major vegetation class present. Differential GPS points were taken at the centre of each quadrat, with in-field accuracy of 0.5 m and a post-processing accuracy of approx. 0.05 m.

2.2.2 Image Acquisition

Multispectral imagery was captured on December 5th 2013 using an RQ-84Z Photogrammetry UAS by Hawkeye UAV (now Hawkeye Systems). The RQ-84Z featured dual mounted Sony NEX 5 (24 megapixel) cameras enabling the concurrent acquisition of both NIR and RGB data. The data were collected flying at an average height of 190 m above sea level, no higher than 219 m above sea level. A timing of three seconds between each image was used, hence camera location is variable across the target area due to flight considerations (such as wind speed and direction).The positioning and orientation (POS) of the camera were determined by the on-board uBlox GPS. The imagery was delivered in the form of 21 image 'tiles' for both the RGB and NIR data (42 in total) with each tile covering approximately 1 km^2. The NIR was split into two different datasets, based on the two independent capture events. The RGB was not divided into the same format for reasons unknown.

2.3 GIS Analysis

The overall aim of the GIS analysis conducted in this study was to recreate the field community data with UAS imagery using image classification and other GIS techniques and methodology. Section 2.3.1 details the initial processing of the imagery. This work focused first on correcting the spatial and spectral discrepancies that existed in the raw image data. The data were then transformed and augmented through the creation of vegetation indices as varying measures of certain image properties. Those indices that contributed most to overall variation were selected and put forward for classification testing. In Section 2.3.2 a series of multiband images were classified using three different image classification techniques. The specific combinations of multiband images and classification algorithms were then ranked by the measure of classification accuracy. The image and

technique with the highest accuracy were then used as the basis for the community analyses for comparison against those of the field data.

2.3.1 Image Preparation

The images were pre-processed by Hawkeye UAV Ltd for sharpness and shadowing then processed in Areo (Version 3.01, © 2014 Areograph Ltd), a multi-ray photogrammetric software, to produce the orthographic imagery with a dependent terrain model and point cloud. Ground Control Points (GCPs) was used to adjust the data to the true ground, with 30 GCPs laid out at selected sites in the target area and surveyed. The data were delivered in LAS 1.2 format (Point Cloud), TIFF (photos), TIFF/TFW (orthophotos) and ESRI Shapefile (index and ground control points). All further GIS analyses and processing was carried out using ArcGIS 10.3 (ESRI, 2014).

Significant spatial and spectral errors that were present in the raw imagery became apparent after the image products had been delivered for the project by Hawkeye UAV. Poor GCP positioning and density resulted in inconsistent spatial accuracy across the images, as well as issues with the coverage of the data, i.e., 'holes' in the imagery at various points. The NIR and RGB data, being captured with two independent sensors and processed in separate operations exhibited a non-satisfactory overlap. The site being flown in two 'halves' (eastern and western ends) also introduced a major discrepancy in spectral quality.

The primary aim of image processing was to create a GIS dataset comparable to that of the field data based on the captured imagery. In order to achieve this, multiple image processing steps were required in order to maximise the spatial and spectral accuracy of the GIS data. These were as follows:

1. Collate the individual RGB and NIR image tile sets into two spatially continuous raster sets for processing.

2. Correct the significant geospatial positioning errors in the raw imagery.

3. Correct the significant geospatial discrepancies between the NIR and RGB data.

4. Collate the individual image tiles into a single, multi-band image.

Raster Creation

Mosaicking and Colour Balancing

Raster mosaicking is the process of joining together multiple raster images into a continuous dataset to enhance image processing speeds and to smooth out -image spectral variations. Using the "Mosaic" tool, the individual RGB and NIR image tile sets were joined together to form larger,

spatially continuous images. The raw NIR dataset was captured in two halves with some overlap between the two, therefore, these images were processed in two stages. To account for any overlap between input datasets, the mosaic operator "blend" was used, which creates a new value for overlapping areas based on a horizontally weighted calculation of the overlapping cells. "Mosaic colourmap" mode "last" was used to set the colourmap of the mosaicked raster to that of the last raster added. The "mosaicking tolerance" was set at 0, meaning that for any misalignment between the target and source pixels, the source pixels are resampled to create a new value based on the average of the two overlapping pixels.

Georeferencing

Further georeferencing was needed to maximise local spatial accuracy in the imagery. As the data had been collected via two independent sensors, there also existed significant spatial discrepancies between the two images. The RGB image was first georeferenced against the Ground Control Points (GCPs) that were manually collected in the field, based on hard reference points, e.g. fence posts, structures and feature boundaries. Once the RGB image was positioned in accordance with the existing GCPs, the NIR image was then georeferenced to the RGB image using a combination of the manually collected GCPs, as well as 275 additional GCPs that were selected using the "georeferencing toolbar". Pairs of corresponding GCPs were identified that link the two images together, with the aim of shifting one raster to the correct position based on the associated point in the target raster. The accuracy of the transformation was calculated via the root square mean error (RMS), which is the difference from where the point in the raster to be transformed was specified to be on the reference raster, compared to where the point was located after the transformation took place. The sum of the RMS of all residual errors was used as a measure of transformation consistency. The forward residual showed the error based on the spatial reference system of the data, whereas the inverse residual showed the error in pixel units (1 pixel = 10 cm).

Spline transformations were used to transform the images in all cases. Spline transformations are best suited to where high local accuracy is required over global accuracy. Pairs of control points are transformed to overlay exactly, while those areas that lay some distance away from control points are shifted for best accuracy. Because the accuracy of these areas cannot be guaranteed, it is important to create a large number of points with good coverage of the image. Exact precision is required for the placement of control points in order to achieve the greatest accuracy.

When selecting reference points to use, physical points, such as fence-lines, corners of buildings, vertices in track intersections and other objects were given priority over living objects, e.g. plants, due to those objects characteristically having more defined borders, allowing higher confidence in

locations across both RGB and NIR images. When no suitable physical objects were available, plants with highly contrasting features, such as hard object boundaries, were selected as reference points.

Kernel-based filters to increase the accuracy of georeferencing

Image Sharpening and edge detection were employed to aid in the detection of suitable control points for georeferencing the two image sets. Images were processed using a series of Convolution Functions (ESRI, 2014) which apply a moving kernel-based filter to the entire image, multiplying the cell values by that of the filter. These are used to improve the quality of an image raster by reducing the local spectral variation and enhance certain image object features such as boundaries (ESRI, 2018a). A "smoothing" filter (Table A. 2) was first applied to reduce image noise, followed by a series of "sharpening" filters (Table A. 3, Table A. 4, Table A. 5 and Table A. 6) to enhance the definition of image object boundaries.
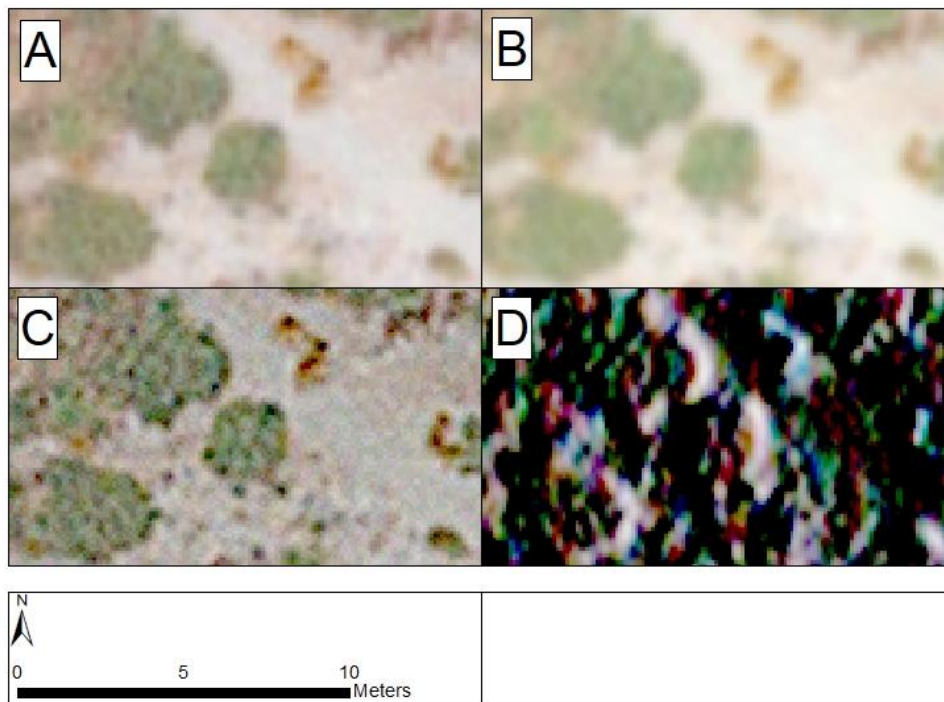
Figure 3. Image sharpening of a sample of the typical dune vegetation at Kaitorete Spit. A = raw image, B = smoothing filter, C = smoothing and sharpening, D = Edge detection.

Vegetation Indices

Vegetation Indices (VIs) are simple and effective algorithms that are applied to remote sensing data in order to derive quantitative and qualitative assessments of vegetation characteristics, such as growth, vigour, structure and cover (Xue & Su, 2017). Most VIs incorporate the difference between the red and NIR spectral bands, as Red reflectance is sensitive to chlorophyll, and NIR is sensitive to the internal leaf structure (Candiago et al., 2015). The greater the difference between the two

reflectance's, the greater the implied amount of living, or "green", vegetation. Small differences can indicate non-living surfaces, such as open ground or dead plant matter (Xu, Guo, Li, Yang, & Yin, 2014).

Creation and evaluation

Seven common VIs were chosen for comparison based on the four discrete bands in the base imagery (Table 1). The SR and NDVI are based on the reflectance of the NIR and RED areas of the spectrum and are used to enhance the differences between the living and non-living ground cover types. While being implemented in monitoring a wide range of ecosystem types, such as salt marshes (Gao & Zhang, 2006; Schalles, Hladik, Lynes, & Pennings, 2013; Sun, Fagherazzi, & Liu, 2018), mountain pastures (Zhumanova, Mönnig, Hergarten, Darr, & Wrage-Mönnig, 2018), dry grasslands (Magiera, Feilhauer, Otte, Waldhardt, & Simmering, 2013; Pearson & Miller, 1972; Weber, Schaepman-Strub, & Ecker, 2018) and sand dune communities (A. V. Bradley, Haughan, Al-Dughairi, & McLaren, 2019; Burgheimer et al., 2006; Shumack et al., 2017) they have been shown to be susceptible to the effect of soil brightness, and increasingly so in areas of sparse vegetation cover (Gilabert, González-Piqueras, García-Haro, & Meliá, 2002; Nagler, Daughtry, & Goward, 2000; Rondeaux, Steven, & Baret, 1996; Xu et al., 2014). The addition of vegetation indices that focus on the green spectrum is due to the fact that for certain species, it is better associated with variations in leaf chlorophyll (Sripada, Heiniger, White, & Meijer, 2006), crop biomass (E. Hunt et al., 2011; Farrell, Gili, & Noellemeyer, 2018), anthocyanin content (Anatoly A. Gitelson, Keydan, & Merzlyak, 2006) and Leaf Area Index (F.-m. Wang, Huang, Tang, & Wang, 2007), as well as being less affected by soil and water reflectance (Motohka, Nasahara, Oguma, & Tsuchida, 2010). Ratios with normalised spectral bands have also been shown to reduce the negative effects of illumination and soil reflectance (Sripada et al., 2006).

Table 1. Seven Vegetation Indices were assessed for their relevance in explaining the difference between image objects.

Names of Vegetation Indices	Equation	Reference
Simple Ratio (SR), also known as the Ratio Vegetation Index (RVI)	$\dfrac{NIR}{Red}$	(Pearson & Miller, 1972)
Normalised Differential Vegetation Index (NDVI)	$\dfrac{NIR - \text{Red}}{\text{NIR + Red}}$	(Rouse Jr, Haas, Schell, & Deering, 1974)

Green Normalised Differential Vegetation Index (GNDVI)	$\dfrac{NIR - Green}{NIR + Green}$	(Anatoly A Gitelson, Kaufman, & Merzlyak, 1996)
Green Red Vegetation Index (GRVI)	$\dfrac{NIR}{Green}$	(Sripada et al., 2006)
Normalised Green (NG)	$\dfrac{Green}{NIR + Red + Green}$	(Sripada et al., 2006)
Normalised Near Infra Red (NNIR)	$\dfrac{NIR}{NIR + Red + Green}$	(Sripada et al., 2006)
Normalised Red (NR)	$\dfrac{Red}{NIR + Red + Green}$	(Sripada et al., 2006)

PCA tests

Many different ancillary variables, such as VI, may be used to increase the accuracies of image classification, however, care must be taken to select only those which are of most relevance for the separation of classes (Lu & Weng, 2007). The addition of too many variables has the potential to reduce overall accuracy (Price, Guo, & Stiles, 2002). Using Model Builder and Map Calculator, The four individual image bands of the composite image were combined to create a series of separate vegetation indices (Table 1). These layers were combined with the original 4 band image using Composite Bands to create an 11 band image layer. This was subjected to a PCA using Principal Components (Table 5).

Composite Image Creation

Following the results of the PCA, the SR and NDVI indices were isolated and combined with the original four band image using Raster Calculator to create a six-band image and as two separate 5 band images (Table 2). The resulting three new multiband images, as well as the original, were then used as the basis for image classification.

Table 2. List of multiband images for classification.

Raster image	Image bands
K2_CompositeBands4	Red, Green, Blue, NIR.

K2_CompositeBands5_SR	Red, Green, Blue, NIR, SR
K2_CompositeBands5_NDVI	Red, Green, Blue, NIR, NDVI
K2_CompositeBands6	Red, Green, Blue, NIR, SR, NDVI

2.3.2 Preliminary Image Analysis

Image Classification

Classification types

Three different classification methods were tested on the four different multiband images (Table 2) using the Image Analysis extension for ArcGIS 10.3 (ESRI, 2014). This included two pixel-based methods, unsupervised Iso Cluster and supervised Maximum Likelihood Classification, and one object-based, supervised image analysis approach, Support Vector Machine. Each of the multiband images was first segmented using the Segment Mean Shift tool. The inputs 'spectral detail' and 'spatial detail' were set to the maximum value, 20. A high 'spectral detail' allows for greater discrimination between image objects with similar spectral characteristics. A high 'spatial detail' is best suited for when the image objects of interest are small or and clustered together (ESRI, 2018b).

Unsupervised classifications are one of the more traditional forms of image classification and are widely used for mapping thematic vegetation cover from remotely sensed image data (Xie et al., 2008). the main advantages of unsupervised classifications, when compared to more advanced techniques, come from its relative ease in application, as well as being readily available in a range of statistical analysis and image processing programs and applications (Langley, Cheshire, & Humes, 2001). MLC is a form of probabilistic classification, in which each pixel or image object is allocated a class with which it exhibits the highest probability of membership (Foody, 1996). Xie et al. (2008), state that MLC is one of the most commonly applied classification techniques for satellite imagery when using pixel or statistical-based distributions. Since MLC rely on the assumption of Gaussian distribution in the data, then classification results may be limited in areas of the highly complex cover of non-normal distribution (Otukei & Blaschke, 2010). SVM classifications use machine learning algorithms to find the optimal separation between classes based on training samples (Huang, Davis, & Townshend, 2002). An important factor of SVMs is that often only the training sample of best fit is used for the description and specification of a class (Mountrakis, Im, & Ogole, 2011). SVMs have been shown to be effective with relatively small and/or incomplete training

datasets, achieving higher classification accuracies when compared to MLC classifications (G. M. Foody & Mathur, 2004; Mantero, Moser, & Serpico, 2005). With training datasets often being highly time-consuming, a reduction in the amount of training data required for accurate classifications can help reduce overall project costs (Foody et al., 2006). Mountrakis et al. (2011) state that the cross-disciplinary application of SVMs can be challenging due to the inherent complexity of the more efficient and effective concepts in certain SVM variants.

Classification method evaluation

To aid in the evaluation and selection of the different image band combinations and classification types, the greater Kaitorete image set was divided into subsets of three smaller test sites. Each of the three sites was selected manually, based on spatial separation and differences in ground cover types. Each site was isolated using the Clip Raster tool with the same polygon used for each clip to ensure each new raster was near exact in spatial extent and cell count. Each site measured approximately 56,500 m^2 for a total of 169,500 m^2, or approximately 0.03% of the total 6 km^2 area.

For each of the test sites, training data sets for the supervised classifications were built using the composite images generated from the RGB and NIR band. The methodology for the selection of training data was based on the recommendations of (Foody et al., 2006). Representative pixels from the major ground cover classes were selected to generate a vector layer consisting of approximately 150 pixels for each class. Once the training data set was complete, the Interactive Image Classification tool was used to produce small, on-the-fly maximum likelihood classifications. The dataset was further refined until the point where either further additions resulted in additional errors, or until the number of pixels within the class, sample reached between 100-150 pixels.

Pixels were selected based on their positioning within an identified target plant. Those pixels located more to the centre of a plant, or those displaying the most saturation in true colouration, were given higher priority. Those pixels outside of these criteria had a higher chance of misrepresenting their class. Edge-pixels covered areas where there was a lower density of foliage, meaning that other plant material affected the pixel's spectral signature. Centre pixels were also less likely to be affected by the geoprocessing errors between the NIR and RGB data in identified plants that were of greater size than the amount of local error.

For each site, SR and NDVI were calculated and combined with the original four bands to create two five-band rasters and one six-band raster before image classification was implimented. These were converted into 8-bit data types from 32-bit, as required for classification. The four multiband images were then classified based on the training data using Maximum Likelihood Classifier, Support Vector

Machine and Iso Cluster Classifications, creating twelve classified images at each site for assessment (36 total).

Accuracy Assessment

Classification accuracies of the three sites were tested using both point and area-based methods. For point-based assessment, 100 pixels were selected for each of the dominant classes (Figure 4). Selection of pixels was based on the same strategies used in classification training. For area-based assessment, ten 56.6 m^2 sample sites (approx. 1% of each site) were located using a random coordinate generator (Figure 5). Within the bounds of each sample, ground cover was manually classified using the polygon drawing tool until 100% coverage was achieved (Figure 6). Sample site size was restricted due to logistical constraints involved with sampling such high-resolution data over a large spatial extent.

For point-based assessment, using ModelBuilder, the results of the image classification were combined with the point shapefile using the Extract Values to Points (Spatial Analyst) tool. For the area based assessment, the results of the classification were converted from raster to vector, and then combined with the assessment polygons using a Merge spatial join.
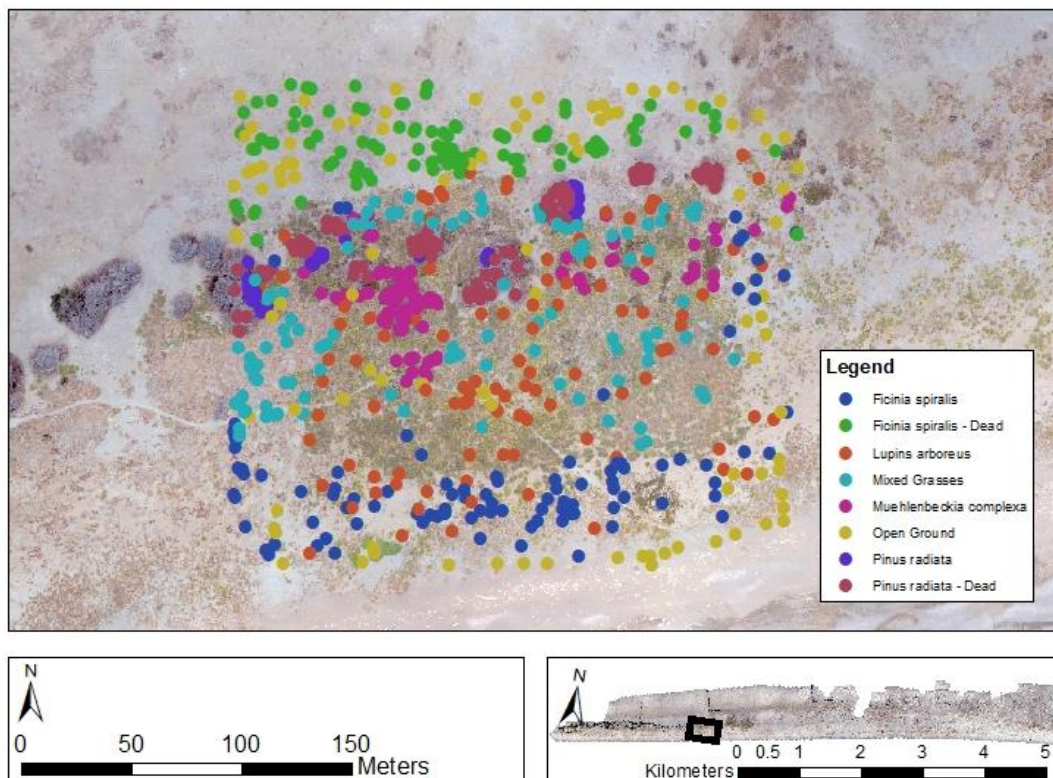
Figure 4. Test Site A showing point locations of plant species for class accuracy assessment.
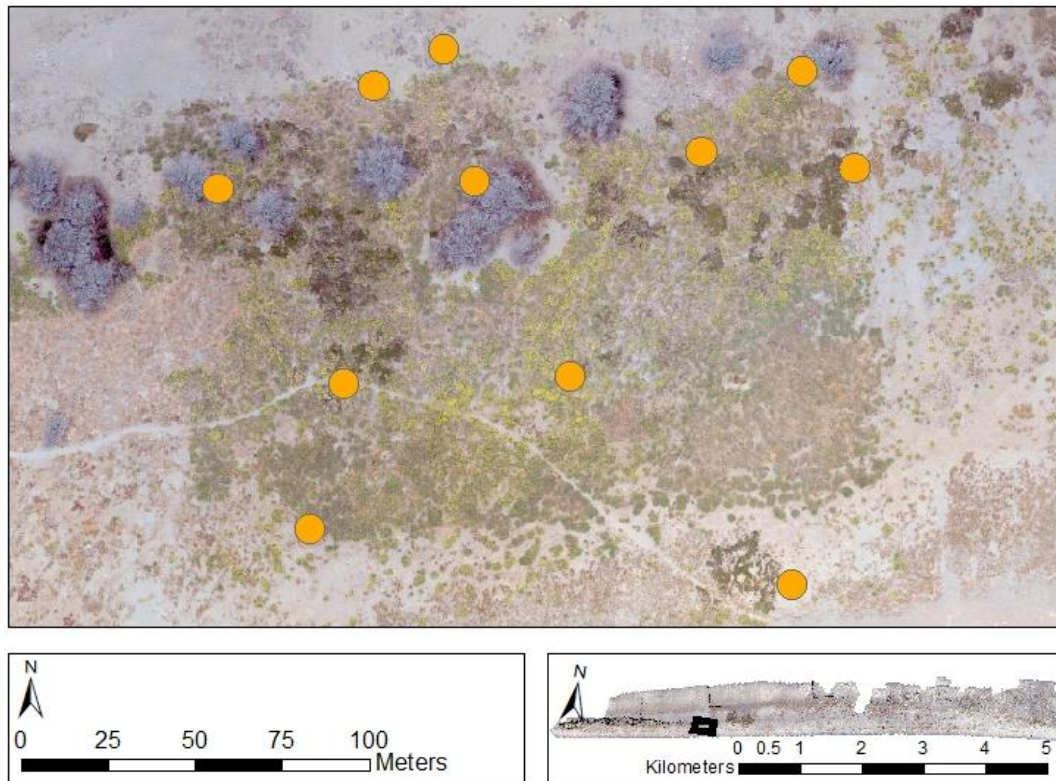
Figure 5. Test Site A showing the locations for area based classification accuracy assessment. Within each circle, the various cover classes were manually classified.
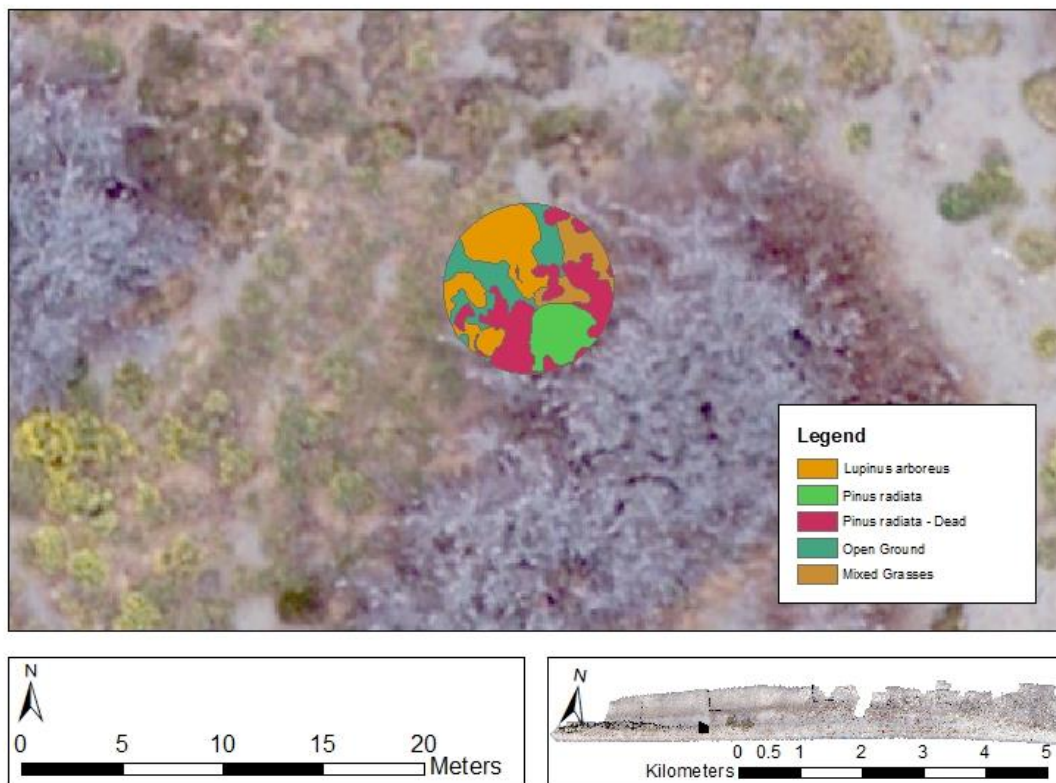
Figure 6. Example of the manually classified assessment area.

The results from the two assessment types were then used in the creation of 36 individual confusion matrices to establish the most accurate combination of spectral bands, vegetation indices and classification algorithms. From the confusion matrices, five different measures of classification accuracy can be determined; Total accuracy, Users accuracy, Producers accuracy, Commission error, Omission error and the Kappa Coefficient.

Table 3. List of measures of accuracy used to asses image classifications.

Accuracy Measure	Equation	Result
Total	$$\text{Accuracy}_{\text{Total}} = \frac{\text{Number of correct cells}}{\text{Total number of cells}}$$	The average accuracy of the classification across all cover types. Does not account for error distribution across classes.
Users accuracy	$$\text{Accuracy}_{User's} = \frac{\text{Number of correct cells in class X}}{\text{Number of cells classified as class X}}$$	For each class, the probability that a randomly chosen point on the map has the same class value in the field.
Producer's accuracy	$$\text{Accuracy}_{Producer's} = \frac{\text{Number of correct cells in class X}}{\text{Total number of cells meant to be in class X}}$$	For each class, the probability that a randomly chosen point in the field has the same value on the map
Commission	$$\text{Commission}_{Error} = \frac{\text{Number of incorrect cells in class X}}{\text{Total number of cells classified as class X}}$$	Measurement of how much the class has been over-classified,
Omission	$$\text{Omission}_{Error} = \frac{\text{Number of cells in class X that were classified as Y}}{\text{Total number of cells meant to be in Class X}}$$	Measurement of how much the class has been under-classified
Kappa coefficient	$\text{Kappa} = (\text{Total number of points} * \text{sum of correct})$ $- \text{sum of all the}(\text{classified points}$ $* \text{ground truth points})$ $/(\text{Total number of points}\wedge 2)$ $- \text{sum of all the}(\text{classified points}$ $* \text{ground truth points})$	Reflects the difference between the actual agreement and the agreement expected by chance.

2.3.3 Final classification and feature extraction

Based on the results of the analyses in Section 2.3.2 the final classification was conducted on the multiband image which contained the NDVI as its fifth layer, using the SVM classification of the segmented image. For this classification, a new and independent classification training dataset was created. This was to have a training dataset that covered a greater amount of area across the entire site and to encompass certain classes that were not present in the test sites, such as Coarse Woody Debris. The final accuracy assessment was based on the same points and areas used in the assessment of the test sites.

Vegetation Sampling Using GIS

Original plant community quadrat GPS locations were identified and a digital polygon of the plot was created and rotated until each point lay within the bounds of its respective polygon. Further spatial joins were used to assign each polygon to its respective transect, plot and quadrat code based on the original GPS data. Due to the large spatial error introduced during data processing, the exact location of each quadrat could not be precisely established. A 10 m buffer around each plot was used to clip the classified image to create localised classification information for faster community analysis processing. To test for the effect of spatial resolution on community analysis, this new layer was resampled at 0.3 m, 0.5 m and 1 m resolution, and the four different spatial resolution layers were converted from raster to vector polygons. These polygons were then joined to the existing quadrat layer, and the respective attribute tables were exported to .csv format for comparative analysis. Figure 7 shows a step-by-step example of the digitisation process.
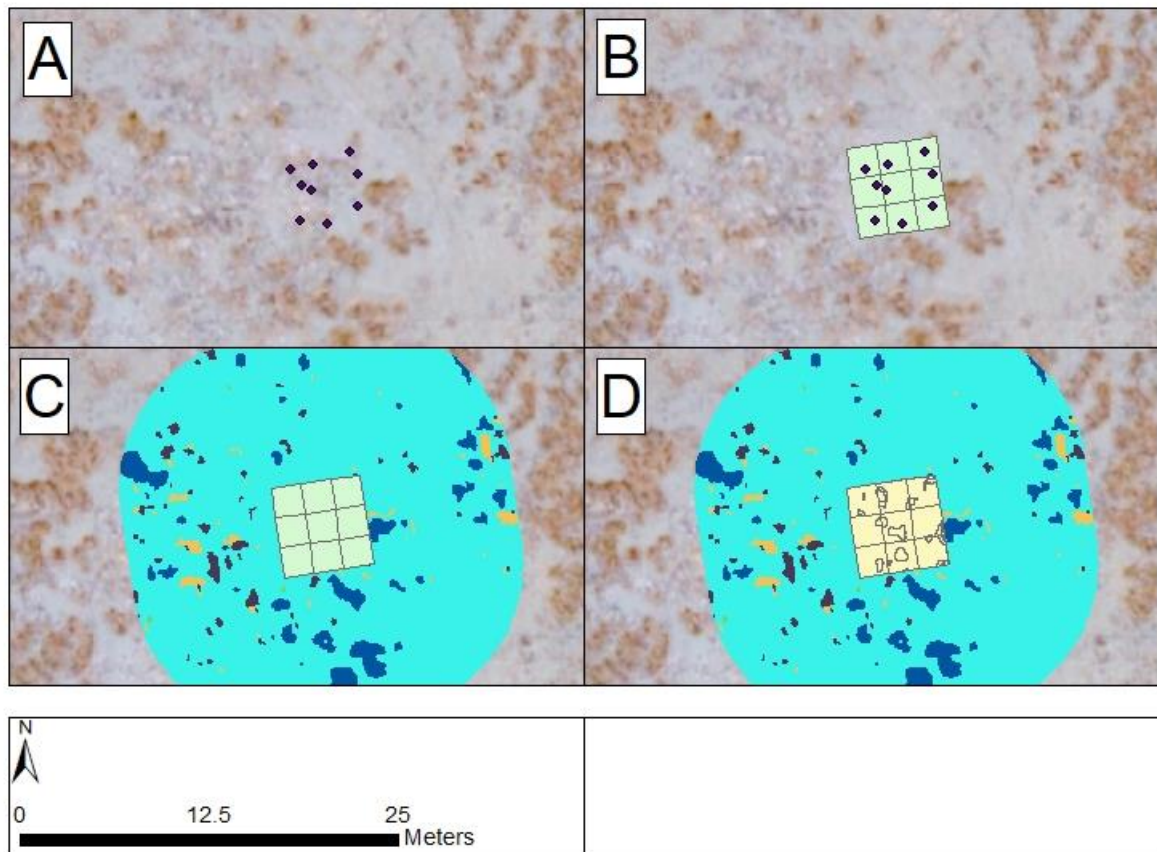
Figure 7. Feature extraction for comparison analysis. A = GPS location of the field quadrats, showing significant spatial error. B = plots were digitally created and manually manipulated to best fit. C= A buffer surrounding the plot was used to clip the classified layer. D = the buffer layer was converted to vector format, and then joined to the plot layer.

2.4 Statistical analysis

All of the following analyses were carried out using R version 3.5.1(R Core Team, 2018).

The plant community data from both the field and GIS data were reshaped into a community abundance matrix by converting percent cover to relative abundance. At this point, all abundance data were at the spatial resolution of the quadrats (2 m x 2 m). As per the field sampling, each plot was made of nine quadrats. For every plot, the relative abundance of the cover class was calculated as the average values from each of its nine quadrats. The community abundance data were then processed at both the quadrat (2 m x 2 m) and plot (6 x 6 m) levels with 576 and 64 units, respectively (Table 4).

Table 4. Community data were analysed at the quadrat and plot levels, with 4 GIS community datasets (1 for each resolution of the data) being compared against 1 field community dataset at both quadrat and plot levels. Observations = the number of sites in each

Dataset	Description	Observations	Number of ground cover classes
Veg	Raw field data at the quadrat (2 m x 2 m)	576	29
Veg2	Raw field data at the Plot (6 m x 6 m)	64	26
Gdat	GIS-derived community data sampled at 0.3 m at the quadrat (2 m x 2 m) level	576	12
gdatII	GIS-derived community data sampled at 0.3 m at the plot (6 m x 6 m) level	64	12
Gdat2	GIS-derived community data sampled at 0.5 m at the quadrat (2 m x 2 m) level	576	11
Gdat2II	GIS-derived community data sampled at 0.5 m at the plot (6 m x 6 m) level	64	11
Gdat3	GIS-derived community data sampled at 1 m at the quadrat (2 m x 2 m) level	576	12
Gdat3II	GIS-derived community data sampled at 1 m at the plot (6 m x 6 m) level	64	12
Gdat4	GIS-derived community data sampled at 0.1 m at the quadrat (2 m x 2 m) level	576	12
Gdat4II	GIS-derived community data sampled at 0.1 m at the plot (6 m x 6 m) level	64	12

2.4.1 Clustering and Ordinations

Modified TWINSPAN

To compare the compositions of the plant communities of Kaitorete Spit, for both the field data, and the GIS data at each of the four spatial resolutions, Modified Two-way Indicator Species Analysis (TWINSPAN(M. Hill, 1979)) was carried out using the twinspanR R package (Zeleny, Smilauer, Hennekens, & Hill, 2016). TWINSPAN is a hierarchical divisive classification technique that is widely used in community ecology (Rolecek, Tichy, Zeleny, & Chytry, 2009). The algorithm places all sites along the first axis of correspondence analysis, then iteratively divides the sites into two using a discriminant function based on a particular species association towards one half or the other(M. O. Hill, Bunce, & Shaw, 1975). Modified TWINSPAN builds upon the original algorithm by adding an additional analysis of cluster heterogeneity prior to each division (Rolecek et al., 2009). TWINSPAN uses the concept of *pseudospecies* to quantifiably model the qualitative concept of *differential species* (i.e. species with distinct niche preferences). For each species, its range of relative abundances (as %) is split into a pre-defined set of dummy variables which are decided by users (Legendre & Legendre, 2012b).

TWINSPAN pseudospecies cut levels were adjusted to 0, 1, 25, 50 and 75 (based on % cover) and the minimum group size was set to 50 and 5 for the quadrat and plot levels, respectively. Maximum cluster number was set at three based on the results of cluster validation from the package clValid (Brock, Pihur, Datta, & Datta, 2008). TWINSPAN was not supported by clValid, so a similar divisive clustering algorithm (Diana) was used in its place. The number of clusters used for each TWINSPAN algorithm was determined for each dataset based on the Objective Function Score from the package RankAggreg (Pihur, Datta, & Datta, 2018). Values were calculated based on the results of clValid, which allows for iterative validation of different cluster amounts for a given clustering algorithm based on a series of validation measures from the R package "clValid".

nMDS Ordinations

Using the R package labdsv (Roberts, 2016), a dissimilarity index based on the Bray-Curtis distance for each of the 10 datasets was calculated. In dissimilarity measures, a value of 1 between a set of objects indicates complete dissimilarity, while a value of 0 indicates an exact match of all descriptors (Legendre & Legendre, 2012a) An asymmetric dissimilarity measure was used, as is typical with species abundances, due to there being a high chance of "double-zero" occurrences (Ricotta & Podani, 2017). The absence of a given species from a site was likely due to a number of reasons, e.g., competitive exclusion from invasives, herbivore damage or the nature of a high-disturbance environment, such as an exposed dune system like Kaitorete Spit. In addition with some species or habitat types being confined to small, distinct areas (pers obs), the higher rates of local rarity would likely further increase the number of double zeros in the species matrix. Therefore, the absence of a species from a pair of sites cannot be used as a measure of similarity with any confidence due to the complexity of the n-dimensional niche of a given species (Borcard, Gillet, & Legendre, 2018).

Nonmetric multidimensional scaling (nMDS) was used to visualise the clusters using the R package "vegan" (Jari Oksanen et al., 2018). For the nMDS, the Bray-Curtis dissimilarity index was used with three dimensions and 200 random starts. The nMDS was used as it has several advantages: first it is capable of utilising a non-Euclidean distance matrix, such as the Bray-Curtis, second data are not assumed to be of normal distribution, last, there is no assumption of a linear relationship between the variables and any underlying gradients (legendre & legendre, 2012c). Non-symmetric Procrustes rotations were used to test the ordination similarity between the field and GIS data at both the quadrat and plot level.

Comparison of ordination and clustering results was done via superimposing the TWINSPAN groups onto the ordination diagrams. Comparison of the GIS data to the field community data was done using Procrustes Rotation from the R package "vegan"

Indicator Species Analysis

Indicator species analysis was carried out using the R package "labdsv". This package uses the function "indval', which is based on the original equations of (Dufrêne & Legendre, 1997), but with minor changes (Roberts, 2016). The identification of species that indicate or characterise a given habitat or community is a core concept in ecology and biogeography. The strength of an indicator species comes from the degree to which it represents a single group of typology and the relative abundance of that species within the sites of a given group.

This duality represents the specificity and fidelity of a species within its environment (Legendre & Legendre, 2012b). The simplified calculation of the Indicator Value for a given species is as follows. For each species j in each cluster of sites k, the specificity (A_{kj}) as a measure of abundance and the fidelity (B_{kj}) as a measure of presence are calculated as:

Where the specificity is defined as:

$$A_{kj} = Nindividuals_{kj}/Nindividuals_{+k}$$

And fidelity is defined as:

$$B_{kj} = Nsites_{kj}/Nsites_{k+}$$

Therefore:

$$INDVAL_{kj} = A_{kj}B_{kj}$$

Chapter 3

Results

3.1 Image Analysis and Preparation

3.1.1 Georeferencing

Two-hundred and seventy five independent 'control points' were manually selected for use in the first transformation (Table A. 1). The total RMS error was Forward: 0.244306 and Forward-Inverse: 0.0337121, where "Forward" is the error in NZTM units (m) and "Forward-Inverse" is the error in Pixels (=0.33cm).

3.1.2 Vegetation indices

Principle components analyses of the 11 band composite image show that over 99% of the total variation in the spectral data is explained by the four original image bands (Table 5) Of the additional vegetation indices, only three accounted for any variability, which were the SR (0.16%), the NDVI (0.01%) and the GNDVI (0.0007%).

Table 5. Principle component results for the composite image band combining seven vegetation indices and the original four spectral image bands. Values are rounding to the nearest 2 decimal places.

Layer		Eigenvalue	Percent of Eigenvalues	Accumulative of Eigenvalues
1	Red	1482.66	80.78%	80.78%
2	Green	314.89	17.16%	97.94%
3	Blue	25.29	1.38%	99.32%
4	Near Infra-red	9.33	0.51%	99.82%
5	Simple Ratio (SR)	2.96	0.16%	99.98%
6	Normalised Differential Vegetation Index (NDVI)	0.27	0.01%	100%
7	Green Normalised Differential Vegetation Index (GNDVI)	0.01	0.00%	100%
8	Green Red Vegetation Index (GRVI)	0.00	0.00%	100%
9	Normalised Green (NG)	0.00	0.00%	100%
10	Normalised Near Infra-Red (NNIR)	0.00	0.00%	100%
11	Normalised Red (NR)	0.00	0.00%	100%

3.1.3 Composite Band Creation

Table 6. Spectral signatures of each of the four original spectral bands and the 2 Vis for the complete Kaitorete Spit imagery.

Site	Band Name	Minimum	Maximum	Mean	Standard Deviation
Kaitorete Spit	Red	0	255	10.41374	21.12342
	Green	0	255	10.03769	20.34674
	Blue	0	255	9.475183	19.40558
	NIR	0	255	13.03982	37.92536
	SR	0	255	2.778049	2.636996
	NDVI	0	200	16.09553	45.71262

3.1.4 Image Classification Testing

Test Site Isolation

Table 7. Spectral signatures of each of the 4 original spectral bands and the 2 Vis across the three test sites at Kaitorete Spit

Site	Band Name	Minimum	Maximum	Mean	Standard Deviation
Site 1	Red	4	150	47.62735	11.25186
	Green	7	142	44.89552	10.41671
	Blue	3	140	39.74252	12.57852
	NIR	0	255	127.3079	37.52974
	SR	0	41	2.39892	1.379468
	NDVI	0	197	150.0206	19.25598
Site 2	Red	0	198	46.72451	10.50411
	Green	0	203	44.65184	11.0324
	Blue	0	195	41.86554	12.65605
	NIR	57	204	100.0896	16.59335
	SR	63	200	140.881	17.26446
	NDVI	0	165	1.805768	1.114341
Site 3	Red	0	222	52.55609	9.579553
	Green	0	222	51.26546	9.959787
	Blue	0	217	49.2131	11.32494
	NIR	49	205	89.20518	15.15717
	SR	59	200	128.6543	15.98858
	NDVI	0	153	1.339265	0.998395

Classification Results and Accuracy Assesment

Classification accuracy was measured by both point and area-based methods for each of the three test sites Figure 8. Classification test results at Site 1. A= True colour image, B = 4bMLC, C = 4bISO and D = 4bSVM.

Table 8, four image band combinations Table 9 and three classification algorithms Table 10. See Table A. 9 for the complete accuracy results. Figure 8 shows an example of the difference in

classifications for a four-band image at Test Site 1. The complete results of the classification tests can be found in the Geodatabase supplied in the digital appendices. The five-band image, containing the four original bands (R, G, B and NIR) combined with the NDVI layer was the most accurate classification as measured by Kappa Coefficient and Total Accuracy (Table 9). Support Vector Machine was the highest performing classification algorithm based on the Kappa Coefficient (62.3%), whereas the Maximum Likelihood Classification achieved the highest average Total Accuracy (71.1%) (Table 10).
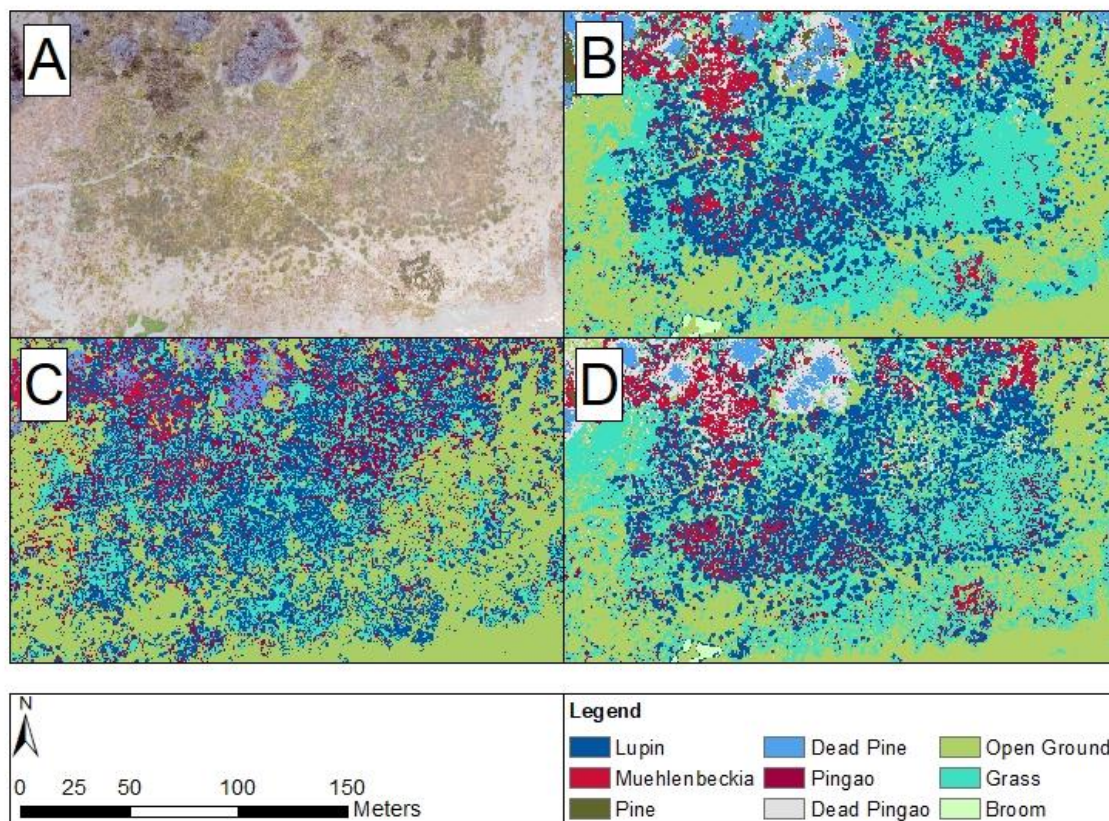
Figure 8. Classification test results at Site 1. A= True colour image, B = 4bMLC, C = 4bISO and D = 4bSVM.

Table 8. Combined accuracy of each test site across all classification methods

	Average accuracy per test site			Average accuracy across test sites
Accuracy Measure	Site 1	Site 2	Site 3	
Kappa	46.7%	44.3%	56.7%	49%
Overall	52.9%	52.1%	62.8%	56%

Table 9. Combined accuracy measures for each of the image band combinations

Image Band Combination	Average Kappa Coefficient	Average Total Accuracy
RGBNIR+SR	49.26%	56.31%
RGBNIR+ NDVI	51.12%	58.04%
RGBNIR+SR+NDVI	47.34%	54.11%

RGBNIR	49.27%	55.30%

Table 10 Combined average Kappa Coefficient and Total Accuracy scores for each classification method applied to the three test sites and four image band combinations.

Classification	Average Kappa Coefficient	Average Total Accuracy
Support Vector Machine	62.3%	68.4%
Maximum Likelihood Classification	61.1%	71.1%
Unsupervised Iso Cluster	24.4%	28.4%

3.2 Final Classification

3.2.1 Classification Inputs

The five-band composite image which performed the best in testing, RGBNIR+SR, was selected for final processing, to which the Support Vector Machine classification was applied. The SVM was chosen due to its higher Kappa Coefficient, which is a better measure of accuracy. A new training sample was created, independent of those used for the classification testing. The spectral signatures of each of the twelve cover classes for the final classification can be found in Table 11.

Table 11. Mean reflectance values for final classification training sample

	Band				
Ground Cover Class	Red	Green	Blue	NIR	NDVI
L.arboreus	47.6	48.01538	24.21538	180.7846	175.8154
M.complexa	24.40909	26.66667	17.07576	143.8939	178.5606
P. radiata	5.72308	11.36923	6.96923	148.1539	190.6923
Dead *P. radiata*	39.5082	43.21311	48.47541	95.40984	130.541
F. spiralis	30.18333	21.55	12.7	158.9833	187.1
Dead *F. spiralis*	37.35484	35.5	41.06452	88.45161	136.5323
Bare Open Ground	62.33846	63.8	64.63077	81.41538	110.2308
Grasses	47.72549	44.78431	39.90196	91.47059	109.1765
C. appressa	45.80328	44.52459	23.16393	162.0328	174.9016
R. australis	111.082	113.082	106.1312	120.3443	105
P. esculentum	25.26984	28.96825	18.11111	182.9524	181.2222
Coarse Woody Debris	125.4194	121.8387	120.8871	69.43548	72.79032

3.2.2 Final Classification Accuracy Results

Twelve different image ground cover classes were identified via SVM classification. Figure 9 shows an example of the results of the final classification for the full site. The fully classified layer is available in the Geodatabase supplied in the digital appendices. Table 12 shows the final number of pixels and area in m^2 for the different classes. Point-based accuracy measures found the highest Kappa (69.73%) and overall/total (72.48%) accuracies, whereas area based accuracy was significantly lower (35.61% and 49.30% for the Kappa Coefficient and Overall/Total Accuracy, respectively). For

the full error matrixes of the accuracy assessments, see Table A. 7 and Table A. 8 for the point and area measures, respectively.

Table 12. Total pixels and amount of area of each of the classified image classes for the five band composite image of Kaitorete Spit.

Ground Cover Class	Pixel Count	Area in M^2
L. arboreus	587146	58.71
M. complexa	21794319	2179.43
P. radiata	1097459	109.75
Dead *P. radiata*	17587201	1758.72
F. spiralis	10110536	1011.05
Dead *F. spiralis*	31188204	3118.82
Bare Open Ground	110898664	11089.87
Grasses	411546748	41154.67
C. appressa	3272928	327.29
R. australis	2746893	274.69
P. esculentum	4403378	440.34
Coarse Woody Debris	4766524	476.65

Table 13 Class specific classification accuracies from the point based accuracy measures. Commission error = rate at which pixels were wrongly classified as this class (over-classified). Omission = number of pixels in class that were wrongly classified as another class (under-classified). Producers = how accurate the map maker was in determining this class. Users = how accurate the map itself is for a given class.

Class	Comission	Omission	Users Accuracy	Producers Accuracy
L. arboreus	100.51%	30.33%	34.67%	53.33%
M. complexa	11.11%	55.67%	82.33%	59.66%
P. radiata	43.78%	4.00%	68.33%	94.47%
Dead *P. radiata*	13.57%	28.33%	84.67%	74.93%
F. spiralis	1.57%	7.67%	98.33%	92.77%
Dead *F. spiralis*	41.31%	22.00%	64.33%	74.52%
Bare Open Ground	26.00%	48.33%	74.00%	74.00%
Grasses	7.82%	51.67%	89.00%	63.27%
C. appressa	24.38%	32.67%	74.00%	69.38%
R. australis	55.84%	2.33%	63.33%	96.45%
P. esculentum	33.54%	42.00%	64.33%	60.50%
Average	32.68%	29.55%	72.48%	73.93%
Max	100.51%	55.67%	98.33%	96.45%
Min	1.57%	2.33%	34.67%	53.33%

Figure 9 Final SVM classification results of the NDVI multiband image.

Table 14 Class specific classification accuracies from the area based accuracy measures. Commission error = rate at which pixels were wrongly classified as this class (over-classified). Omission = number of pixels in class that were wrongly classified as another class (under-classified). Producers = how accurate the map maker was in determining this class. Users = how accurate the map itself is for a given class.

Class	Comission	Omission	Producers Accuracy	Users Accuracy
L. arboreus	92.21%	1.47%	98.53%	7.79%
M. complexa	36.16%	55.26%	44.74%	63.84%
P. radiata	68.30%	31.54%	68.46%	31.70%
Dead *P. radiata*	85.25%	85.21%	14.79%	14.75%
F. spiralis	84.11%	58.02%	41.98%	15.89%
Dead *F. spiralis*	76.34%	83.99%	16.01%	23.66%
Bare Open Ground	37.55%	11.44%	76.34%	62.45%
Grasses	26.38%	57.02%	42.98%	73.62%
C. appressa	80.38%	79.73%	20.27%	19.62%
R. australis	74.76%	48.89%	51.11%	25.24%
P. esculentum	95.78%	98.29%	1.71%	4.22%
Average	68.84%	55.53%	43.36%	31.16%
Maximum	95.78%	98.29%	98.53%	73.62%
Minimum	26.38%	1.47%	1.71%	4.22%

3.3 Community Analyses

3.3.1 Species presence

Field Data

Twenty-five distinct ground cover classes were found across 64 plots at Kaitorete Spit. These were divided into living and non-living classes, with 14 living cover classes, of which 10 were identified to the species level, and 11 non-living classes, of which eight were identified to the species level, two were non-identifiable standing dead matter or coarse woody debris (driftwood) and one was bare open ground.

Table 15. List of ground cover classes as found during field observations.

Ground cover type	Ground Cover Class
Identifiable Species	*C. appressa* *F. spiralis* *L. arboreus* *Lycium ferocissimum* (Miers) *Melicytus alpinus* (Forster & Forster) *M. complexa* *Pimelea prostrata* *P. cita* *P. esculentum* *R. australis*
Mixed species cover	Bryophytes Forbs

	Grasses
	Lichens
Non-living identifiable species	dead *C. appressa*
	dead *F. spiralis*
	dead *L. arboreus*
	dead *L. ferocissimum*
	dead *M. complexa*
	dead *P. cita*
	dead *P. esculentum*
	dead *R. australis*
Other ground cover type	Bare Open Ground (OG)
	Dead Standing Biomass
	Coarse Woody Debris

GIS Data

12 distinct ground cover classes were identified as part of the GIS classification training across 64 plots at Kaitorete Spit (Table 16). These can be divided into living and non-living classes, with eight living cover classes of which seven were identified to the species level, and four non-living classes, of which two were identified to the species level, one was bare open ground and one was coarse woody debris (CWD). All cover species were present at all sample locations, except for *F. spiralis* which, due to resampling conditions, was not detected at 0.5 m resolution.

Table 16. List of Final cover classes

Ground cover type	Ground Cover Class
Identifiable Species	*C. appressa*
	F. spiralis
	L. arboreus
	M. complexa
	P. esculentum
	R. australis
	P. radiata
Mixed species cover	Grasses and Forbs
Non-living identifiable species	dead *F. spiralis*
	dead *P. radiata*
Other ground cover type	Bare Open Ground (OG)
	CWD

3.3.2 Field Based Plant Community Analysis

Ordination

mNDS Ordination was carried out on the field data at the quadrat and plot levels using a Bray\Curtis dissimilarity index (Figure 10). The number of axes were set at three, at which point the ordination stress vs. dimensionality approaches 0.1 (Table 17). Clarke (1993) proposes that for acceptable stress values: <0.05 = excellent fit, <0.10 = good fit, <0.20 = ok fit, >0.20 = poor fit. Final ordination stress was 0.1106805 (Quadrat) and 0.09520376 (Plot), indicating an acceptable ordination fit for both.
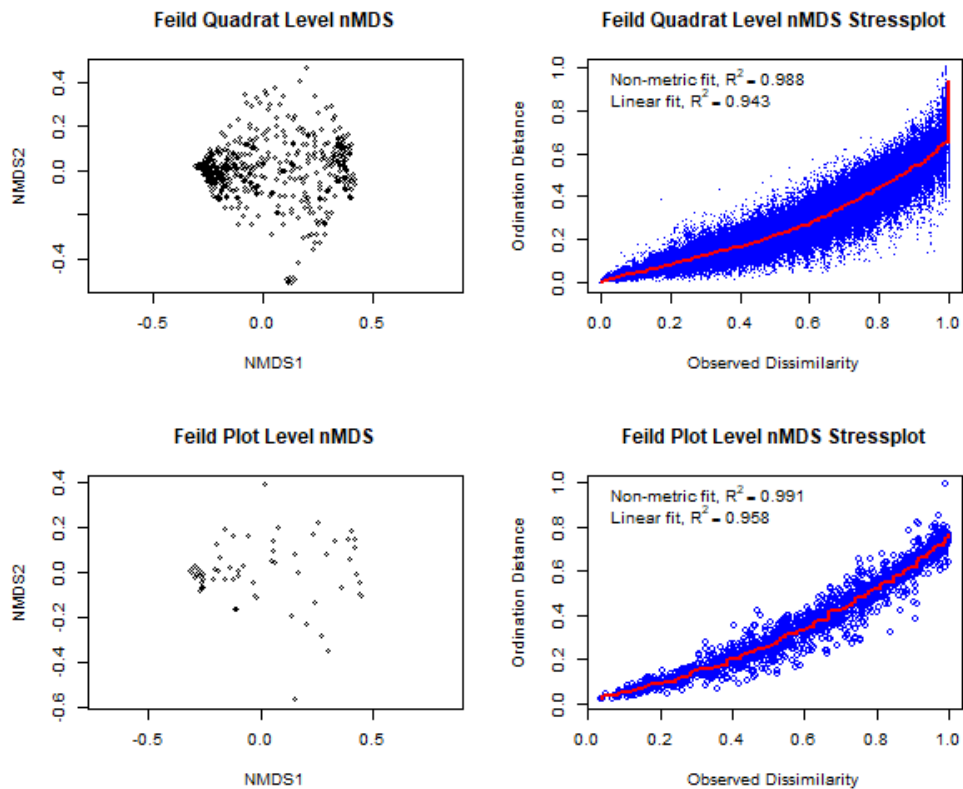
Figure 10. nMDS Ordination and Shepard's diagram of the Field data at the Quadrat and Plot levels. The nonmetric fit is based on stress (S) and defined as R2 = 1-S*S, whereas linear fit is the squared correlation between ordination distances and dissimilarities.

Table 17. nMDS ordination dimensionality and stress from the Field data at the quadrat and plot levels.

Number of Axes	Stress	
	Veg quad	Veg plot
1	0.288	0.266
2	0.161	0.140
3	0.111	0.095
4	0.086	0.070
5	0.072	0.056
6	0.060	0.048

TWINSPAN Divisive Clustering

Modified TWINSPAN was used to divide the field data into 3 distinct clusters for the field data for both the quadrat and plot levels. The number of clusters (divisions) was set by the R package RankAggreg with Objective Function Scores of 4.67 and 5.49 for the quadrat and plot data levels, respectively (Table 18). Figure 11 shows the clustering results overlaid upon the nMDS ordination of the quadrat and plot level data.

Table 18. Optimal number of TWINSPAN clusters (divisions) and Objective Function Score for field data at the quadrat and plot levels at determined via…

Dataset	Number of clusters	Objective Function Score
Veg Quad	3	4.667622
Veg Plot	3	5.484706
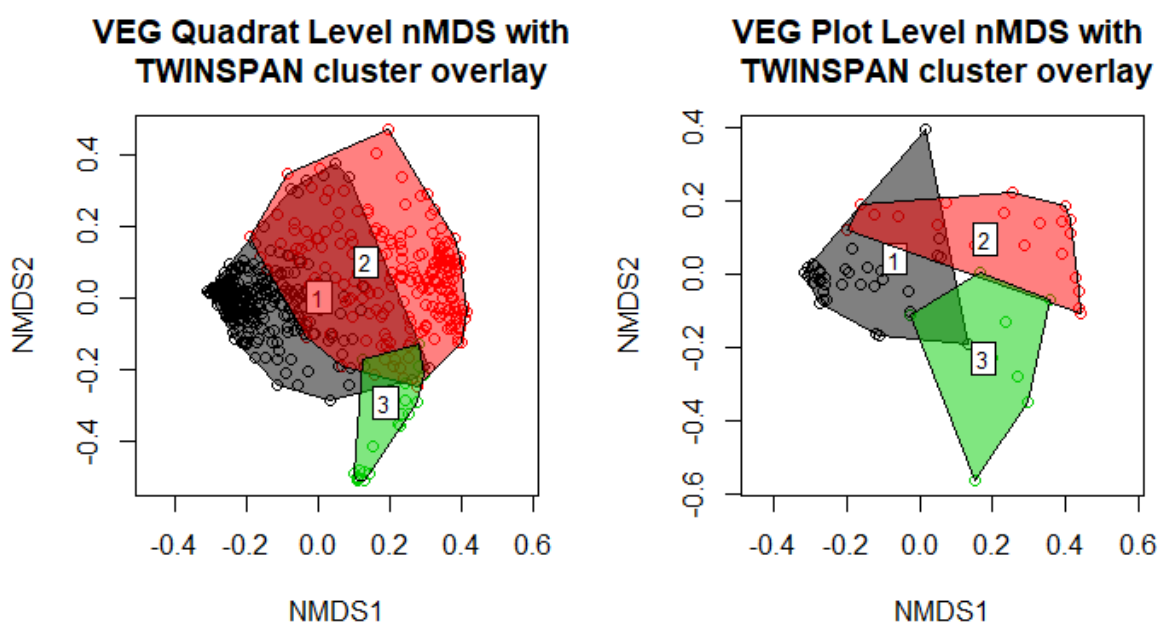
Figure 11. Comparison of ordination results from nMDS of the field data at the quadrat and plot levels with clustering results from Modified TWINSPAN overlaid as bounding polygons.

Indicator Species Analysis

Indicator species analyses of the TWINSPAN results found that different species were indicative of each community type at both the quadrat (Table 19) and plot (Table 20) levels. For both datasets, the number of clusters with significant indicators (3) matched the total number of classes from the modified TWINSPAN analysis (3). Sixteen significant indicators were identified at the quadrat level, with 5, 8 and 3 significant indicators for each of the three classes, respectively. For the plot level data, ten significant indicators were identified, with 3, 4 and 3 for each of the three classes, respectively.

Table 19. Indicator species analysis of the Modified TWINSPAN clustering results for the quadrat level field data. Sum of probabilities = 5.607. Sum of Indicator Values = 8.65. Sum of Significant Indicator Values = 8.37.

Cluster	Ground Cover Class	Indicator value	Probability
1	Bare Open Ground	0.8783	0.001
	Dead *F. spiralis*	0.6674	0.001

	F. spiralis	0.5367	0.001
	Coarse Woody Debris	0.3358	0.009
	A. arenaria	0.0521	0.04
2	Forbs	0.7097	0.001
	Grasses	0.5881	0.001
	Bryophytes	0.5874	0.001
	Lichens	0.3887	0.009
	P. cita	0.315	0.001
	C. appressa	0.2966	0.001
	M. complexa	0.2353	0.002
	R. australis	0.1899	0.016
3	Dead *P. esculentum*	0.9349	0.001
	P. esculentum	0.9183	0.001
	Dead Standing Biomass	0.7402	0.001

Table 20. Indicator species analysis of the Modified TWINSPAN clustering results for the quadrat level field data. Sum of probabilities = 6.419. Sum of Indicator Values = 10.23. Sum of Significant Indicator Values = 7.1.

Cluster	Ground Cover Class	Indicator value	Probability
1	Dead *F. spiralis*	0.7707	0.001
	F. spiralis	0.7296	0.001
	Bare Open Ground	0.726	0.001
2	*P. cita*	0.6963	0.001
	C. appressa	0.6939	0.001
	Grasses	0.5236	0.038
	R. australis	0.4222	0.022
3	Dead *P. esculentum*	0.9923	0.001
	P. esculentum	0.8627	0.001
	Dead Standing Biomass	0.6855	0.001

3.3.3 GIS 0.1 m Resolution Based Plant Community Analysis

Ordination

nMDS Ordination to test for relationships between sites and species was carried out on the GIS 0.1 m data at the quadrat and plot levels using a Bray\Curtis dissimilarity index (Figure 12). The number of axes were set at three, at which point the ordination stress vs. dimensionality approaches 0.05 and the reduction of stress from additional dimensionality is low (Table 21). Final ordination stress was 0.06814165 (Quadrat) and 0.05825607 (Plot), indicating a good and excellent fit for the quadrat and plot level GIS 0.1 m data, respectively (Clarke, 1993).

Figure 12. nMDS Ordination and Shepard's diagram of the GIS 0.1 m data at the Quadrat and Plot levels. The nonmetric fit is based on stress (S) and defined as R2 = 1-S*S, whereas linear fit is the squared correlation between ordination distances and dissimilarities.

Table 21 Optimal number of TWINSPAN clusters (divisions) and Objective Function Score for GIS 0.1 m data at the quadrat and plot levels.

Number of Axes	Stress	
	0.1 m Quad	0.1 m Plot
1	0.233	0.211
2	0.116	0.100
3	0.068	0.058
4	0.048	0.040
5	0.036	0.030
6	0.028	0.023

Canonical Analysis

Non-symmetric Procrustes rotations were used to test the ordination similarity between the field and GIS 0.1 m data at both the quadrat and plot level. Figure 13 shows the GIS 0.1 m data superimposed and rotated to fit the field data, with the residuals of each transformation plotted. At the quadrat level, the sum of squares was 42.99202 with an RSME of 0.2732012. Permutation testing gave a Procrustes sum of squares (m_{12}^2) value of 0. 8562 with a significance of 0.001. At the plot

level, the sum of squares was 5.217996 with an RSME of 0.2855367. Permutation testing gave a Procrustes sum of squares (m_{12}^2) value of 0.8307 with a significance of 0.001.
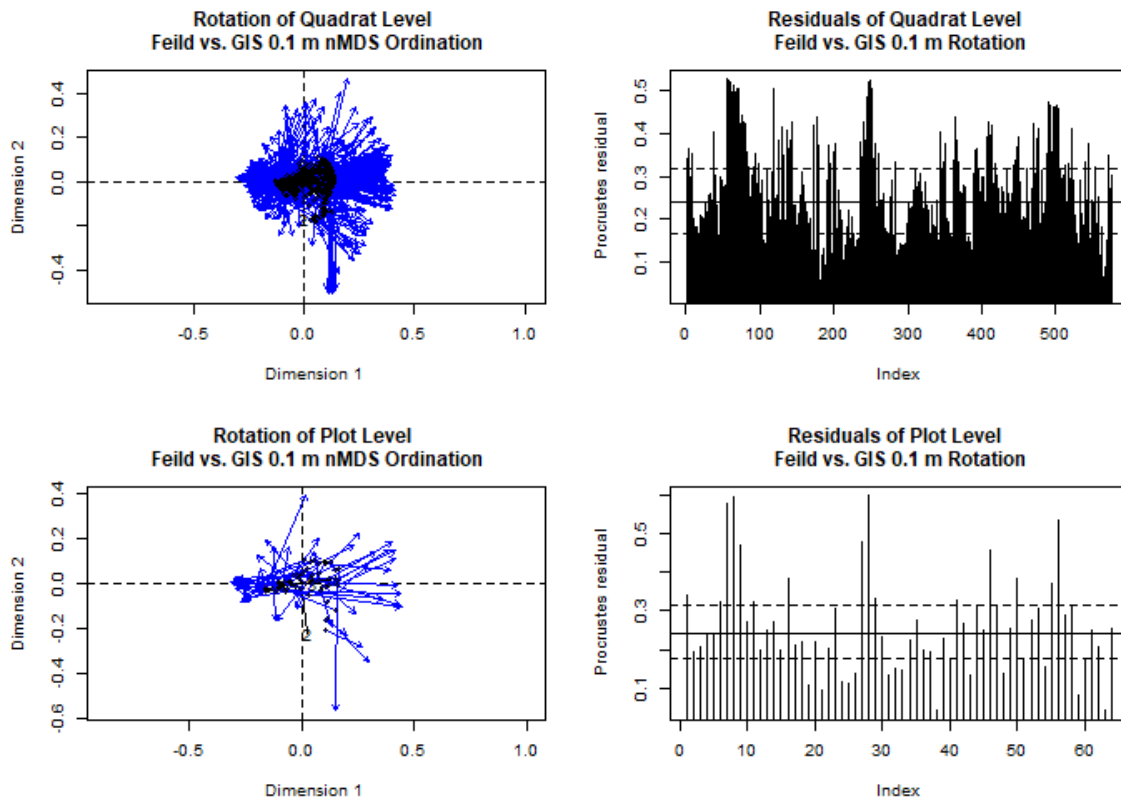
Figure 13. Procrustes rotation and residuals of Field and GIS 0.1 m data nMDS ordinations at Quadrat and Plot level.

TWINSPAN Divisive Clustering

Modified TWINSPAN was used to divide the data into 4 distinct clusters for the GIS 0.1 m data for both the quadrat and plot levels. The number of clusters (divisions) was set by the R package RankAggregwith Objective Function Scores of 7.74 and 6.16 for the quadrat and plot data levels, respectively (Table 22). Figure 14 shows the clustering results overlaid upon the nMDS ordination of the quadrat and plot level data.

Table 22 Optimal number of TWINSPAN clusters (divisions) and Objective Function Score for field data at the quadrat and plot levels.

Dataset	Number of clusters	Objective function Score
0.1 m Quad	4	7.744942
0.1 m Plot	4	6.163798

Figure 14. Comparison of ordination results from nMDS of the 0.1 m GIS data at the quadrat and plot levels with clustering results from Modified TWINSPAN overlaid as bounding polygons

Indicator Species Analysis

Indicator species analyses of the TWINSPAN results found that different species were indicative of each community type at both the quadrat (Table 23) and plot (Table 24) levels. For both datasets, the number of clusters with significant indicators (4) matched the total number of classes from the modified TWINSPAN analysis (4). Ten significant indicators were identified at the quadrat level, with 2, 2, 3 and 3 significant indicators for each of the four classes. For the plot level data, six significant indicators were identified, with 1, 1, 2 and 2 for each of the four classes.

Table 23. Indicator species analysis of the Modified TWINSPAN clustering results for the quadrat level GIS 0.1 m data. Sum of probabilities = 0.687. Sum of Indicator Values = 5.14. Sum of Significant Indicator Values = 4.99.

Cluster	Ground Cover Class	Indicator value	Probability
1	Bare Open Ground	0.6748	0.001
	Dead *F. spiralis*	0.1403	0.041
2	*P. radiata*	0.5903	0.001
	Grasses and Forbs	0.4369	0.001
3	*C. appressa*	0.8181	0.001
	A. arenaria	0.7055	0.001
	P. esculentum	0.6489	0.001
4	*M. complexa*	0.5652	0.001
	Standing Dead Biomass	0.3524	0.006
	F. spiralis	0.0583	0.025

Table 24. Indicator species analysis of the Modified TWINSPAN clustering results for the plot level GIS 0.1 m data. Sum of probabilities = 3.673. Sum of Indicator Values = 6.26. Sum of Significant Indicator Values = 4.88.

Cluster	Ground Cover Class	Indicator value	Probability
1	Bare Open Ground	0.861	0.001
2	*M. complexa*	0.6909	0.029
	C. appressa	0.8055	0.025
3	*P. radiata*	0.7725	0.006
	Dead *F. spiralis*	0.9543	0.001
4	Standing Dead Biomass	0.7983	0.021

3.3.4 GIS 0.3 m Resolution Based Plant Community Analysis

Ordination

nMDS Ordination to test for relationships between sites and species was carried out on the GIS 0.3 m data at the quadrat and plot levels using a Bray\Curtis dissimilarity index (Figure 15). The number of axes were set at three, at which point the ordination stress vs. dimensionality approaches 0.05 and the reduction of stress from additional dimensionality is low (Table 24). Final ordination stress was 0.06737749 (Quadrat) and 0.05631183 (Plot), indicating a near excellent fit for both the quadrat and plot level GIS 0.3 m data (Clarke, 1993).

Figure 15. nMDS Ordination and Shepard's diagram of the GIS 0.3 m data at the Quadrat and Plot
levels. The nonmetric fit is based on stress (S) and defined as R2 = 1-S*S, whereas linear
fit is the squared correlation between ordination distances and dissimilarities.

**Table 25. The optimal number of TWINSPAN clusters (divisions) and Objective Function Score for GIS
0.3 m data at the quadrat and plot levels.**

Number of Axes	Stress	
	0.3 m Quad	0.3 m Plot
1	0.295	0.282
2	0.126	0.106
3	0.067	0.056
4	0.049	0.038
5	0.037	0.030
6	0.028	0.021

Canonical Analysis

Non-symmetric Procrustes rotations were used to test the ordination similarity between the field
and GIS 0.3 m data at both the quadrat and plot level. Figure 16 shows the GIS 0.3 m data
superimposed and rotated to fit the field data, with the residuals of each transformation plotted. At
the quadrat level, the sum of squares was 45.60269 with an RSME of 0.281374. Permutation testing
gave a Procrustes sum of squares (m_{12}^2) value of 0.9082 with a significance of 0.001. At the plot level,
the sum of squares was 5.617939 with an RSME of 0. 2962774. Permutation testing gave a Procrustes
sum of squares (m_{12}^2) value of 0.8944 with a significance of 0.002.

Figure 16. Procrustes rotation and residuals of Field and GI7S 0.3 m data nMDS ordinations at Quadrat and Plot level.

TWINSPAN Divisive Clustering

Modified TWINSPAN was used to divide the data into 9 and 5 distinct clusters for the GIS 0.3 m data for quadrat and plot levels, respectively. The number of clusters (divisions) was set by the R package RankAggreg with Objective Function Scores of 7.43 and 9.76 for the quadrat and plot data levels, respectively (Table 26). Figure 17 shows the clustering results overlaid upon the nMDS ordination of the quadrat and plot level data.

Table 26. Optimal number of TWINSPAN clusters (divisions) and Objective Function Score for GIS 0.3 m data at the quadrat and plot levels.

Dataset	Number of clusters	Objective function Score
0.3 m Quad	9	7.431347
0.3 m Plot	5	9.769342
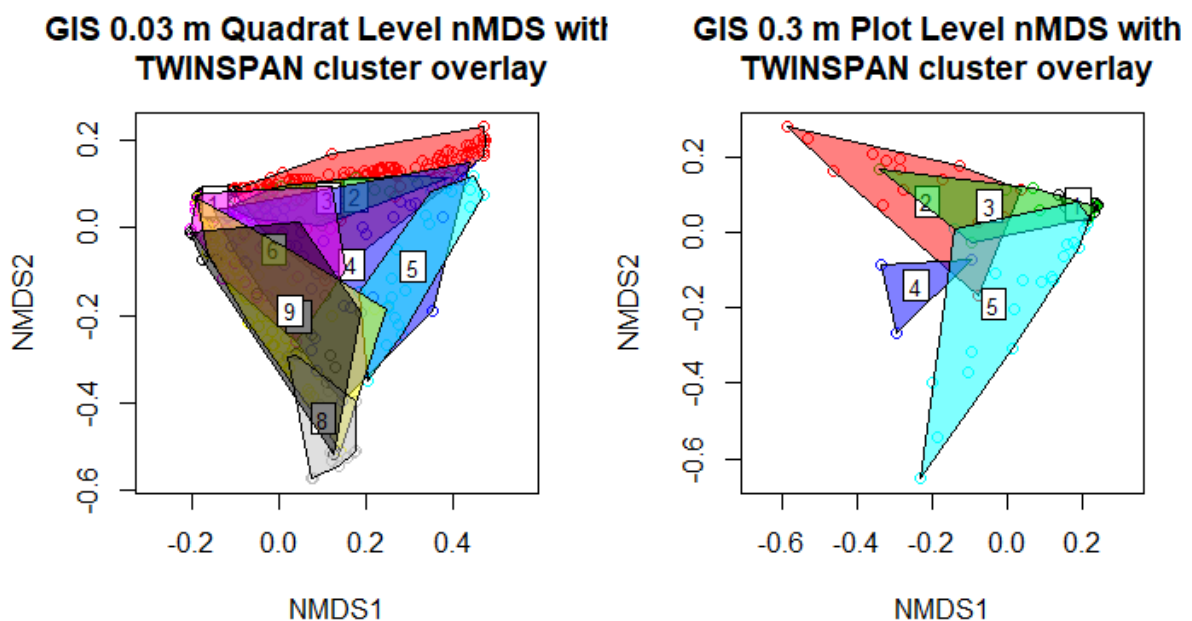
Figure 17. Comparison of ordination results from nMDS of the 0.03 m GIS data at the quadrat and plot levels with clustering results from Modified TWINSPAN overlaid as bounding polygons

Indicator Species Analysis

Indicator species analyses of the TWINSPAN results found that different species were indicative of each community type at both the quadrat (Table 27Table 23) and plot (Table 28) levels. The number of clusters with significant indicators at both the quadrat (6) and plot (4) did not match the total

number of classes from the modified TWINSPAN analysis, which was 9 and 5 for the quadrat and plot levels, respectively. Ten significant indicators were identified at the quadrat level, with 1, 2, 1, 2, 1 and 3 significant indicators for each of the six classes. For the plot level data, 10 significant indicators were identified, with 1, 3, 2 and 4 for each of the four classes.

Table 27 Indicator species analysis of the Modified TWINSPAN clustering results for the quadrat level GIS 0.3 m data. Sum of probabilities = 0.671. Sum of Indicator Values = 4.79. Sum of Significant Indicator Values = 4.71.

Cluster	Ground Cover Class	Indicator value	Probability
1	Grasses and Forbs	0.2487	0.001
2	Bare Open Ground	0.3924	0.001
	Coarse Woody Debris	0.1206	0.01
3	*P. radiata*	0.4336	0.001
5	Dead *F. spiralis*	0.6733	0.001
	Standing Dead Biomass	0.5717	0.001
8	*M. complexa*	0.5731	0.001
	C. appressa	0.6171	0.001
	P. esculentum	0.5711	0.001
	A. arenaria	0.5089	0.001

Table 28 Indicator species analysis of the Modified TWINSPAN clustering results for the quadrat level GIS 0.3m data. Sum of probabilities = 0.846. Sum of Indicator Values = 6.03. Sum of Significant Indicator Values = 5.67.

Cluster	Ground Cover Class	Indicator value	Probability
1	Grasses and Forbs	0.3181	0.001
2	Bare Open Ground	0.6373	0.001
	R. australis	0.5532	0.006
	Coarse Woody Debris	0.5345	0.012
4	Standing Dead Biomass	0.8455	0.001
	Dead *F. spiralis*	0.811	0.002
5	*M. complexa*	0.6516	0.003
	C. appressa	0.6221	0.005
	P. esculentum	0.4179	0.037
	A. arenaria	0.2756	0.022

3.3.5 GIS 0.5 m Resolution Based Plant Community Analysis

Ordination

nMDS Ordination to test for relationships between sites and species was carried out on the GIS 0.5 m data at the quadrat and plot levels using a Bray\Curtis dissimilarity index (Figure 18). The number of axes were set at three, at which point the ordination stress vs. dimensionality approaches 0.05 and the reduction of stress from additional dimensionality is low (Table 29). Final ordination stress

was 0.0673079 (Quadrat) and 0.05693242 (Plot), indicating a near excellent fit for both the quadrat and plot level GIS 0.3 m data (Clarke, 1993).
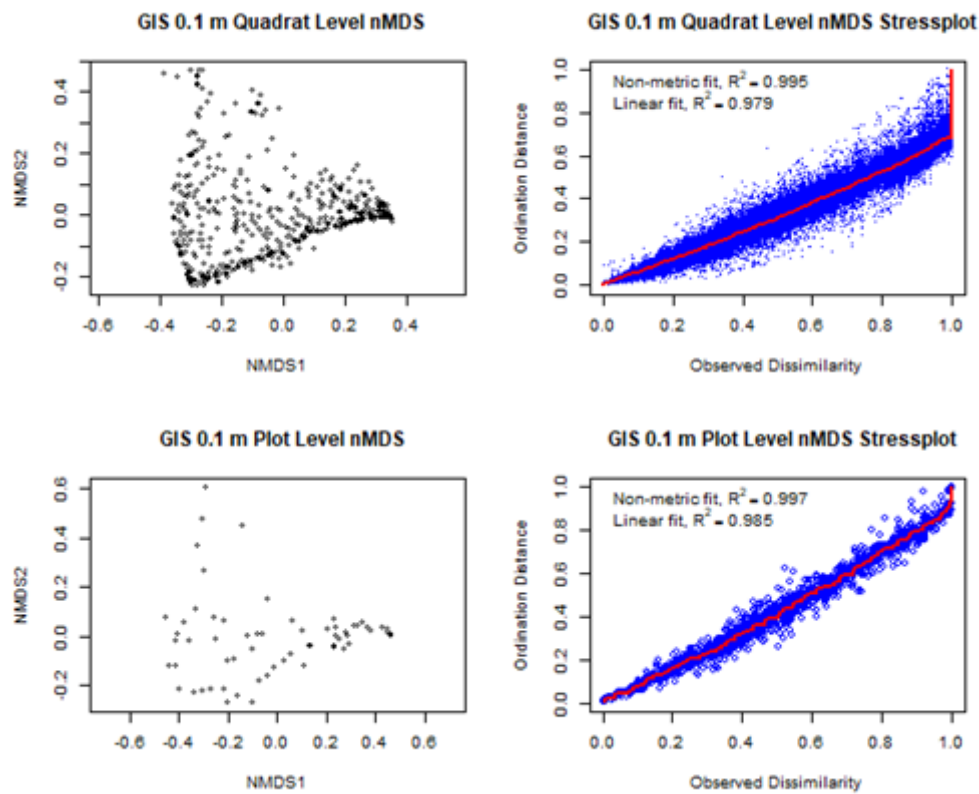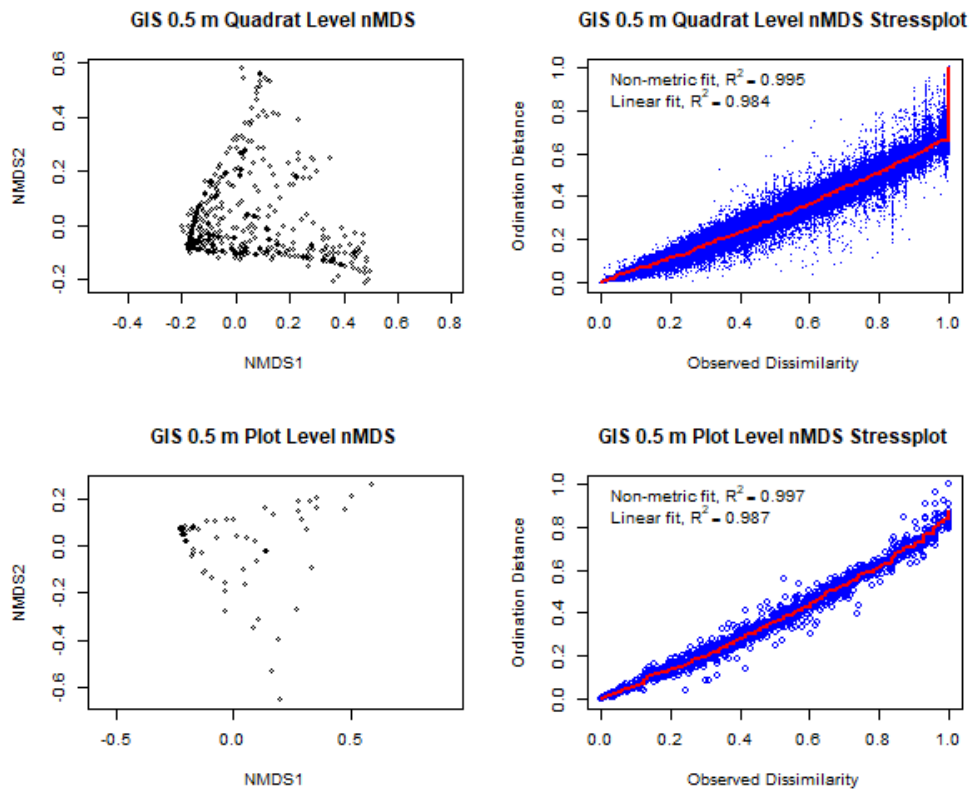

Figure 18 nMDS Ordination and Shepard's diagram of the GIS 0.5 m data at the Quadrat and Plot levels. The nonmetric fit is based on stress (S) and defined as R2 = 1-S*S, whereas linear fit is the squared correlation between ordination distances and dissimilarities.

Table 29 Optimal number of TWINSPAN clusters (divisions) and Objective Function Score for GIS 0.5 m data at the quadrat and plot levels.

Number of Axes		
	0.5 m Quad	0.5 m Plot
1	0.285	0.278
2	0.124	0.107
3	0.067	0.057
4	0.048	0.039
5	0.038	0.030
6	0.029	0.021

Canonical Analysis

Non-symmetric Procrustes rotations were used to test the ordination similarity between the field and GIS 0.5 m data at both the quadrat and plot level. Figure 19 shows the GIS 0.5 m data superimposed and rotated to fit the field data, with the residuals of each transformation plotted. At the quadrat level, the sum of squares was 45.6029 with an RSME of 0.2813747. Permutation testing

gave a Procrustes sum of squares (m_{12}^2) value of 0.9082 with a significance of 0.001. At the plot level, the sum of squares was 5.601834 with an RSME of 0.2958524. Permutation testing gave a Procrustes sum of squares (m_{12}^2) value of 0.8918 with a significance of 0.002.
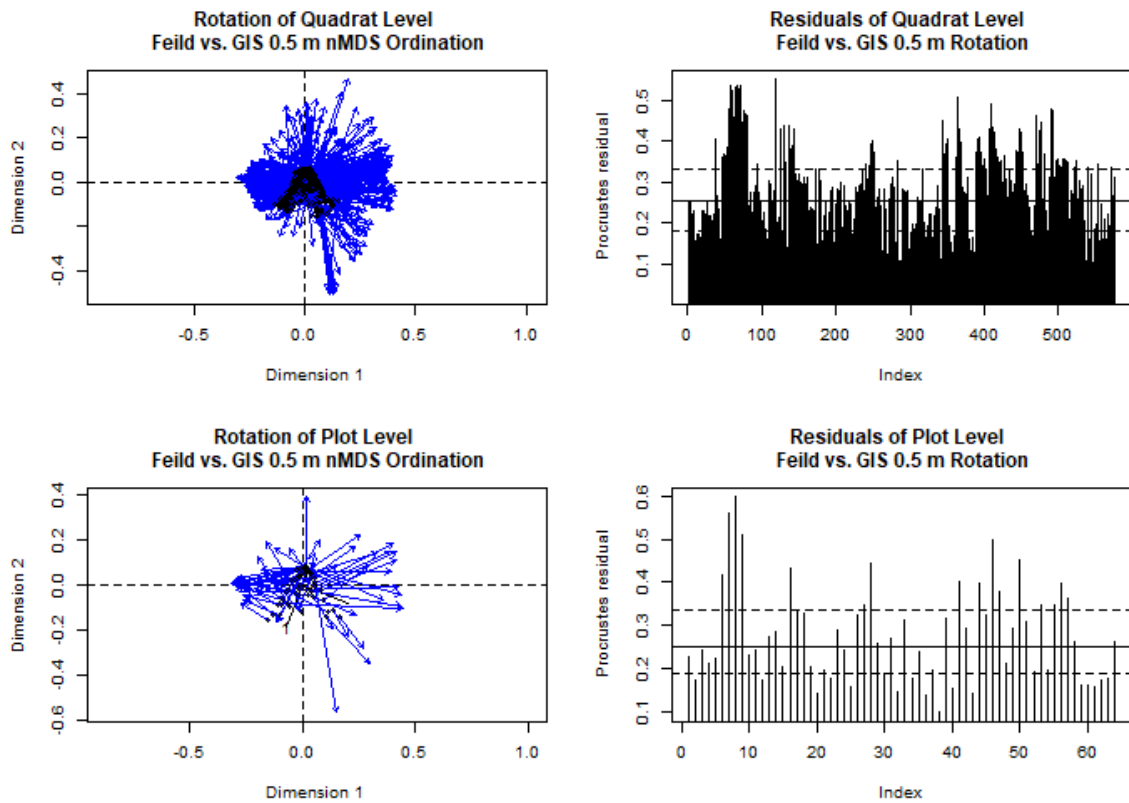
Figure 19 Procrustes rotation and residuals of Field and GIS 0.5 m data nMDS ordinations at Quadrat and Plot level. Quadrat level sum of squares = 45.6029, RSME = 0.2813747. Plot-level sum of squares = 5.601834, RSME = 0.2958524

TWINSPAN Divisive Clustering

Modified TWINSPAN was used to divide the data into 5 and 10 distinct clusters for the GIS 0.3 m data for quadrat and plot levels, respectively. The number of clusters (divisions) was set by the R package RankAggreg with Objective Function Scores of 7.85 and 7.48 for the quadrat and plot data levels, respectively (Table 30). Figure 20 shows the clustering results overlaid upon the nMDS ordination of the quadrat and plot level data.

Table 30 Optimal number of TWINSPAN clusters (divisions) and Objective Function Score for GIS 0.5 m data at the quadrat and plot levels.

Dataset	Number of clusters	Objective function Score
0.5 m Quad	5	7.848975
0.5 m Plot	10	7.483927
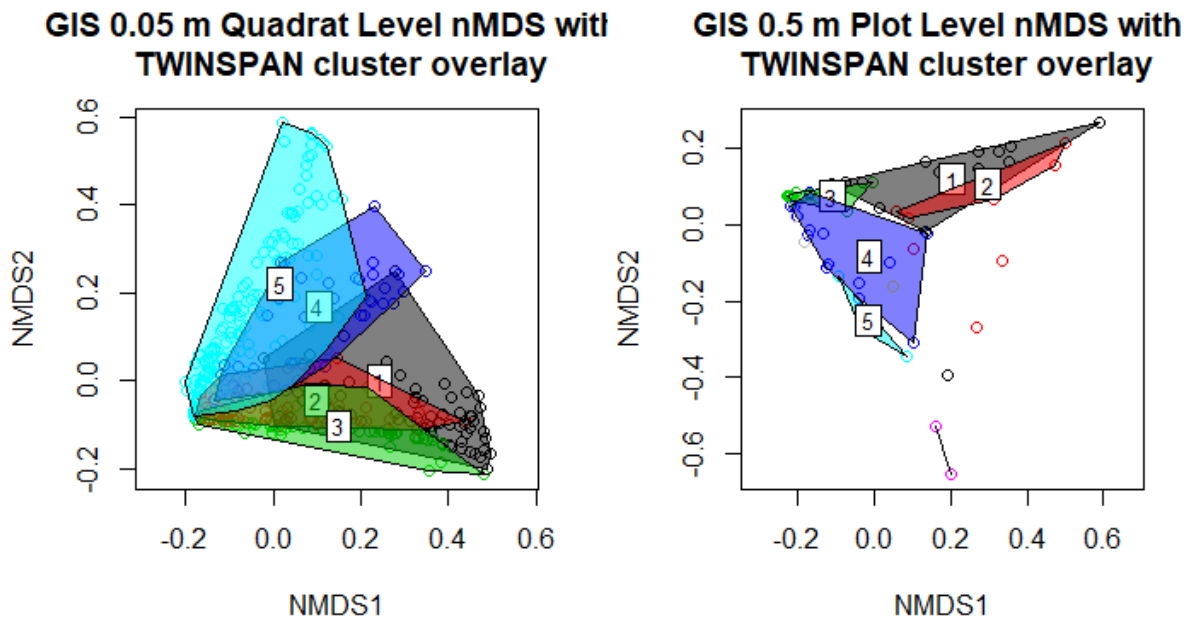
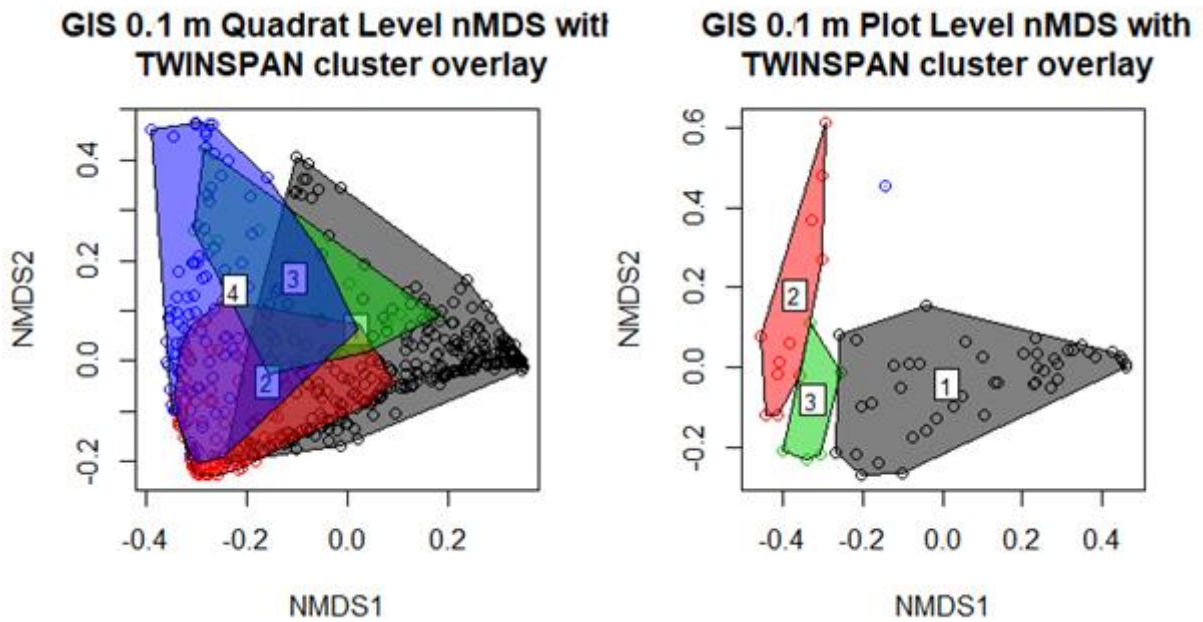**Figure 20. Comparison of ordination results from nMDS of the 0.05 m GIS data at the quadrat and plot levels with clustering results from Modified TWINSPAN overlaid as bounding polygons**

Indicator Species Analysis

Indicator species analyses of the TWINSPAN results found that different species were indicative of each community type at both the quadrat (Table 31) and plot (Table 23) levels. The number of clusters with significant indicators at the quadrat (5) level matched the number of TWINSPAN clusters (5). At the plot level, however, the number of clusters with significant indicators (2) did not match the total number of classes from the modified TWINSPAN analysis (10). Nine significant indicators were identified at the quadrat level, with 1, 1, 2, 3 and 2 significant indicators for each of the five classes. For the plot level data, 2 significant indicators were identified, with 1 each of the two classes.

Table 31 Indicator species analysis of the Modified TWINSPAN clustering results for the quadrat level GIS 0.5 m data. Sum of probabilities = 0.197. Sum of Indicator Values = 3.44. Sum of Significant Indicator Values = 3.31.

Cluster	Ground Cover Class	Indicator value	Probability
1	Bare Open Ground	0.4717	0.001
2	*P. radiata*	0.4016	0.001
3	Coarse Woody Debris	0.355	0.001
	R. australis	0.1324	0.001
	Standing Dead Biomass	0.7721	0.001
	Dead *F. spiralis*	0.5397	0.001
	M. complexa	0.2643	0.001
5	Grasses and Forbs	0.2835	0.001

	C. appressa	0.0928	0.029

Table 32 Indicator species analysis of the Modified TWINSPAN clustering results for the quadrat level GIS 0.5m data. Sum of probabilities = 1.66. Sum of Indicator Values = 4.71. Sum of Significant Indicator Values = 0.96.

Cluster	Ground Cover Class	Indicator value	Probability
8	Grasses and Forbs	0.2012	0.001
9	A. arenaria	0.7598	0.049

3.3.6 GIS 1 m Resolution Based Plant Community Analysis

Ordination

nMDS Ordination to test for relationships between sites and species was carried out on the GIS 1 m data at the quadrat and plot levels using a Bray\Curtis dissimilarity index (Figure 21). The number of axes were set at three, at which point the ordination stress vs. dimensionality approaches 0.05 and the reduction of stress from additional dimensionality is low (Table 33). Final ordination stress was 0.07730923 (Quadrat) and 0.06223447 (Plot), indicating a near excellent fit for both the quadrat and plot level GIS 0.5 m data (Clarke, 1993).
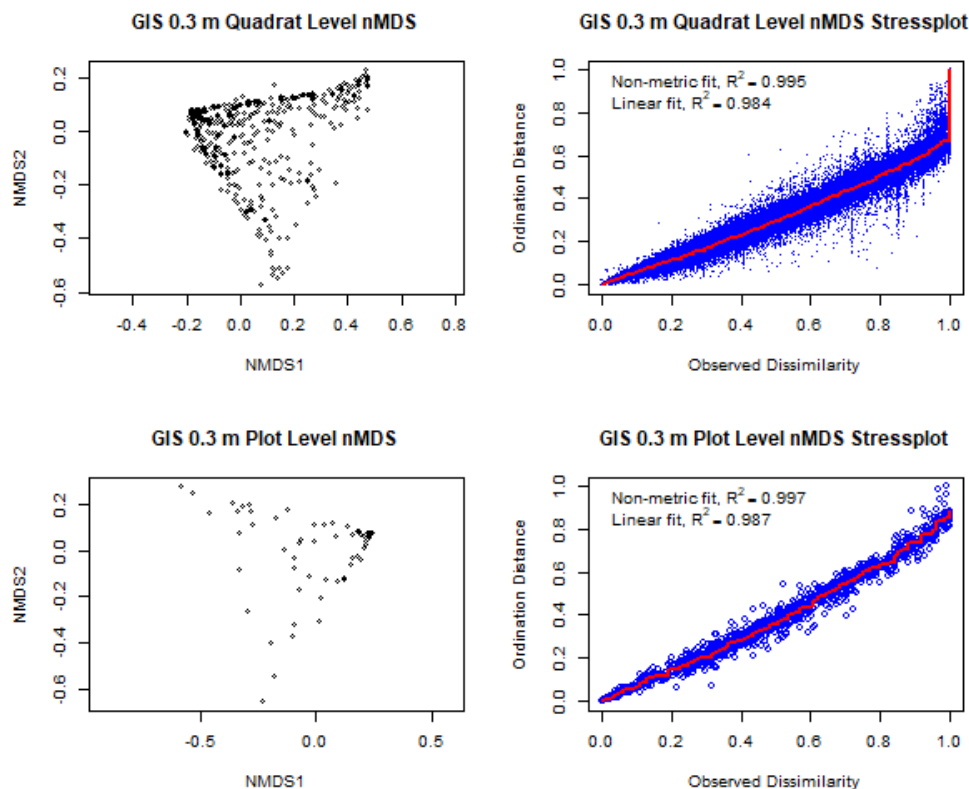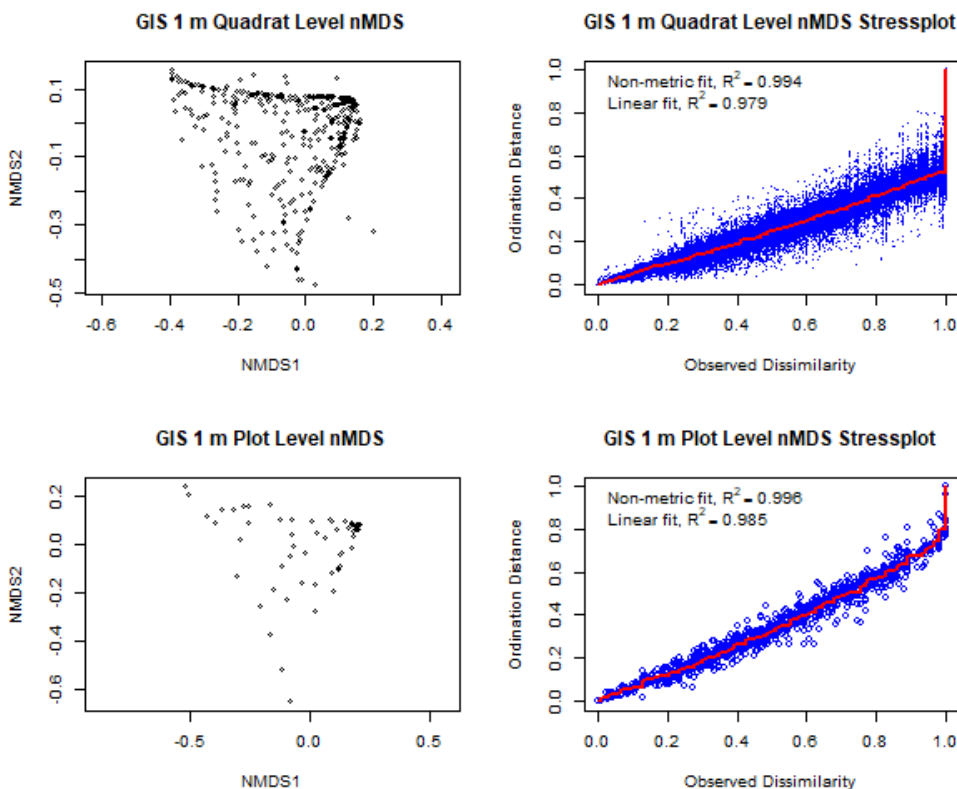
Figure 21 nMDS Ordination and Shepard's diagram of the GIS 1 m data at the Quadrat and Plot levels. The nonmetric fit is based on stress (S) and defined as R2 = 1-S*S, whereas linear fit is the squared correlation between ordination distances and dissimilarities.

Table 33 Optimal number of TWINSPAN clusters (divisions) and Objective Function Score for GIS 0.5 m data at the quadrat and plot levels.

Number of Axes		
	1 m Quad	1 m Plot
1	0.279	0.275
2	0.135	0.109
3	0.078	0.062
4	0.053	0.043
5	0.041	0.032
6	0.033	0.024

Canonical Analysis

Non-symmetric Procrustes rotations were used to test the ordination similarity between the field and GIS 1 m data at both the quadrat and plot level. Figure 16 shows the GIS 1 m data superimposed and rotated to fit the field data, with the residuals of each transformation plotted. At the quadrat level, the sum of squares was 46.01828 with an RSME of 0.2826532. Permutation testing gave a Procrustes sum of squares (m_{12}^2) value of 0.9165 with a significance of 0.001. At the plot level, the sum of squares was 5.603201 with an RSME of 0.2958885. Permutation testing gave a Procrustes sum of squares (m_{12}^2) value of 0.892 with a significance of 0.001.
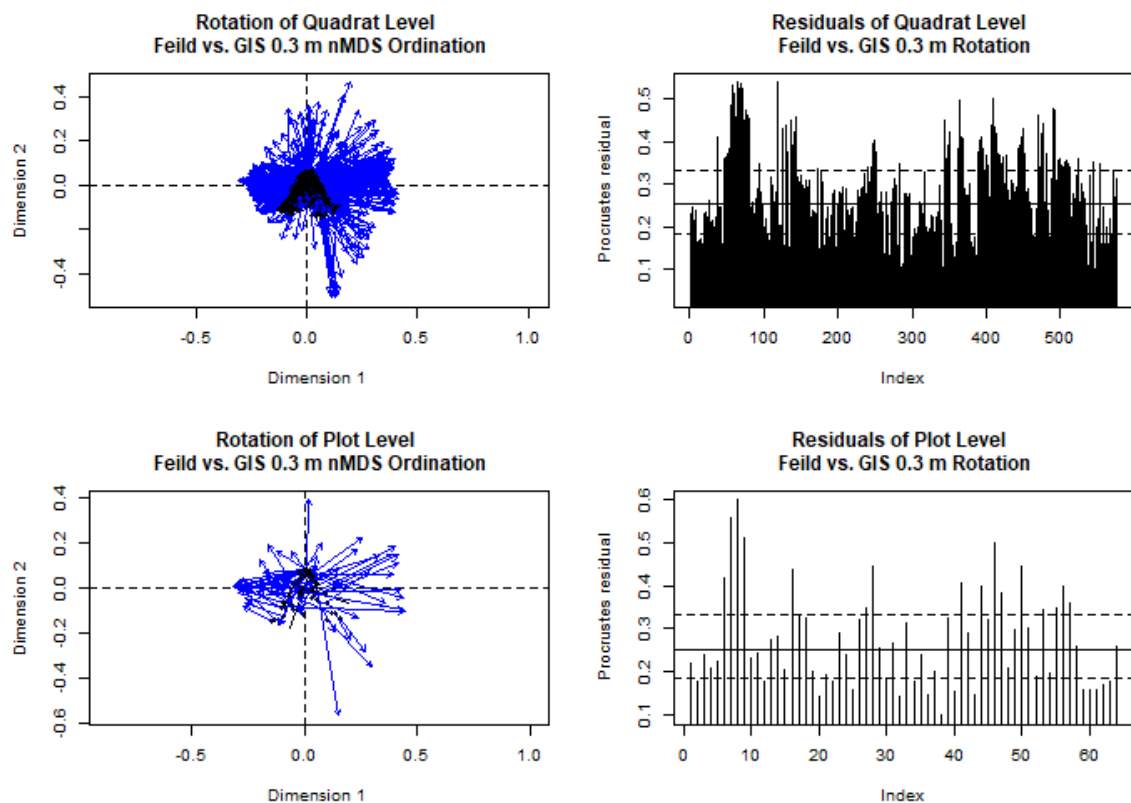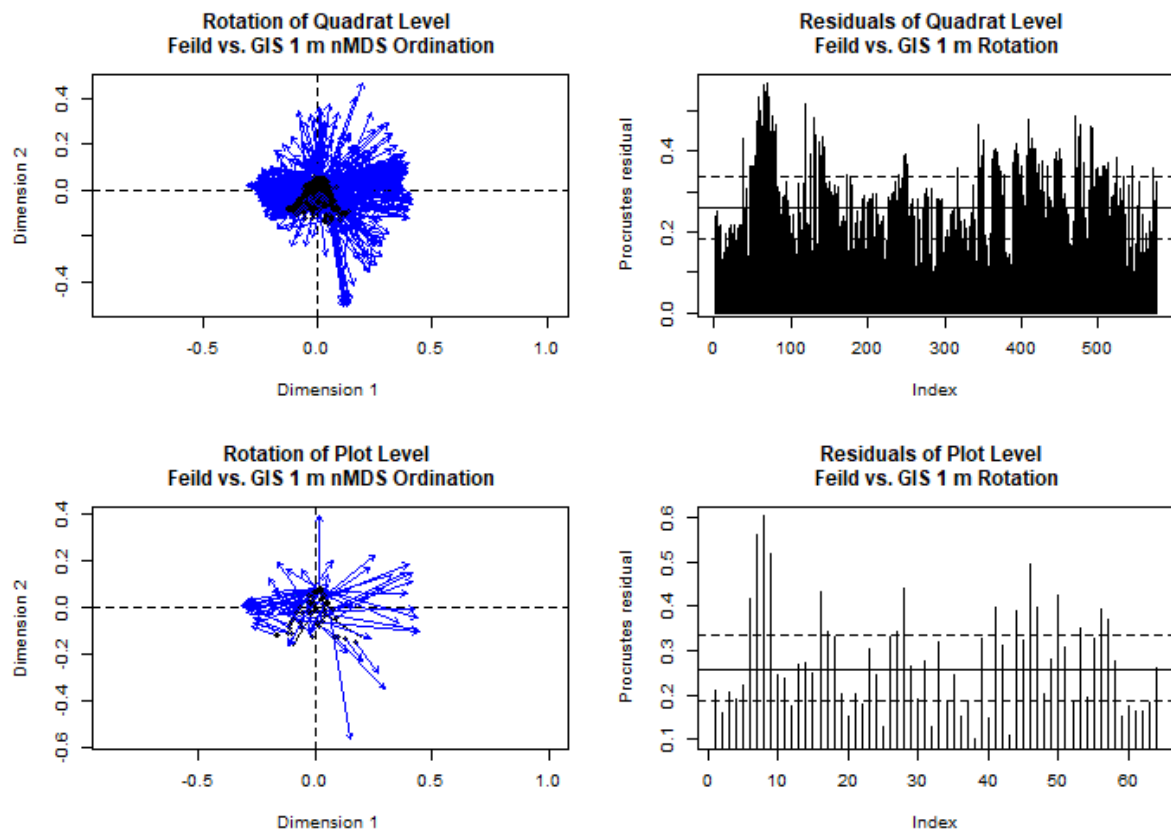
Figure 22 Procrustes rotation and residuals of Field and GIS 1 m data nMDS ordinations at Quadrat and Plot level. Quadrat level sum of squares = 46.01828, RSME = 0.2826532. Plot-level sum of squares = 5.603201, RSME = 0.2958885.

TWINSPAN Divisive Clustering

Modified TWINSPAN was used to divide the data into 10 distinct clusters for the GIS 1 m data for both the quadrat and plot levels. The number of clusters (divisions) was set by the R package RankAggreg with Objective Function Scores of 6.28 and 6.68 for the quadrat and plot data levels, respectively (Table 34). Figure 23 shows the clustering results overlaid upon the nMDS ordination of the quadrat and plot level data.

Table 34 Optimal number of TWINSPAN clusters (divisions) and Objective Function Score for GIS 1 m data at the quadrat and plot levels.

Dataset	Number of clusters	Objective function Score
1 m Quad	10	6.283789
1 m Plot	10	6.675333
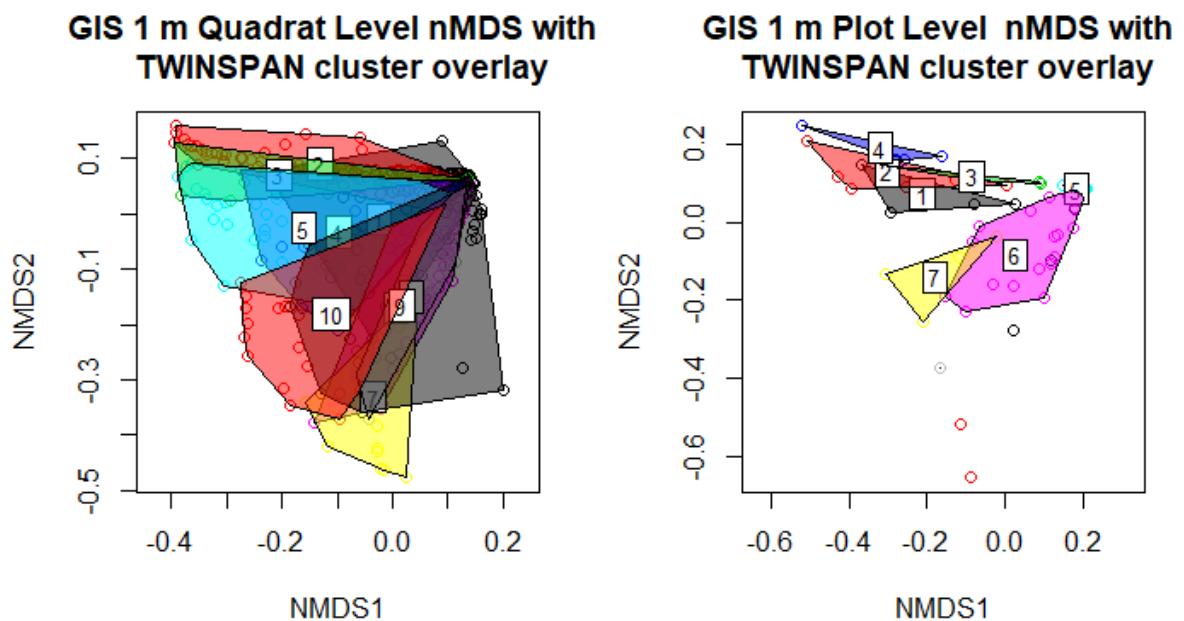
Figure 23. Comparison of ordination results from nMDS of the 1 m GIS data at the quadrat and plot levels with clustering results from Modified TWINSPAN overlaid as bounding polygons.

Indicator Species Analysis

Indicator species analyses of the TWINSPAN results found that different species were indicative of each community type at both the quadrat (Table 35) and plot (Table 36) levels. The number of clusters with significant indicators at both the quadrat and plot level (10) did not match the total number of classes from the modified TWINSPAN analysis, which was 5 and 4 for the quadrat and

plot levels, respectively. 9 significant indicators were identified at the quadrat level, with 2, 1, 1, 3, and 2 significant indicators for each of the nine classes. For the plot level data, 6 significant indicators were identified, with 1, 1, 3 and 1 for each of the four classes.

Table 35. Indicator species analysis of the Modified TWINSPAN clustering results for the quadrat level GIS 1 m data. Sum of probabilities = 0.878. Sum of Indicator Values = 3.35. Sum of Significant Indicator Values = 3.24.

	cluster	indicator_value	probability
GFMHW	1	0.2054	0.001
P. radiata	1	0.165	0.006
OG	2	0.3334	0.001
M. complexa	7	0.4445	0.001
C. appressa	9	0.5616	0.001
P. esculentum	9	0.3992	0.001
L. arboreus	9	0.1719	0.001
dFISsp	10	0.5596	0.001
SDM	10	0.4036	0.001

Table 36 Indicator species analysis of the Modified TWINSPAN clustering results for the plot level GIS 1 m data. Sum of probabilities = 2.124. Sum of Indicator Values = 4.79. Sum of Significant Indicator Values = 2.74.

	cluster	indicator_value	probability
GFMHW	5	0.2219	0.001
SDM	7	0.5388	0.048
dFISsp	8	0.7156	0.027
L. arboreus	8	0.6645	0.037
C. appressa	8	0.5836	0.032
M. complexa	10	0.5533	0.02

3.4 Comparison of field and GIS data community analysis

3.4.1 Ecological meaning of the cluster divisions

Field data

The field community data were divided into three distinct and ecologically relevant clusters using modified TWINSPAN analysis. Table 19 shows the most significant indicators across the three clusters (Table A. 13 shows the complete distribution of all indicators at each site). These three clusters are characteristic of distinct fore-dune (Cluster 1), mid-dune (Cluster 2) and rear-dune Kaitorete Spit communities (Cluster 3).

Sites that were classified in cluster 1 were dominated by pīngao, both live (0.54) and dead (0.67), marram grass (0.05), open ground (0.88) and coarse woody debris (0.34), e.g. driftwood. In these areas, the sites are likely more exposed to the main 'erosion front' where Aeolian forces create an unstable sand environment, meaning that slower-growing species are unable to use the limited time and shelter in which to colonise. Cluster 2 is characteristic of the mid-rear-dune environment; larger species, such as *M. complexa* (0.24) and *C. appressa* (0.30), are common on the more-stable and sheltered areas of the dunes and are frequently seen growing together. Grasses (0.59) and Forbs (0.71) are also able to grow in these areas, as the level of disturbance is low enough to allow for colonisation of the shorter-lived species. In the low-lying areas of the mid-dune, large areas of gravel and sand beds are dominated by low-density grasses and forbs, as well as areas of *R. australis* (0.19). The stability of these areas is such that it allows for lichens and bryophytes to take hold. *R. australis*, *M. alpinus* and *P. cita* were unique to Cluster 2, which further supports the mid-rear-dune environment. Cluster 3 is characterised by the presence of both live and dead *P. esculentum* (0.92 and 0.93, respectively) and dead standing biomass (0.74). *P. esculentum* was unique to Cluster 3, indicating that this cluster was made up of sites that lay towards the rear of the dunes.

The plot level data shows a similar distribution of environmental indicators to the quadrat data. Fewer significant indicators were identified at the plot level (Table 20) compared to the quadrat data, however more non-significant identifiers (Table A. 12) were found in total. For Cluster 1 (fore-dune), coarse woody debris (0.35) and *A. arenaria* (0.06) were no longer identified as significant indicators of the cluster, which at the larger sampling scale likely became rarer relative to the rest of the plot. For Cluster 2 (mid-dune), *M. complexa* (0.10) is no longer a significant ecological indicator alongside lichens and bryophytes. The loss of *M. complexa* was interesting, as it was a key vegetation feature of the mid-dune in field observations. Cluster 3 retained the same indicators as at the quadrat level, however, there was an increase in indicator value for dead *P. esculentum* (0.93 increased to 0.99) and a decrease for *P. esculentum* (0.92 decreased to 0.86) and standing dead biomass (0.74 decreased to 0.69).

Changing the sampling resolution affected the significance of the presence of dead plant material as an ecological indicator at the relatively lower indicator levels (Table A. 13, Table A. 12). Dead *C. appressa* was identified for Cluster 2 at the quadrat level (0.14) but not at the plot level for any cluster. Dead *L. arboreus* increased in significance for Cluster 1 (0.07 increased to 0.15) and was a new indicator for Cluster 3. Dead *R. australis* (0.08) and dead *P. cita* (0.10) were new indicators for Cluster 1 and Cluster 2, respectively. Standing dead biomass was no longer a significant indicator for Cluster 2.

GIS data

The results of the clustering and indicator species analysis for the GIS data are slightly less intuitive than the field data, however, cluster divisions do seem to have been made based on ecological differences. For both the quadrat (Table 23) and plot data (Table 24), four different plant communities were identified, each with unique ecological identifiers. At the quadrat level, Cluster 1 shows dead *F. spiralis* and bare open ground as being the only significant identifiers, although also included in the cluster are standing dead biomass, coarse woody debris, grasses and forbs (Table A. 14). This cluster is the only one to show coarse woody debris as an indicator, which suggests that it may relate to the fore-dune environment. Cluster 2 shows *P. radiata* and mixed grasses as the significant indicators, but also includes *M. complexa*, *R. australis* and *C. appressa* (Table A. 14), all of which are indicative of mid-rear-dune vegetation. Cluster 3 has *C. appressa*, *A. arenaria* and *P. esculentum* as significant indicators, yet also includes mixed grasses, *M. complexa*, *P. radiata* and bare open ground. The presence of both pines and bracken fern indicates sites belonging to the rear-dune systems. Broom and *Muehlenbeckia* are also found in the Rear-dunes, often growing together in a densely tangled structure. Cluster 4 is indicated by the presence of *Muehlenbeckia* and standing dead biomass, as well as *R. australis*, mixed grasses, *P. esculentum* and *F. spiralis*. This was the only cluster that registered pīngao as an indicator at the quadrat level for GIS 0.1 m. Based on these indicators, it is likely that these sites are indicative of the early-mid-dune, in that we see sites along the back of the active fore-dunes, the gravel and raoulia beds of the dune hollows and the stabilised mid-dunes that contain the standing dead matter and *Muehlenbeckia*.

At the plot level, the GIS 0.1 m data becomes a little less clear regarding how it translates into the real world distribution of sites (Table 24, Table A. 15). Clusters 1 & 2 are characterised by only one significant indicator each; bare open ground and *M. complexa*, respectively. The also share coarse woody debris, mixed grasses, *P. esculentum* and *R. australis* as less significant indicators. CWD was attributed more towards Cluster 1 (0.25) than Cluster 2 (0.06), which alongside the significance of bare open ground (0.86) would indicate areas near or including the fore-dune. The presence of *P. radiata* (0.12), *P. esculentum* (0.10) and *R. australis* (0.13) in Cluster 1 would suggest sites more towards the rear, however, these low values may be attributed to classification error. Compared to Cluster 1, Cluster 2 shows the unique indicators of *C. appressa* and SDM, although at relatively low levels (0.07 and 0.11, respectively). The lack of OG as an indicator for Cluster 2, in combination with those that *are* present, suggests the mid-rear-dunes are typically stable enough to allow for higher levels of ground cover. Cluster 3 was indicated by both *C. appressa* (0.81) and *P. radiata* (0.77). Cluster 3 was the only cluster to register *L. arboreus* (0.31), which, in combination with mixed grasses (0.37), *M. complexa* (0.20), *P. esculentum* (0.25) and OG (0.08) would again indicate areas towards the mid-rear-dunes. How this differs from Cluster 2 could be explained by the narrowness of the

western end of the dune system compared with the eastern end. The old *P. radiata* shelterbelt and the surrounding *L. arboreus* populations at the western end of the site is in close proximity to the Mid and Fore-dunes in that area. These results would suggest that Clusters 1 & 2 represent relatively similar mid-rear-dune environments, although they are separated by the difference in dune structure from the western (Cluster 2) and eastern (Cluster 3) ends of the site. Cluster 4 is significantly indicated by dead *F. spiralis* (0.95) and SDM (0.80). The remainder of the indicators for Cluster 4 are relatively low compared to these; *P. esculentum* (0.10), *M. complexa* (0.06) and mixed grasses (0.05). Based on these results, Cluster 4 may be representative of the back of the Mid-dune, however, this comes with a degree of uncertainty.

Chapter 4

Discussion

4.1 The suitability for UAS Remote Sensing for monitoring Kaitorete Spit

In order to achieve effective management of natural habitats, sound knowledge and understanding of their inherent ecological characteristics and qualities are required (Spanhove et al., 2012). Kaitorete Spit, and the important ecological communities that reside there are expansive and both structurally and ecologically diverse. Accurate field-based monitoring of processes is typically unfeasible due to time and financial constraints. To gain an understanding of the health and functioning of ecosystems and communities, we must understand the key ecological drivers and quality indicators that define these communities. This thesis research sought to evaluate the use of UAS based remote sensing imagery for the detection and analysis of at-risk plant communities at Kaitorete Spit. Using both data types, the major plant communities of the dune system at Kaitorete Spit, i.e. the fore, mid and rear-dunes, were able to be identified using modified TWINSPAN clustering and Indicator Species Analysis. The results show that community analyses based on UAS imagery can be used to identify some, but not all, plant species and ground cover to an acceptable standard of accuracy. These data can then be used to identify meaningful ecological indicators for distinct, real-world dune communities. The relevance of the UAS imagery to the effective management of Kaitorete Spit depends on the scale at which we monitor habitat quality and the type of ecological monitoring we are attempting to conduct.

Characterising the scale of ecological patterns is critical for their spatial and spectral identification in both field and RS techniques (Corbane et al., 2015). If we can use UAS imagery to monitor coarse scale plant community and dune habitat, then does the lack of direct fine-scale species monitoring matter? In order to answer this, we need to break down the methods and scales at which we measure community health. Kaitorete Spit is home to a number of rare and threatened species. Many of the key indicators that were identified in the field data, however, were not present in the GIS data; the potential reasons for which will be discussed below.

4.1.1 The scale of ecological phenomena at Kaitorete Spit

The field data, based on real-world information, showed ecologically stronger clustering compared with that of the GIS information. Comparing the number of cover classes for each dataset alone found 25 and 12 classes for the field and GIS data, respectively. Much of this undoubtedly came from the ability to identify rare species, as well as to identify the type of standing dead material to the species level.

Identification of species using GIS imagery was challenging. Training samples for classification classes could only be built when a positive identification of cover was achieved. Much of the knowledge required for this came from exploratory observations into the field site. Rare species that were identified in the field data (e.g. *L. ferocissimum*, *M. alpinus*, and *P. prostrata*) were either not seen in the imagery or misidentified as another ground cover type. For the field data, we also saw a differentiation between grasses and forbs, which were combined in the GIS data into mixed grasses. The classes of lichens and bryophytes were not included in the GIS data, as their typically sub-pixel size meant that they were indistinguishable from the surrounding cover type, which was likely open ground.

The greater number of species and cover types available in the field data allowed for better differentiation of clusters and cluster indicators. When comparing the types of indicators shown to be significant for cluster divisions at the quadrat level there are classes from the field data (Table 19) that were not identified in the GIS analyses (Table 23). *A. arenaria* were indicative of Cluster 1 (fore-dune) for the field data. For Cluster 2 (mid-dune), the presence and differentiation of grasses, forbs, bryophytes and lichens made for easier ecological interpretation of the results compared to the GIS data. At the non-significant level for the field data (Table A. 12), *M. alpinus* (0.17) and *P. cita* (0.7) were identified as indicators for Cluster 2. At the plot level (Table A. 13), *P. cita* (0.70), grasses (0.52) and bryophytes (0.45) were significant indicators of Cluster 2. These differences between the field and GIS data made interpretation of the GIS community data somewhat challenging, reducing its overall effectiveness and explanatory power.

4.1.2 Detectable indicators of community division and health

Common species with high detection ability define certain ecological communities

GIS data were able to delineate similar course-scale ecological communities when compared to the field data based on a similar, but not identical, set of ecological factors. At this level, the data are arguably of value, as it would enable broad-scale monitoring of these key habitats. The majority of the existing literature surrounding the use of UAS for habitat monitoring focuses on coarse-scale dynamics, such as quantifying the total amount of vegetation or a mixed species community (Zahawi et al., 2015), plant functional types (Roth, Roberts, Dennison, Peterson, & Alonzo, 2015) or the amount of open ground and water (Gong, Jiao, Zhou, & Li, 2011). While informative, at these broad scales the fine-scale ecological drivers of differences in community health and structure can be lost (Elliott & Jules, 2005). Failure to link course-scale habitat features to single biophysical characteristics restricts the application of habitat characterisation (Groom, Mücher, Ihse, & Wrbka, 2006).

The mixed performance of the GIS data in separating the mid-dune plant communities is a significant limitation of the application of RS for monitoring Kaitorete Spit. The main conservation values of the mid-dunes based on field observations come from the structural heterogeneity of this area. This zone has a mixture of environmental gradients, with more exposed areas allowing for dune colonising species, such as pīngao to establish, and more sheltered and stable areas that facilitate higher within-class diversity. This diversity and the high ecological value it provides comes at a cost when trying to characterise the habitat using remote sensing, as habitats within such dynamic systems can occur in a mosaic pattern, making clear delineation and assessment challenging (Evans, 2006). These within-habitat communities may also display differences in the timing and duration of phenological events, which can further increase the spectral variability within a given class (Klosterman et al., 2018). Differentiation at the between and within-habitat levels can be challenging, although the scale at which habitats are characterised will not be the same for all habitats within a given area (Vanden Borre et al., 2011).

For Kaitorete Spit, while a reduction in the spatial resolution of the remote sensing data led to a decrease in the ability to detect key drivers of community differentiation, the results of increasing sampling sizes (smaller quadrats to larger plots) indicate that 2 m x 2 m sample size is too fine-scale for analyses. Comparing the nMDS ordination stress of the field and native GIS data at the quadrat vs. plot scale shows a reduction in ordination stress and an increase of linear fit for both the field and GIS data at each of the four resolutions. Further evidence for the fact that the vegetation dynamics at Kaitorete Spit exist as a fine scale matrix across larger spatial extent comes from a 1992 study of the vegetation in the same area of this study. Partridge (1992) used a nested sampling design of six 200 m x 220 m sampling sites within the mid-dune (with one at 240 m), in which 111, 5 m x 5 m plots were assessed for species relative abundance at the 1 m x 1 m scale. The intricate detail of this sampling design allowed for the differentiation of 20 different plant communities based on the 31 most abundant species found and their respective abundances when compared to dune topography and distance from the shoreline. Pudji (1997) conducted a similar study using nested study sites which were 200 m across at the end parallel to the high-tide line, and extending north between 300 m and 750 m depending on dune vegetation distribution. These were divided into 50 m x 50 m blocks, in which a 2 m x 2 m quadrat was sampled for species presence and relative abundance. Using TWINSPAN, these were divided into 8 different plant communities based on Indicator Species Analysis across 5 major plant vegetation zones. It should be noted that the authors used a much more robust level of species identification, especially for the different grasses, forbs and bryophytes found. The five zones matched those discussed in this current study; the fore-dunes, deflation hollows, inner dunes (mid-dunes), sandy plains (grassfields) and old dunes (P. *esculentum* dominant areas). For this study, sampling transects extended from the shoreline out to the very back

of the dunes and the beginning of the grass fields and were placed at 300 m intervals with plot sizes of 6 m x 6 m and cover estimates based on a 2 m x 2m sampling unit. This sampling design was not very effective at describing the highly variable mid-dune environment, as is evident in the lack of definitive, ecologically relevant classes in the GIS data.

Of the easily detectable species that strongly indicate community divisions, the native or ecologically significant species, while locally common, are often rare or threatened at the regional and national scale. This is particularly true for the active fore and mid-dune environment where the prevalence of the native sand-binder, pīngao, forms part of the largest remaining natural population of this at-risk species (Lettink, 2008). The direct detection of larger species, such as *C. appressa*, *M. complexa* and *R. australis*, which were indicative of the mid-dune environments, is also of significance. *C. appressa* is one of the only vascular plant species endemic to Kaitorete Spit and all three species, as well as pīngao, are important host species for many of the 130 Lepidoptera species found at Kaitorete Spit, of which 6 are endemic to the area itself (Patrick, 1994). The fleshy fruit of *M. complexa* is also an important food source for native lizards, which are, in turn, important for seed dispersal (Whitaker, 1987). The structural density of *M. complexa* and *C. appressa* also provide habitat for lizards that is safe from most predatory species (Lettink, 2008).

The mid and rear dunes are characterised by a wide range of vegetation with most of the species detected in these areas being shared right across the mid and rear-dunes. Rather than species presence and absence, for much of these communities the differences exist in the physical growth structure and the degree to which each species contributes to the overall species assemblage. These inherent biological features of the dune vegetation at Kaitorete Spit again limit the current application of UAS based remote sensing. The results of this study are in agreement with other studies which show that in heterogeneous environments, with fine-scale features and continuous between-habitat variability, such as those found at Kaitorete Spit, mapping accuracy is reduced (Varela, Rego, Iglesias, & Sobrino, 2008). In these scenarios, detection of the indicators of these environments may be limited to relatively course-scale homogenous cover (Irisarri, Oesterheld, Verón, & Paruelo, 2009). Zweig et al. (2015) in a recent and rather similar study stated that they were one of the first studies to use UAS imagery not as a photo or map, but rather as data for fine-scale community classification. However, the authors used expert knowledge of their system to define communities, not using the presence or absence of different species, but rather by estimating the density of those species within the community itself. Of the nine classes used in their classifications, eight were either mixed species assemblages or variations of a cover type based on the surrounding cover. The only single species cover was also only identified to the genus level. Zweig et al. (2015) further increased classification accuracies by reducing the total number of plant communities from 9 to 3 by aggregating similar or related community types. While some fine-scale

features were lost, more important features, such as major structural differences (wet prairie vs. slough (waterbody-based vegetation)), were retained. Marceau et al. (1994) in a much larger study using aerial imagery ranging from 5 m – 10 m found that the aggregation of certain clusters can lead to increased classification accuracies, however, results were heavily dependent on class species membership and the resolution of the imagery.

Increasing the resolution of the data, both spatial and spectral, to better match the scale of ecological indicators can aid in species detection. Husson, Ecke, and Reese (2016), in a study of non-submerged aquatic vegetation, were able to accurately identify individual species using 5 cm RGB imagery, although classification accuracy decreased when vegetation complexity increased. A similar reduction of accuracy from increased complexity was found in an earlier study by (Husson, Hagner, & Ecke, 2014). When communities are lacking any distinct spatial or spectral features, community level classifications have been shown to perform poorly.

In certain situations however, a decrease in spatial resolution may be more beneficial. With an increase in the spatial resolution of RS imagery comes with an increase of the within-class spectral variability, causing a 'salt and pepper' effect which can reduce the accuracy of classification results (Pu, Landry, & Yu, 2011). In a study using hyperspectral data to detect individual and mixed invasive species, a reduction in spatial resolution still resulted in significantly accurate classifications, however, this was attributed to the large spatial extent and the dominant cover of certain species (Underwood et al., 2007). Roth et al. (2015) found an increase in pixel size from roughly 3 m to 20 m led to an overall increase in the classification of plant communities based on plant functional types. Zweig et al. (2015) stressed the importance of matching image resolution in wetland communities to that of the texture of ecological phenomena being studied. In their research, which focused more on habitat structure than species presence, for this broader level of community differentiation, the authors found the native 5 cm imagery to be of too high resolution compared to the texture of these plant communities. The authors found that by resampling the image to 0.5 m (a ten-fold increase in spatial resolution) they could produce more intuitive and accurate results. When compared to this study, which focused primarily on the identification of individual species, resampling the classification data to a lower accuracy resulted in a loss of the overall indicator values for the site, as well as an increase in ordination and Procrustes rotational stress.

Ecologically significant species are actively controlled, creating artificial rarity and an increased within-class spectral variation.

When we consider the types of risks that these dune communities face, the most important indicators of fore-dune habitat quality exist at a fine ecological scale, such as the detection of ecologically significant species. The detection of invasive species at Kaitorete Spit is just as important

as detecting native species for habitat quality and risk monitoring. The active dunes – both fore and mid, are at risk from invasive plant species that function to stabilise the dunes. Once stabilised, the native species are out-competed and the amount of open-ground and other suitable habitats for plants, invertebrates and vertebrates is reduced (Molloy et al., 1991; Partridge, 1992).

For the fore-dune habitat, the three main species that pose the greatest risk are *P. radiata*, *L. arboreus* and *A. arenaria*. A significant issue in assessing the detection of invasive species within a nature reserve, such as the Kaitorete Spit Science and Conservation Area, is that *these species are actively controlled within the area*. Because of this, the total population number is typically quite low. For species such as *L. arboreus*, which can rapidly colonise available habitat, there exists a wide range of plant ages and phenological states. This would undoubtedly affect the ability to detect and effectively characterise the populations when building training samples for classification, as within-class spectral variability is increased (Klosterman et al., 2018). When detecting multiple invasive species, different species will require different levels of spatial and spectral resolution in order to maximise accuracy in detection (Underwood et al., 2007). An example of species size and growth form affecting its spectral characteristics at Kaitorete Spit would be *P. radiata*. Individual trees can be readily identified; however, their inherent structural complexity and within-class spectral variation undoubtedly contribute to the classes' lower accuracy. Roth et al. (2015) state that minimising such internal spectral variation is crucial for accurate identification of species with complex canopy structures. Detection of fine-scale canopy components and environmental effects, such as shadowing, leads to an increase of within-class spectral variation, which has been shown to negatively affect classification accuracies (Clark, Roberts, & Clark, 2005). Relatively course-scale imagery has the effect of spatial and spectral averaging of canopy structure and individual tree crown geometry, which can improve classification accuracies up to a certain resolution (Roth et al., 2015).

Underwood et al. (2007) found that when an invasive species is spectrally distinct and present within a relatively homogenous cover type with low within-class spectral variability, then the spectral rather than spatial resolution is of greater significance to classification and detection. However, in heterogeneous mixed-species environments, such as those in the mid and rear-dunes at Kaitorete Spit, accurate detection of invasive species required higher spectral resolution. The authors found that when using multiband imager rather than hyperspectral, classification accuracy of the intact heterogeneous communities (those without invasive species) reduced from 81% to 26% as measured by User's Accuracy.

Deciding on the most appropriate scale requires trade-offs depending on the relevance or perceived risk for each species in question. Most, if not all other UAS studies start with *a priori* knowledge of

the specific habitat or community types that are present in their study (Franke, Keuck, & Siegert, 2012; Gonçalves et al., 2016; Mucher et al., 2013; Rapinel, Rossignol, Hubert-Moy, Bouzille, & Bonis, 2018; Vanden Borre et al., 2011). Underwood et al. (2007) state that appropriate spatial resolutions for a given species could be derived *a priori* from limited field data using tests to determine the highest correlation of spatial resolution and explain community variability. In addition to a better definition of optimal spatial resolution for a given species, creating a spectral training sample for individual classes from independent sources could also be a potential solution. Roth et al. (2015) found that training samples based on fine-scale imagery could be used to classify coarse-scale images. Schaaf, Dennison, Fryer, Roth, and Roberts (2011) also found that when fine-scale training samples are used on coarse-scale imagery, they perform better than coarse-scale training samples derived from the same image. Using training data from independent RS imagery at the same spatial and spectral scales has been shown to create accurate classifications on separate images (Su & Gibeaut, 2017). Before the implementation of these techniques at Kaitorete Spit, more testing would be recommended, as using training data from other areas would likely also increase the chance of errors from between-site spectral variation.

The consideration of the amount of effort and resources to invest for the monitoring of invasive species is relevant when bearing in mind the potential impacts of delaying control operations until populations are large enough to detect accurately via RS. For larger species such as *P. radiata* that take years to reach reproductive age, this is perhaps less of an issue. For species like *L. arboreus* which can rapidly colonise an area and cause sudden ecosystem change (Pickart, 2004), the best time to control such a species might be when they are too small to detect via RS. The monitoring of populations with low-density or detectability can be instrumental in the effective control of invasive species, as they can enable detection of recently established "founder" populations that can be targeted for control (Lodge et al., 2006). Outright eradication of these species is likely unfeasible at this point in time due to the prominence of source populations in the surrounding landscape. Continued control operations are important, however, as a reduction in population density can be enough to significantly increase the effect of stochastic events in reducing population densities even more. At Kaitorete Spit, herbivorous predation and fungal pathogens are known to periodically cause crashes in the local *L. arboreus* populations (Molloy et al., 1991).

Other detectable factors

The ability of the GIS data to differentiate plant communities were negatively affected by its inability to differentiate between different types of standing dead biomass. The ability of the field data to detect and identify types of standing dead matter also enhanced the separability of clusters. Dead *F. spiralis* was able to be identified in the GIS data and were indicative of the fore-dune environment

for both datasets. This was the only identifiable dead matter class for the GIS data. The field data, for which species identification was much more readily available, readily benefited from this level of identification. Dead *P. esculentum* was a significant indicator of the rear-dunes from the field data at both the quadrat and plot levels. While not identified *per se* in the GIS data, due to the way the training samples were made it is likely the class for *P. esculentum* included both live and dead material as they were typically in immediate proximity to each other in the field. At the non-significant level, dead *L. arboreus* was indicative of Cluster 1 for the quadrat level and for both Cluster 1 and 3 at the plot level. The relevance of identifiable dead material was much more pronounced at the plot level, which further enhanced cluster separability in the field data compared to the GIS. Dead *R. australis* was indicative of Cluster 1, and dead P*. cita* and *C. appressa* were indicators of Cluster 2.

Quantification of dead matter accumulation is used an as an indicator of disturbance (Christina Eisfelder, Kuenzer, & Dech, 2010), fire risk modelling (Arroyo, Pascual, & Manzanera, 2008; Garcia et al., 2011; Rollins, Keane, & Parsons, 2004; Shin et al., 2018) and bioaccumulation/nutrient cycling (G. D. Cook, Meyer, Muepu, & Liedloff, 2016) and productively (C. Eisfelder, Kuenzer, Dech, & Buchroithner, 2013; Pullanagari, Kereszturi, & Yule, 2017). The detection of non-photosynthetic components within multispectral imagery is a challenge due to the fact that the reflectance of such material is similar to that of bare soil (Qi & Wallace, 2002) or features such as moss and lichen (Xu et al., 2014). The presence of dead material at Kaitorete Spit indicates the difference in disturbance between the fore-dune and mid-dunes; however, it may also be present as a result of invasive species control operations. In fact, the potential for UAS imagery to detect negative effects of weed control on species such as pīngao was one of the initial management questions for this study. The risk of fire to the dune vegetation at Kaitorete Spit is also a serious threat to biodiversity and dune stability, and remote sensing is used in coastal environments to monitoring ecosystem-level responses to such events (Shumack et al., 2017). Hyperspectral imagery can be used to detect non-photosynthetic vegetation via the use of vegetation indices such as the Cellulose Absorption Index (CAI) (Guerschman et al., 2009; Ren & Zhou, 2012). (Xu et al., 2014) investigated the relationship between NDVI and varying amounts of dead matter in grassland ecosystems and found that dead matter influences the relationship between live material and the NDVI. This may have implications for classifying vegetation in that when building training samples for a given species which exists in high and low disturbance environments, the presence of dead material in close proximity (or within the same pixel) will contribute towards greater within-class spectral variation.

4.1.3 Non-detectable indicators of community division and health

There are three main explanations for rarity and or reduced representation in ecological data: highly specific endemism, naturally sparse distribution, and poor detection based on insufficient data collection (Kunin & Gaston, 1993). Understanding how a particular species may fit into one of these categories is of vital importance to effective environmental monitoring and planning (de Siqueira, Durigan, de Marco Júnior, & Peterson, 2009).

Common species with sub-pixel spatial extents define ecologically important zones that are not detectable via remote sensing

The mid-dune community, according to the indicator species analysis of the field data, was most characterised by small species, such as grasses, forbs, bryophytes and lichens. Larger species, such as *C. appressa* and *M. complexa*, are also indicative, but less so than the smaller species. These smaller species make up the dominant vegetation of a significant community type that lays within this mid-dune in the dune hollows (referred to as gravel basements in (Partridge, 1992)). These areas are large, flat and stable gravel beds which are formed either naturally from dune deflation, or are remnants of historical mining in the area (Partridge, 1992) The dune hollows are important breeding sites for shore-breeding bird species, and also are home to the endemic plant *C. 'kaitorete'* whose low growth-form is easily outcompeted by taller exotics. *Craspedia sp.* and *R. australis*, other key species found in these areas, were listed as host species for a number of native moths in the area (Patrick, 1994). Apart from grasses that can form larger areas of relatively high cover, the remainder of these indicative cover types typically, grow to sizes that would be in the sub-pixel range, even when using very high-resolution data like that used in this study. While not identified as a different cluster in the TWINSPAN analysis, further method revisions would likely have identified these zones as a separate cluster. If the key indicator species for these areas are too fine-scale to be detected via GIS based on the methods used in this study, then monitoring of these environments would not be viable.

Outside of the mid-dune hollows, detection of the sub-pixel indicator species mentioned above, as well as similarly sized ecologically significant species within the grassland areas was further limited because these species characteristically form part of diverse species assemblages within habitats. The issues surrounding the identification of individual species in mixed-species assemblages were discussed in Chapter 1.3. In this case, direct detection of these species remains unachievable without sub-decimetre pixel resolution. Roth et al. (2015) found that even with hyperspectral data, classes with patch sizes approaching or less than the spatial resolution of the data could not be mapped accurately at coarse resolutions. Underwood et al. (2007) found that when classifying heterogeneous scrub communities, a lack of defining spatial or spectral patterning meant that

similar classification accuracies were achieved regardless of spectral or spatial resolution. Spanhove et al. (2012) state that despite recent developments in RS technology and statistical data analysis approaches, the successful identification of small individual plants whether as individuals or part of heterogeneous habitat matrixes remains a highly significant barrier towards the application of RS in ecological monitoring. While the loss of fine-scale classes at relatively lower resolutions can be safely assumed, it represents an important limitation of classifying to the species level in that there is an inherent bias to large, more dominant species (Roth et al., 2015). This bias likely contributed to a reduction of the spectral variation between classes in the GIS data. Of the species that *were* able to be identified most, if not all, were shared between the other communities to a varying degree. This small change in microclimate or other micro-environmental conditions may result in increased within-class spectral variability (Klosterman et al., 2018)

Detection of rare species is possible via the modelling of its known ecological niche. de Siqueira et al. (2009) used 16 different rasters to model the environmental conditions from a single occurrence of a rare Brazilian plant species that was thought to be locally extinct. Using these data, the authors were able to isolate a range of sites with matching environmental conditions, at which they were able to locate previously unknown populations of the species in question at five of the nine sites identified. These models, however, were of the entire state of Sao Paulo, Brazil. Replicating fine-scale environmental modelling of a site such as Kaitorete Spit would be currently unfeasible, as for the most part, these data do not yet exist. Structural information of the dunes could be created via SFM techniques that could help in environmental modelling.

Rare species that assist in the differentiation of certain ecological communities were either not encountered or could not accurately be described via remote sensing

L. ferocissimum, *M. alpinus* and *P. prostrata* are examples of locally rare species that were identified as significant indicators in the field data yet were not identified via GIS. Unlike the aforementioned species with sub-pixel spatial extents, these species can grow to relatively large sizes. Their naturally sparse densities combined with an ineffective GIS sampling methodology likely resulted in their non-detection when image classification training was being conducted. Of the few individuals that were seen in the field, there were too few observations from which to build a training sample of sufficient spatial and spectral resolution. *M. alpinus* was also likely confused for *M. complexa* in the imagery, as both species share a very similar growth form and foliage colour.

Observer bias and the difference in observer skill in the detection of low-density populations has been shown to significantly affect the reliability of data from the field (Bergstedt et al., 2009; Fitzpatrick, Preisser, Ellison, & Elkinton, 2009; Trevithick, Muir, & Denham, 2012; Vittoz & Guisan,

2007) and remote sensing based surveys (Cagney, Cox, & Booth, 2011; Frederick, Hylton, Heath, & Ruane, 2003). In Zweig et al. (2015) the authors explicitly state: "expert knowledge was critical to producing our classification, both in terms of on the ground and remote sensing knowledge". For this study, the ability to discern image objects with any level of confidence was a combination of image quality and my own knowledge of the plant communities of the dune system itself.

4.2 Factors in the final results

4.2.1 Overall accuracy

The overall accuracy of the classification has a significant influence on the reliability of the data and the strength of any ecological conclusions. For the sake of simplifying the discussion, the Kappa coefficient will be used for comparisons between studies whereas the user's accuracy will be used to discuss the implications of different accuracies of the classes that exist within this study. An explanation of the two measures can be found in Section 3.2.2. The Kappa coefficient is a widely used metric that describes the overall relationship between the classification and the associated reference data. The use of the Kappa coefficient allows for the direct comparison between different classifications (Congalton & Green, 2008). The Users' accuracy is the more useful measure of individual class accuracy to land managers (Underwood et al., 2007) as it is a measure of how reliable the map or classified image is in relation to what it actually on the ground (Story & Congalton, 1986).

In this study, point and area-based accuracy measures were used. Point-based accuracy measures found the highest Kappa (69.73%) and overall/total (72.48%) accuracies, whereas area based accuracy was significantly lower (35.61% and 49.30% for the Kappa Coefficient and Overall/Total Accuracy, respectively). Based on the standard proposed by Landis and Koch (1977), these results range from "fair" for the area assessment to "substantial" for the point assessment. These ranges put the results in line with recent similar studies. Zweig et al. (2015) achieved an overall accuracy of 69% with a Kappa coefficient of 0.65, as measured by point-based accuracy for nine vegetation classes at 0.5 m resolution. Fraser, Olthof, Lantz, and Schmitt (2016) used 0.1 m RGB imagery to classify arctic shrubland with an accuracy of 72% (overall/total accuracy) using point-based accuracy. (Chabot et al., 2017) used 0.05 m multiband imagery to classify broad-scale vegetation dynamics with an overall accuracy of 78% and a Kappa coefficient of 0.61 using point-based accuracy. Chabot et al. (2018) achieved accuracies ranging from 84% - 92% (overall/total) and 75% - 88% (Kappa coefficient) when using ~13 0.13 multispectral (including red-edge) imagery and 0.04 RGB imagery.

The accuracy of key indicator species

The strength of any ecological conclusion that are drawn from remote sensing data are heavily dependent on the specific accuracies of the data themselves. As such, these measures of evaluation

should be made available to users for objective verification before deciding if and how the end products can be used (Xie et al., 2008). While a direct measure of classification accuracy is of some value, they do not show how well a classified image or map may relate to that landscape's structure and function (Lunetta & Lyon, 2004). By comparing the class-specific accuracy against the classes' apparent relevance to a sites community analysis, we can derive a basic idea of the suitability of any classification products derived from the data (Figure 24). For each cover class, the relevance of its accuracy will relate to whether its detection is important for direct monitoring of the species *per se*, or rather its value as an indicator species for monitoring coarse-scale habitats.

Table 37 shows the specific class accuracies as measured by the User's Accuracy. Of the 16 significant indicators for the plot level field data, only eight could be directly identified. The other eight were either not detected at all, or formed part of a mixed species class. Of the species that are of the highest ecological importance to Kaitorete Spit, only *M. complexa* showed an acceptable average Users' accuracy. The highest average was of the mixed-grass species class, at 81%. While a significant indicator of a specific community, as discussed previously the ecological value of this cover class is of less importance relative to single species classes such as *M. complexa.* Of the most distinctive indicator species for each of the three clusters, only Bare Open Ground could be directly detected. With an indicator value of 0.88, its accuracy of 68% relative to the other classes would make for a relatively confident identification. *F.* spiralis, which was the cover class of the highest ecological value in this cluster only achieved an average Users accuracy of 57%. Using point based methods rather than the average however shows an accuracy of 98%, the highest overall accuracy rating for all classes.

The areas-based accuracies are lower for every class compared to the point-based measures. As mentioned in section 2.3.2 the points used in the accuracy assessment were all manually selected. Point-based accuracy works well with high-resolution data, as a definitive point with small spatial extent is less likely to exhibit more than one vegetation type at the sub-pixel level (Xie et al., 2008). Manual selection of points, however, does introduce selection bias, in that I was more likely to select points that they have the highest relative confidence in identifying. This is in direct contrast for the methods used in the area-based assessments for this study. The areas were randomly placed and the cover classes within were manually classified by drawing a bounding polygon around each class. While the knowledge and skills surrounding my ability to identify cover types was the same for each method, issues in the identification of mixed cover and boundary pixels were apparent. When delineating cover classes at this resolution, defining individual plant or class boundaries was difficult (Figure 25). High-resolution imagery comes with finer class boundaries and a subsequent increased need for accurate boundary definition (Underwood et al., 2007). The mixed species ground cover and its highly variable distribution and density would have also resulted in high within-class spectral

variation. *F. spiralis*, *C. appressa* and *P. esculentum* all showed large differences between the point and area-based assessments. For *F. spiralis* and *C. appressa*, this may be due to their low-density growth forms. When designating image object boundaries for these species, the fine-scale variations in the presence of open ground or other cover types that exist at the boundaries would have been undoubtedly included. For *P. esculentum* rather, the high density of its growth form and the high-occurrence of standing dead biomass would have significantly increased the within-class variation for the cover class.
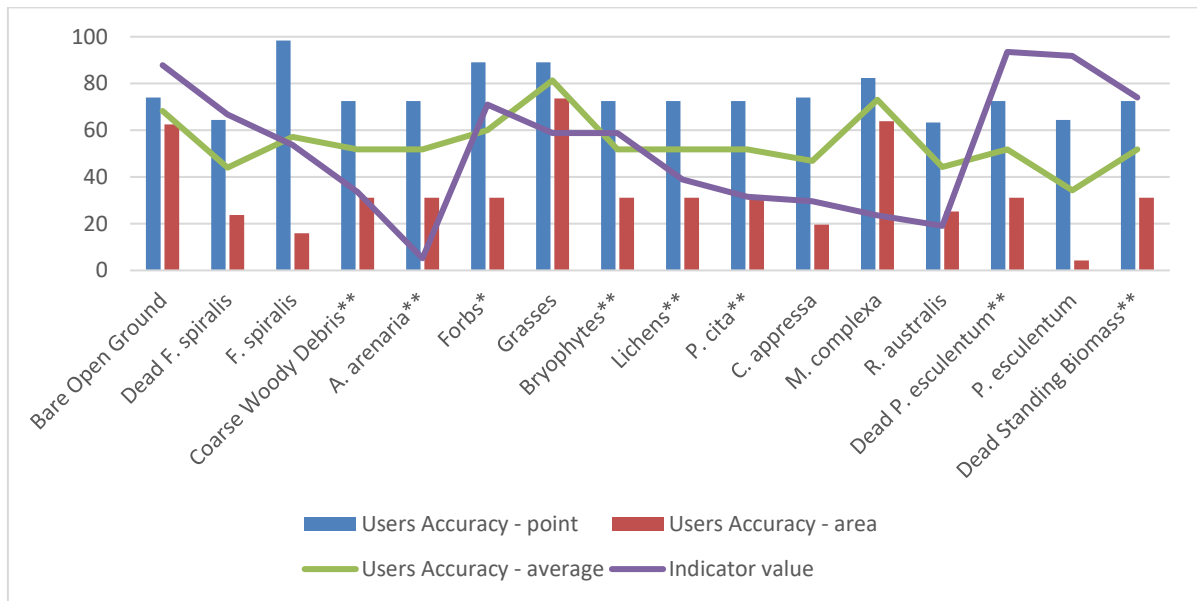
Figure 24. Significant indicator species from plot-based field community and User's accuracy based on point assessment, area assessment and the average of the two methods.
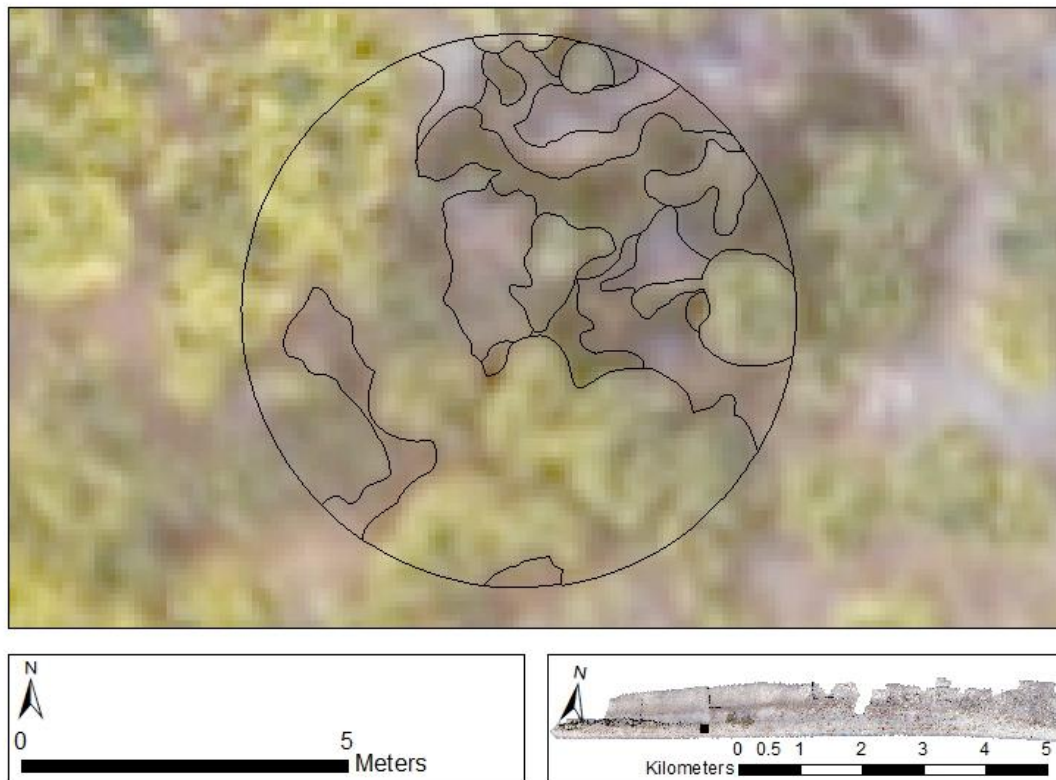
Figure 25. Designation of the boundaries between perceived image cover classes was challenging.

Table 37 Significant indicator species from plot-based field community data with the User's accuracy for each class from the point and area-based accuracy assessment, and the average of the two measures. When the cover class was not detected directly via UAS image classification, the total average accuracy of all classes was used as indicated by *.

Cluster	Ground Cover Class	Indicator value	Users Accuracy - point	Users Accuracy - area	User Accuracy - Average
1	Bare Open Ground	0.8783	74.00%	62.45%	68.23%
	Dead *F. spiralis*	0.6674	64.33%	23.66%	44.00%
	F. spiralis	0.5367	98.33%	15.89%	57.11%
	Coarse Woody Debris*	0.3358	72.48%*	31.16%*	51.82%*
	*A. arenaria**	0.0521	72.48%*	31.16%*	51.82%*
2	Forbs*	0.7097	72.48%*	31.16%*	51.82%*
	Grasses	0.5881	89.00%	73.62%	81.31%
	Bryophytes*	0.5874	72.48%*	31.16%*	51.82%*
	Lichens*	0.3887	72.48%*	31.16%*	51.82%*
	*P. cita**	0.315	72.48%*	31.16%*	51.82%*
	C. appressa	0.2966	74.00%	19.62%	46.81%
	M. complexa	0.2353	82.33%	63.84%	73.09%
	R. australis	0.1899	63.33%	25.24%	44.29%
3	Dead *P. esculentum**	0.9349	72.48%*	31.16%*	51.82%*
	P. esculentum	0.9183	64.33%	4.22%	34.28%

		Dead Standing Biomass*	0.7402	72.48%*	31.16%*	51.82%*

4.2.2 Factors affecting accuracy

The main sources of error for the image classification results in this study came from errors in the methodology of data collection and processing. Issues with the initial UAS image data quality and the post-processing steps carried out in an attempt to rectify them were outlined in section 2.3.1. In the following section a more detailed discussion of the sources and implications of these errors.

Image quality

Upon first assessment of the imagery, distinct spectral and spatial distortion of the data were apparent. Spectral distortion (spectral accuracy) can include variation in image colour, contrast and brightness. Many factors can contribute towards spectral error, such as atmospheric effects, the perspective and positioning (e.g. altitude and velocity) of the sensor optics, the degree of motion and stability of the sensor and sensor platform, and terrain relief (Conlin et al., 2018). Spatial distortion (spatial accuracy) refers to the degree of accuracy in the exact positioning of pixels in an image.

Many of the data quality issues may be related to the methodologies involved in the image capture. Two separate capture events at Kaitorete Spit were used in order to maximise the spatial coverage of the limited amount of GCPs that were available for use. The eastern side was flown first with relatively optimal GCP coverage. The western side was flown later in the day and without proper GCP coverage. In remote sensing, GCPs are of particular importance in UAS studies, as the onboard GPS positioning systems of UAS compared to other systems is of relatively poor accuracy (Duffy et al., 2018). The decision to split the site into the two flights to maximise GCP coverage was due to the significant gains in accuracy from using a higher density of GCPs (Agüera-Vega, Carvajal-Ramírez, & Martínez-Carricondo, 2017). However, proper GCP coverage i.e. complete and stratified distribution has been shown to be important for increasing the accuracy of UAS imagery (K. L. Cook, 2017; Martinez-Carricondo et al., 2018). It should be noted that the decision to fly the second half of the flights without proper GCP coverage was the professional decision of Hawkeye UAV. Proof of this was conveniently captured via a RQ-84Z Photogrammetry UAS by Hawkeye UAV at around 200 m above sea level (Figure 26).

The split capture events and lack of proper GCP coverage likely significantly contributed to the amount of spectral and spatial distortion. Timing image capture events to be as close as possible is important for minimising the amount of spectral variability from changes in the environmental

conditions (Duffy et al., 2018). For example the amount of wind, the presence of water in the atmosphere or as water-based surfaces, and the position of the sun as a degree of showing and light intensity can all affect accuracy in remote sensing (Aber, Marzolff, & Ries, 2010; Husson et al., 2016). Duffy et al. (2018) state that the complex winds that come about from differences in land and sea temperature should be strongly considered when operating UAS in coastal areas.

The difference in image appearance and quality between the western and eastern halves of the images is present in both the RGB and NIR imagery. For the RGB images, the eastern side is marred by multiple areas of image warping, distinct changes in image contrast, as well as issues with incomplete data coverage. The western side does not display such significant errors in image distortion, although issues of spectral distortion in the form of image 'banding' from differences in contrast in colour do exist. Alterations to the UAS between the two sides resulted in a slight shadowing on the western imagery due to the positioning of the camera on the mount. The issues of image warp and tearing most likely came from incomplete coverage of GCPs. Any pre-processing georeferencing would have resulted in larger shifts in image data around the physical GCPs, whereas areas where the data were georeferenced against the point cloud likely received a smoother, yet less spatially accurate translation.
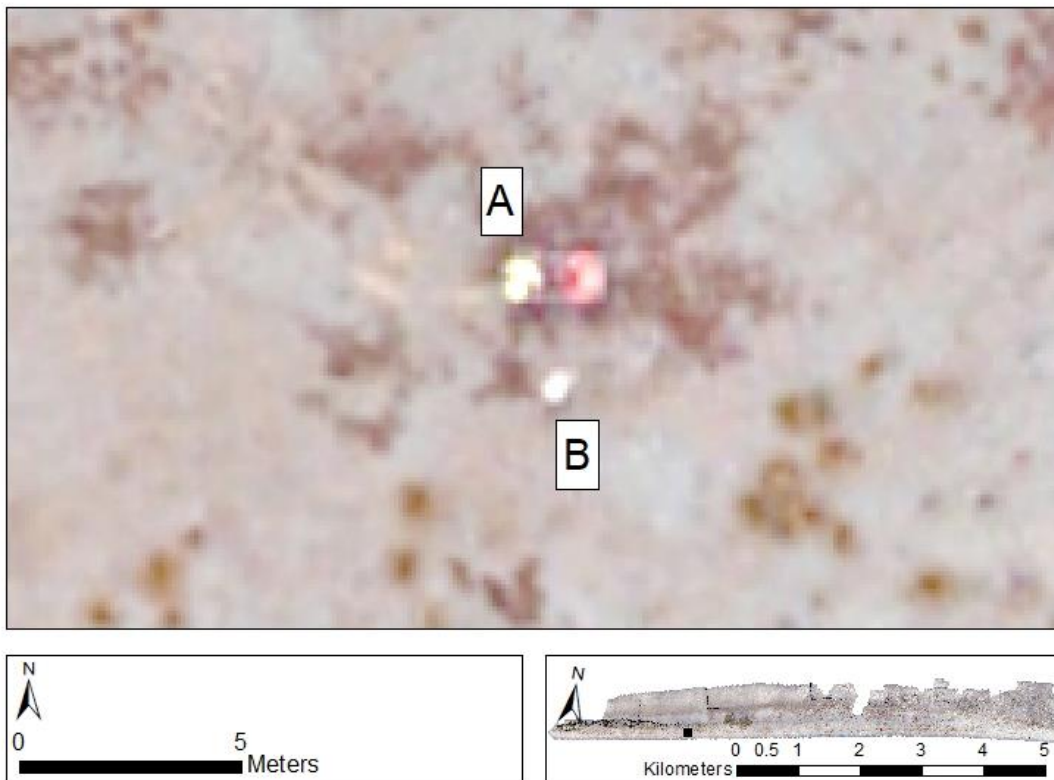
Figure 26. GCPs (A) on the back of a quad bike and in the process of being laid out by the author (B).

Spectral variation and classification training data

Where possible, the training data used for the classifications followed the recommended methodologies from Foody et al. (2006). The aforementioned spectral discrepancies, as well as the relatively large area of the study, meant that creating a truly representative sample was quite challenging. The aim of classification training is to create the smallest possible training sample that accurately represents a cover class yet also minimises the with-in class spectral variation. Over such a large area, there likely exists cover classes or species that were present yet either not detected in the imagery (see section 4.1.3), or not detected in both the field and remote sensing data. When in situations such as this where the object(s) of interest are individual species rather than broad community types, traditional supervised techniques may be of limited use (Foody et al., 2006), as these techniques assume that the set of classes within the images have been comprehensively defined (Congalton & Green, 2008). Poorly defined classes or even those not defined at all, can lead to substantial classification errors in the resultant products (G. Foody, 2002).

The less-than-satisfactory geopositioning errors in the imagery would have more than likely significantly affected the accuracy of the classifications. The separate capture of the NIR and RGB imagery using two different sensors also resulted in the two data sets not displaying a direct pixel-to-pixel spatial overlay. The two datasets were processed independently, in that different image spectral and spatial translations were applied to each dataset; subsequently, errors in one dataset did not occur in the other. While a reduction in total error may seem like a desirable goal, unless an exact match between the NIR and RGB data is achieved, the resulting data will have higher spectral variation within image pixel or object class. This error was likely further exacerbated by the choice of georeferencing translation used in the current study. Spline transformations are known as an example of a 'rubber sheeting' method, in that they do not apply an equal shift to every pixel. Transformation or movement of pixels is higher in areas in close proximity to GCPs, and less so, for areas further away; this allows for a higher degree of local spatial accuracy at the cost of a higher spectral discrepancy in other areas. The different effects of, and methods for correcting various geospatial errors can be found in (Aspinall, Marcus, & Boardman, 2002), however spatial discrepancies between image objects and known validation points are a significant source of classification errors (Underwood et al., 2007).

4.2.3 Techniques to improve accuracy

Fuzzy clustering is a classification technique that assigns a probability that a given pixel or object belongs to any given class (Zadeh, 1965). Fuzzy clustering has been shown to be effective in areas of high heterogeneity, where broad classes and coarse-scale pixels can show high within class spectral

variation (Rapinel et al., 2018). Amiri, Solaimani, and Miryaghoubzadeh (2013) found that Fuzzy Classification was useful in areas with gradual or fine-scale differences between community types. When compared to MLC, Fuzzy Clustering has been shown to be more accurate (Wang, 1990) and have faster processing times (Amiri et al., 2013). Foody (1996) states that Fuzzy Classifications may enable a more realistic representation of land and vegetation cover. Such techniques may be of use for monitoring of Kaitorete Spit as its vegetation communities are characterised by fine-scale features and changes within a highly heterogeneous environment.

Many examples of the use of additional environmental data such as topography to aid in vegetation classification exist in the recent literature. Baena et al. (2017) used UAS multispectral data and photogrammetric point clouds to achieve an overall classification accuracy of 94.10%. The study, however, was in low-density Peruvian dry forest, and clear delineation of trees was easily achieved. When used for monitoring smaller vegetation at mixed densities, the accuracies of photogrammetric point clouds can be reduced. K. L. Cook (2017) used a low-cost UAS to study the structure of the Daan River gorge in Taiwan. The author found that when in low-densities, grasses and shrubs could not be detected by SFM techniques. High-density vegetation presented another issue, however, in that the SFM methods were returning points from below the canopy yet above the ground. The detection of small-scale variation in surfaces could be improved by increasing image sampling, however, this significantly increases processing time and the noise within the resulting point cloud. Conlin et al. (2018) assessed multiple different UAS and remote sensing techniques in modelling the structural components of coastal dune systems. The authors conclude that an increase in spatial resolution would have likely increased the ability of the SFM techniques to distinguish image features. Strong evidence for this comes from Fraser et al. (2016), who used extremely high spatial resolution RGB imagery (0.0075 m) of artic scrublands to generate a point cloud that was capable of detecting a change in vegetation height of between 10 cm and 30 cm. In Conlin et al. (2018), the structural complexity of dunes and spatial variation in vegetation density and height resulted in reduced accuracy of SFM surface models. This was due to the need for an increase flight height for capturing accurate dune imagery, and lack of existing methodologies for accurately determining individual vegetation heights.

The benefits and advantages of hyperspectral data in remote sensing are both well known and widely available in the scientific literature and such will not be discussed at length in comparison to the present study. As a brief overview however: hyperspectral data allows for single-species mapping in a multispecies environment (Neumann, Itzerott, Weiss, Kleinschmit, & Schmidtlein, 2016), and therefore could be of use for delineating those species indicative of the dune hollows and other fine-scale habitat features at Kaitorete. Increased spectral resolution also aids in the differentiation of invasive species (He et al., 2011; Mullerova, Pergl, & Pysek, 2013; Skowronek et

al., 2017), especially so when they have distinct phenological stages (Ouyang et al., 2013). Using hyperspectral data, more informative studies of specific species can be conducted, such as differentiating between plant age (Knox et al., 2013) and successional/reproductive stage (Carvalho et al., 2013). These methodologies could potentially be of use for fine-scale monitoring of community health, particularly in regards to recovery from disturbance events, or to ascertain information regarding population age structure.

4.3 Conclusions and recommendations

This thesis research sought to evaluate the use of UAS based remote sensing imagery for the monitoring and management of the coastal dune plant communities at Kaitorete Spit. UAS derived, high resolution, multi-spectral imagery was collected, processed and classified into 12 different major cover classes at, for the most part, the individual species level. These data were then used in a study of the plant communities at the site, from which distinct ecological zones were able to be distinguished. Field-based studies of plant community composition were undertaken and then used as a direct comparison to the GIS-based data in a somewhat second-order ground-truthing of the data.

The suitability and applicability of the results of this study towards the monitoring of the dunes at Kaitorete Spit are somewhat mixed. The dune environment and the communities that lay within this area are structurally and ecologically complex as well as diverse. For effective management of such a site, the scale and type of ecological management and monitoring needs to change with the natural scale of those systems and key components to be studied. The main conclusions of this study are as follows:

The specific methodologies of this study resulted in a generalised measure of the plant communities, with an ability to correctly identify some, but not all, key species. The ability to directly monitor species, such as pīngao, *M. complexa* and *C. appressa,* provides a valuable conservation tool in and of itself, but also allows for the potential indirect monitoring of the types and amount of habitat available for other species living at the site, such as native lizards and invertebrates. Monitoring invasive species, such as *L. arboreus* was also possible, however, the specific management practices in use at Kaitorete Spit likely affected its overall detectability.

The UAS data were not able to detect fine-scale community compositional changes and features with any acceptable form of accuracy. The high heterogeneity of the landscape features of Kaitorete Spit provide some of the most valuable outcomes in terms of biodiversity. This complexity, however, makes the detection and modelling of these key habitats challenging via UAS imagery based on the methods used in this study.

There were significant sources of error in the final classifications and subsequent comparisons of the GIS and field data:

A lack of proper GCPs during image acquisition meant there was poor confidence in final geospatial positioning.

Using two separate capture events resulted in significant spectral discrepancies within and between the two halves of the site.

Using two separate sensors for the capture of the NIR and RGB data, in combination with the geospatial issues, resulted in significant and independent spectral distortion and a lack of an acceptable overlay between the two data types. This resulted in a significantly large within-class spectral variation that likely reduced classification accuracies.

Issues with the specific GPS unit used in the field data acquisition meant that the field sites could not be accurately located, reducing the strength of the comparisons between it and the GIS community data.

Based on these results and the data available with the methodologies used in this thesis, the following recommendations are made:

Due to the spectral distortions and discrepancies of the NIR imagery, these should be excluded from use in any image classifications based on these data.

Fuzzy classification methods may be more suitable for use with the spatial and spectral resolutions used in this study. These may prove to be more suited for the highly complex vegetation environments that dominate the dunes.

If this study were to be repeated, then the design of the field sampling should be altered to better reflect those of previous studies of the vegetation at Kaitorete Spit. The sampling sizes used in this study were more effective over a larger area; therefore increasing sampling coverages will likely increase the ability to discern meaningful community results for comparison. The size of the GIS sampling window can be changed to match any that can be done in the field.

If further studies of the application of UAS in the monitoring of the dunes at Kaitorete Spit are to be carried out, then the following recommendations are made:

The collection of UAS imagery should be treated like any other method of ecological data acquisition in that they should be tailored to specific conservation and management goals.

Methods to increase the spatial resolution of the data should be employed to enable detection of the various fine-scale habitat features.

In summary, the main benefits of these data are dependent of the different conservation and management needs of those who are responsible for the long-term management of the site. Aerial imagery is of most use to those who have intrinsic knowledge of the site. In many other studies, expert knowledge was key in the successful collection and implementation of aerial data. These data are in no way a replacement for field-based monitoring efforts, but rather serve best to augment the management practices instead. UAS can provide a new type of data that should be integrated into traditional methods. This is because while we can provide using this technology data at smaller and smaller scales, these may not always be of use. The cost-benefit ratio of these sources of data should be considered before they are widely applied to a range of habitats and ecosystems.

Lastly, the results of this study also support the need for more interdisciplinary communication between ecologists and remote sensing professionals. In this study, field-based questions were applied to digitally sourced data, without much consideration for how well they would translate between the two. That being said, more studies such as these are crucial if we are to further our understanding of UAS as a tool for fine-scale ecological monitoring.

Appendix A

A.1 Georeferecing

Table A. 1 Spline Link table for final georeferencing operation

X1	Y1	X2	Y2
1568108	5146753	1568113	5146753
1566003	5146576	1566008	5146575
1566846	5147277	1566853	5147276
1567160	5147261	1567165	5147260
1567547	5146958	1567552	5146957
1566866	5146663	1566871	5146662
1565403	5146899	1565408	5146899
1563419	5146373	1563424	5146373
1565582	5146940	1565586	5146940
1566743	5147025	1566749	5147024
1566554	5146812	1566558	5146811
1565335	5146472	1565339	5146472
1565244	5146606	1565248	5146604
1566171	5147047	1566176	5147046
1565063	5146370	1565066	5146370
1564757	5146557	1564763	5146556
1564498	5146182	1564503	5146184
1564231	5146463	1564238	5146463
1564712	5146311	1564716	5146312
1564611	5146440	1564616	5146440
1564478	5146504	1564484	5146504
1564459	5146527	1564465	5146526
1568074	5146784	1568079	5146784
1568121	5146924	1568126	5146923
1568064	5146913	1568069	5146913
1567877	5147098	1567882	5147097
1567902	5147122	1567908	5147121
1567800	5147199	1567805	5147197
1565631	5146521	1565636	5146520
1565665	5146449	1565669	5146447
1565544	5146478	1565548	5146476
1565461	5146627	1565465	5146626
1565430	5146650	1565434	5146649
1565438	5146731	1565443	5146730
1565191	5146695	1565197	5146695
1565124	5146588	1565129	5146587
1563634	5146324	1563641	5146325

1563663	5146443	1563671	5146445
1563480	5146346	1563486	5146345
1563427	5146314	1563432	5146314
1563447	5146251	1563453	5146252
1563381	5146229	1563386	5146231
1563238	5146131	1563245	5146129
1563137	5146118	1563144	5146116
1562946	5146000	1562953	5145998
1562346	5146108	1562351	5146107
1562254	5146101	1562259	5146100
1563963	5146183	1563971	5146185
1563945	5146188	1563953	5146189
1563911	5146116	1563919	5146118
1563820	5146355	1563828	5146355
1563910	5146438	1563917	5146439
1563993	5146539	1564001	5146538
1564083	5146560	1564090	5146559
1564241	5146595	1564248	5146595
1564750	5146731	1564755	5146729
1564653	5146703	1564659	5146702
1564457	5146652	1564464	5146651
1564381	5146613	1564388	5146613
1564144	5146548	1564149	5146547
1564293	5146288	1564299	5146289
1564213	5146267	1564220	5146269
1564190	5146298	1564197	5146300
1563689	5146302	1563697	5146302
1563660	5146274	1563668	5146275
1563291	5145975	1563299	5145974
1563348	5146005	1563356	5146005
1562585	5145932	1562590	5145929
1562549	5145901	1562553	5145899
1562556	5145906	1562561	5145903
1562554	5145896	1562559	5145894
1562439	5145881	1562443	5145879
1562291	5145900	1562295	5145899
1562829	5146200	1562835	5146201
1562788	5146183	1562794	5146181
1562774	5146191	1562781	5146189
1562650	5146144	1562656	5146141
1562575	5146150	1562582	5146151
1562501	5146093	1562507	5146090
1563351	5146641	1563354	5146639
1563248	5146579	1563252	5146576
1561932	5145729	1561935	5145730
1561925	5145792	1561930	5145792

1561884	5145770	1561888	5145772
1561764	5145722	1561769	5145725
1561782	5145838	1561789	5145836
1561712	5145875	1561717	5145877
1561823	5145842	1561827	5145844
1562067	5146048	1562071	5146047
1562192	5146081	1562197	5146079
1567989	5146757	1567994	5146756
1568770	5146899	1568773	5146902
1568547	5147432	1568550	5147431
1568092	5147245	1568097	5147244
1568324	5147099	1568329	5147099
1566003	5146846	1566008	5146844
1566001	5146852	1566006	5146849
1565934	5146714	1565939	5146712
1563619	5146074	1563627	5146074
1563609	5146125	1563616	5146126
1563624	5146271	1563631	5146271
1566398	5146700	1566402	5146698
1565613	5146825	1565619	5146823
1565549	5146903	1565555	5146901
1564012	5146553	1564020	5146552
1563718	5146709	1563725	5146710
1566271	5147113	1566275	5147111
1566268	5147168	1566272	5147167
1566440	5146927	1566444	5146926
1568493	5146978	1568497	5146979
1568324	5146890	1568329	5146891
1568287	5146871	1568292	5146872
1568235	5146872	1568239	5146872
1568735	5147240	1568739	5147241
1568482	5146917	1568486	5146920
1568489	5146865	1568493	5146868
1568415	5146830	1568420	5146833
1568152	5147009	1568157	5147009
1568197	5147067	1568201	5147067
1567339	5146715	1567344	5146715
1567242	5147100	1567246	5147099
1562282	5146439	1562287	5146437
1562293	5146458	1562298	5146456
1562295	5146454	1562300	5146452
1562620	5146526	1562627	5146522
1562789	5146537	1562797	5146532
1562796	5146539	1562803	5146534
1562893	5146527	1562900	5146523
1563168	5146652	1563173	5146647

1563301	5146689	1563304	5146684
1563494	5146602	1563499	5146601
1563526	5146432	1563532	5146432
1562853	5146100	1562860	5146098
1562969	5146099	1562976	5146097
1563095	5146025	1563102	5146023
1563168	5146280	1563174	5146278
1562962	5146267	1562968	5146264
1561984	5145780	1561988	5145781
1561978	5145778	1561982	5145779
1561963	5145772	1561966	5145773
1561998	5145786	1562002	5145787
1561779	5145752	1561783	5145755
1561882	5145820	1561886	5145821
1561952	5145823	1561956	5145824
1562016	5145855	1562020	5145855
1562002	5145914	1562006	5145915
1561823	5145999	1561828	5145999
1561940	5146292	1561946	5146289
1563050	5145943	1563057	5145941
1563079	5145954	1563085	5145952
1563110	5145965	1563116	5145963
1563135	5145944	1563142	5145943
1563194	5146035	1563201	5146033
1563188	5146040	1563195	5146038
1563199	5145988	1563206	5145987
1562718	5146066	1562724	5146063
1562692	5146047	1562698	5146044
1562244	5145836	1562247	5145834
1562215	5145818	1562218	5145817
1562382	5145833	1562386	5145831
1562319	5145806	1562322	5145804
1562093	5145768	1562097	5145769
1562087	5145772	1562091	5145772
1562422	5145824	1562426	5145821
1562957	5145935	1562963	5145933
1562857	5145961	1562863	5145959
1562861	5145962	1562867	5145959
1562908	5145915	1562914	5145912
1566568	5146582	1566573	5146582
1566546	5146579	1566550	5146578
1566467	5146636	1566471	5146636
1566392	5146597	1566397	5146596
1566254	5146580	1566258	5146579
1566176	5146595	1566180	5146594
1565742	5146671	1565747	5146669

1565748	5146978	1565755	5146974
1567202	5146832	1567208	5146831
1567759	5146781	1567763	5146781
1567386	5146784	1567392	5146784
1567918	5146855	1567922	5146855
1567915	5146779	1567919	5146779
1567604	5146705	1567609	5146706
1567622	5146692	1567627	5146693
1567717	5146711	1567721	5146712
1567776	5146728	1567779	5146729
1567790	5146723	1567794	5146724
1567810	5146733	1567814	5146734
1567840	5146771	1567843	5146771
1567601	5146863	1567606	5146863
1567591	5146855	1567596	5146856
1567922	5146738	1567926	5146739
1567958	5146798	1567962	5146798
1567985	5146830	1567989	5146830
1568013	5146845	1568017	5146845
1568070	5146845	1568074	5146844
1567143	5146649	1567148	5146649
1567059	5146635	1567065	5146635
1566976	5146670	1566981	5146670
1566900	5146656	1566905	5146655
1566899	5146685	1566904	5146684
1566691	5146707	1566696	5146706
1566689	5146652	1566693	5146651
1566692	5146660	1566696	5146659
1566951	5146961	1566957	5146960
1566914	5146978	1566920	5146977
1566930	5146847	1566936	5146846
1566919	5146842	1566925	5146840
1564842	5146383	1564846	5146383
1565274	5146407	1565277	5146407
1565221	5146387	1565225	5146387
1565093	5146375	1565097	5146375
1564608	5146344	1564612	5146345
1564530	5146336	1564534	5146338
1564398	5146290	1564403	5146292
1564334	5146216	1564340	5146218
1564343	5146194	1564349	5146197
1564134	5146132	1564142	5146135
1564199	5146144	1564206	5146147
1564220	5146157	1564227	5146159
1564279	5146153	1564286	5146156
1563474	5145999	1563482	5145999

1563364	5146132	1563370	5146131
1563510	5146142	1563517	5146142
1563787	5146118	1563795	5146119
1563728	5146181	1563735	5146182
1564378	5146501	1564384	5146500
1564891	5146263	1564894	5146263
1564857	5146254	1564861	5146255
1564564	5146263	1564568	5146265
1564476	5146255	1564481	5146257
1563733	5146058	1563741	5146059
1564171	5146359	1564178	5146359
1563431	5146167	1563438	5146166
1561885	5146215	1561891	5146213
1562698	5145877	1562703	5145874
1562739	5145890	1562744	5145887
1562787	5145903	1562793	5145900
1562784	5145908	1562790	5145905
1562610	5145859	1562615	5145856
1562593	5145869	1562598	5145866
1562669	5145892	1562674	5145889
1562508	5145857	1562512	5145854
1562342	5145945	1562346	5145943
1562239	5146023	1562243	5146020
1562316	5146041	1562321	5146038
1562163	5145956	1562167	5145954
1562524	5145953	1562529	5145950
1562887	5146017	1562893	5146014
1563387	5145982	1563395	5145981
1563423	5145979	1563431	5145979
1563461	5146079	1563469	5146079
1566231	5146494	1566236	5146493
1566254	5146499	1566258	5146499
1566133	5146534	1566137	5146533
1566091	5146574	1566095	5146572
1566130	5146587	1566134	5146585
1566164	5146631	1566168	5146629
1566203	5146651	1566207	5146649
1566055	5146690	1566059	5146687
1565842	5146530	1565847	5146528
1565448	5146352	1565450	5146350
1565959	5146453	1565964	5146452
1566023	5146451	1566028	5146450
1566108	5146638	1566113	5146636
1566088	5146664	1566092	5146661
1567792	5147314	1567797	5147312
1568105	5147162	1568110	5147161

1567770	5146769	1567774	5146769
1567346	5146829	1567351	5146829
1567307	5146820	1567312	5146819
1567249	5146796	1567255	5146795
1567161	5146762	1567167	5146761
1565589	5146442	1565593	5146440
1565226	5146550	1565230	5146549
1565002	5146470	1565006	5146469

A.2 Convolution Functions

Table A. 2 'Smoothing 3x3' filter kernel

	C0	C1	C2
R0	1	2	1
R1	2	4	2
R3	1	2	1

Table A. 3 'Sharpen 3x3' filter kernel

	C0	C1	C2
R0	-1	-1	-1
R1	-1	9	-1
R3	-1	-1	-1

Table A. 4 'Laplacian 3x3' filter kernel

	C0	C1	C2
R0	0	-1	0
R1	-1	4	-1
R3	0	-1	0

Table A. 5 'Sobel Horizontal 3x3' filter kernel

	C0	C1	C2
R0	-1	-2	1
R1	0	0	0
R3	1	2	1

Table A. 6 'Sobel Vertical 3x3' filter kernel

	C0	C1	C2
R0	-1	0	1
R1	-2	0	2
R3	-1	0	1

A.3 Classification results

Table A. 7 Point based accuracy confusion matix of classification results. Green cells indicate correctly classified pixels. 1 = *L. arboreus*, 2 = *M. complexa*, 3 = *P. radiata,* 4 = Dead *P. radiata*, 5 = *F. spiralis*, 6 = Dead *F. spiralis*, 7 = Bare Open Ground, 8= Grasses, 9 = *C. appressa*, 10 = *R. australis*, 11 = *P. esculentum*

	Classified Image											
Ground Truth	1	2	3	4	5	6	7	8	9	10	11	Grand Total
1	104	22		6		1	24	24	33	6	80	300
2	2	247	6		4	4		1			36	300
3		60	205			1	10		23		1	300
4				254		24	1	14	7			300
5		1			295		1	2	1			300
6		24	3	34		193	1	45				300
7				16		2	222	60				300
8		3		4	12	10	3	267		1		300
9	55	5			6			4	222		8	300
10	34			21		16	38			190	1	300
11		52	3	4	1	8		5	34		193	300
Grand Total	195	414	217	339	318	259	300	422	320	197	319	3300

Table A. 8 Area based accuracy confusion matix of classification results. Green cells indicate correctly classified pixels. 1 = *L. arboreus*, 2 = *M. complexa*, 3 = *P. radiata,* 4 = Dead *P. radiata*, 5 = *F. spiralis*, 6 = Dead *F. spiralis*, 7 = Bare Open Ground, 8= Grasses, 9 = *C. appressa*, 10 = *R. australis*, 11 = *P. esculentum*

Ground Truth	Classification Result											Grand Total
	1	2	3	4	5	6	7	8	9	10	11	
1	1609	5749		51	513	40	553	3845	5150	92	3047	20649
2		9777	155	108	790	545	117	3196	225		402	15315
3		776	395			12					63	1246
4		944	3	782		2808	10	746			7	5300
5		210		399	2457	753	6099	5377	140		25	15460
6		358	20	760	14	1726	1273	3124	2	8	10	7295
7		268		2006	26	2033	40443	19877	14	48	46	64761
8		2228	4	938	1394	2188	3793	30289	172	2	137	41145
9	24	875		33	659	164	231	3804	1450	26	125	7391
10				41		20	457	27		184		729
11		667		169		494		190			67	1587

Grand Total	1633	21852	577	5287	5853	10783	52976	70475	7153	360	3929	180878

Table A. 9. Accuracy assessment results from classification method testing across the three test sites.

Image	Classification	Assessment type	Measure	Site 1	Site 2	Site 3
RGBNIR+SR	SVM	Area	Kappa	27.9%	26.3%	62.7%
			Overall	43.2%	39.1%	76.4%
		Point	Kappa	77.6%	60.2%	83.0%
			Overall	80.4%	64.6%	85.1%
	MLC	Area	Kappa	49.4%	47.2%	58.0%
			Overall	58.9%	61.7%	71.0%
		Point	Kappa	85.4%	52.1%	86.4%
			Overall	87.3%	57.4%	88.1%
	ISO	Area	Kappa	24.9%	28.1%	31.5%
			Overall	28.4%	31.7%	29.9%
		Point	Kappa	30.0%	25.2%	30.7%
			Overall	35.0%	32.8%	42.8%
RGBNIR+NIR	SVM	Area	Kappa	48.1%	41.8%	84.6%
			Overall	58.0%	59.2%	86.5%
		Point	Kappa	77.6%	66.9%	83.0%
			Overall	80.4%	70.4%	85.1%
	MLC	Area	Kappa	48.7%	43.8%	55.4%
			Overall	58.3%	58.4%	68.5%
		Point	Kappa	84.3%	76.1%	62.7%
			Overall	86.3%	78.8%	76.4%
	ISO	Area	Kappa	22.6%	18.8%	21.5%
			Overall	26.8%	27.6%	25.2%
		Point	Kappa	24.1%	27.1%	33.0%
			Overall	34.4%	30.1%	34.4%
RGBNIR+SR+NDVI	SVM	Area	Kappa	48.7%	47.6%	59.3%
			Overall	58.4%	62.2%	72.4%
		Point	Kappa	7.1%	78.0%	86.6%
			Overall	18.8%	80.4%	88.3%
	MLC	Area	Kappa	50.5%	41.8%	62.7%
			Overall	60.3%	59.2%	76.4%
		Point	Kappa	77.6%	68.1%	83.0%
			Overall	80.4%	71.6%	85.1%
	ISO	Area	Kappa	16.8%	25.0%	25.8%
			Overall	20.6%	28.8%	27.5%
		Point	Kappa	27.4%	26.7%	19.4%
			Overall	30.0%	31.7%	22.0%
RGBNR	SVM	Area	Kappa	48.9%	41.5%	49.9%
			Overall	58.4%	55.4%	63.0%
		Point	Kappa	85.4%	79.0%	84.9%

			Overall	87.3%	81.3%	86.8%
	MLC	Area	Kappa	77.6%	41.8%	62.7%
			Overall	80.4%	59.2%	76.4%
		Point	Kappa	37.9%	68.1%	83.0%
			Overall	48.7%	71.6%	85.1%
	ISO	Area	Kappa	21.6%	18.5%	22.4%
			Overall	24.5%	20.3%	24.1%
		Point	Kappa	21.7%	12.7%	29.4%
			Overall	25.0%	17.3%	30.6%

Table A. 10 Class specific classification accuracies from the point based accuracy measures.

Class	Comission	Omission	Users Accuracy	Producers Accuracy
L. arboreus	100.51%	30.33%	34.67%	53.33%
M. complexa	11.11%	55.67%	82.33%	59.66%
P. radiata	43.78%	4.00%	68.33%	94.47%
Dead *P. radiata*	13.57%	28.33%	84.67%	74.93%
F. spiralis	1.57%	7.67%	98.33%	92.77%
Dead *F. spiralis*	41.31%	22.00%	64.33%	74.52%
Bare Open Ground	26.00%	48.33%	74.00%	74.00%
Grasses	7.82%	51.67%	89.00%	63.27%
C. appressa	24.38%	32.67%	74.00%	69.38%
R. australis	55.84%	2.33%	63.33%	96.45%
P. esculentum	33.54%	42.00%	64.33%	60.50%
Average	32.68%	29.55%	72.48%	73.93%
Max	100.51%	55.67%	98.33%	96.45%
Min	1.57%	2.33%	34.67%	53.33%

Table A. 11 Class specific classification accuracies from the area based accuracy measures.

Class	Comission	Omission	Producers Accuracy	Users Accuracy
L. arboreus	92.21%	1.47%	98.53%	7.79%
M. complexa	36.16%	55.26%	44.74%	63.84%
P. radiata	68.30%	31.54%	68.46%	31.70%
Dead *P. radiata*	85.25%	85.21%	14.79%	14.75%
F. spiralis	84.11%	58.02%	41.98%	15.89%
Dead *F. spiralis*	76.34%	83.99%	16.01%	23.66%
Bare Open Ground	37.55%	11.44%	76.34%	62.45%
Grasses	26.38%	57.02%	42.98%	73.62%
C. appressa	80.38%	79.73%	20.27%	19.62%
R. australis	74.76%	48.89%	51.11%	25.24%
P. esculentum	95.78%	98.29%	1.71%	4.22%

A.4 TWINSPAN

Table A. 12 Indicator Species Analysis results for the field data at the quadrat level

	1	2	3
A. arenaria	0.05	.	.
Bare Open Ground	0.88	0.06	.
Bryophytes	.	0.59	0.1
C. appressa	.	0.3	.
Coarse Woody Debris	0.34	0.05	.
Dead *F. spiralis*	0.67	.	.
Dead *L. arboreus*	0.07	.	.
Dead *P. esculentum*	.	.	0.93
Dead Standing Biomass	0.16	0.06	0.74
F. spiralis	0.54	.	.
Forbs	0.09	0.71	0.08
Grasses	0.14	0.59	0.17
Lichens	0.13	0.39	.
L. arboreus	0.07	.	.
M. alpinus	.	0.06	.
M. complexa	.	0.24	0.08
P. cita	.	0.32	.
P. esculentum	.	.	0.92
R. australis	.	0.19	.

Table A. 13 Indicator Species Analysis results for the field data at the plot level

	1	2	3
A. arenaria	0.06	.	.
Bare Open ground	0.73	0.12	0.08
Bryophytes	.	0.45	0.21
C. appressa	.	0.69	.
Coarse Woody Debris	0.36	.	0.27
Dead *C. appressa*	.	0.14	.
Dead *F. spiralis*	0.77	.	.
Dead *L. arboreus*	0.15	.	0.14
Dead *P. cita*	.	0.1	.
Dead *P. esculentum*	.	.	0.99
Dead *R. australis*	0.08	.	.
Dead Standing Biomass	0.26	.	0.69
F. spiralis	0.73	.	.
Forbs	0.09	0.53	0.33
Grasses	0.16	0.52	0.32
Lichens	0.2	0.48	.
L. arboreus	0.18	.	0.22

M. alpinus	.	0.17	.
M. complexa	.	0.1	0.21
P. prostrata	.	0.11	.
P. cita	.	0.7	.
P. esculentum	.	.	0.86
R. australis	.	0.42	.

Table A. 14 Indicator Species Analysis results for the GIS 0.1 m data at the quadrat level

	1	2	3	4
C. appressa	.	0.09	0.82	.
Coarse Woody Debris	0.08	.	.	.
Dead *F. spiralis*	0.14	.	.	.
F. spiralis	.	.	.	0.06
Grasses	0.12	0.44	0.09	0.28
L. arboreus	.	.	0.71	.
M. complexa	.	0.06	0.3	0.57
Bare Open Ground	0.67	.	0.12	.
P. radiata	.	0.59	0.16	.
P. esculentum	.	.	0.65	0.07
R. australis	.	0.05	.	0.07
Standing Dead Matter	0.19	.	.	0.35

Table A. 15 Indicator Species Analysis results for the GIS 0.1 m data at the plot level

	1	2	3	4
C. appressa	.	0.07	0.81	.
Coarse Woody Debris	0.25	0.06	.	.
Dead *F. spiralis*	.	.	.	0.95
Grasses	0.2	0.37	0.37	0.05
L. arboreus	.	.	0.31	.
M. complexa	.	0.69	0.2	0.06
Bare Open Ground	0.86	.	0.08	.
P. radiata	0.12	.	0.77	.
P. esculentum	0.1	0.28	0.25	0.1
R. australis	0.13	0.14	.	.
Standing Dead Matter	.	0.11	.	0.8

References

Aber, J. S., Marzolff, I., & Ries, J. (2010). *Small-format aerial photography: Principles, techniques and geoscience applications*: Elsevier.

Agüera-Vega, F., Carvajal-Ramírez, F., & Martínez-Carricondo, P. (2017). Assessment of photogrammetric mapping accuracy based on variation ground control points number using unmanned aerial vehicle. *Measurement, 98*, 221-227. doi:https://doi.org/10.1016/j.measurement.2016.12.002

Albuquerque, M. D., Alves, D. C. L., Espinoza, J. M. D., Oliveira, U. R., & Simoes, R. S. (2018). Determining Shoreline Response to Meteo-oceanographic Events Using Remote Sensing and Unmanned Aerial Vehicle (UAV): Case Study in Southern Brazil. *Journal of Coastal Research*, 766-770. doi:10.2112/si85-154.1

Alexander, C., Korstjens, A. H., Hankinson, E., Usher, G., Harrison, N., Nowak, M. G., . . . Hill, R. A. (2018). Locating emergent trees in a tropical rainforest using data from an Unmanned Aerial Vehicle (UAV). *International Journal of Applied Earth Observation and Geoinformation, 72*, 86-90. doi:10.1016/j.jag.2018.05.024

Almeida-Neto, M., & Ulrich, W. (2011). A straightforward computational approach for measuring nestedness using quantitative matrices. *Environmental Modelling & Software, 26*(2), 173-178. doi:10.1016/j.envsoft.2010.08.003

Amiri, M., Solaimani, K., & Miryaghoubzadeh, M. (2013). Fuzzy Classification for Mapping Invasive Species from Multispectral Imagery. *Journal of the Indian Society of Remote Sensing, 41*(4), 749-755. doi:10.1007/s12524-013-0261-8

Anderson, K., & Gaston, K. J. (2013). Lightweight unmanned aerial vehicles will revolutionize spatial ecology. *Frontiers in Ecology and the Environment, 11*(3), 138-146. doi:10.1890/120150

Andrew, M. E., & Ustin, S. L. (2009). Habitat suitability modelling of an invasive plant with advanced remote sensing data. *Diversity and Distributions, 15*(4), 627-640. doi:10.1111/j.1472-4642.2009.00568.x

Andrews, B., Gares, P. A., & Colby, J. D. (2002). Techniques for GIS modeling of coastal dunes. *Geomorphology, 48*(1), 289-308. doi:https://doi.org/10.1016/S0169-555X(02)00186-1

Anteau, M. J., Wiltermuth, M. T., Sherfy, M. H., & Shaffer, T. L. (2014). Measuring and predicting abundance and dynamics of habitat for piping plovers on a large reservoir. *Ecological Modelling, 272*, 16-27. doi:10.1016/j.ecolmode1.2013.08.020

Aplin, P. (2005). Remote sensing: ecology. *Progress in Physical Geography, 29*(1), 104-113. doi:10.1191/030913305pp437pr

Arroyo, L. A., Pascual, C., & Manzanera, J. A. (2008). Fire models and methods to map fuel types: the role of remote sensing. *Forest Ecology and Management, 256*(6), 1239-1252.

Aspinall, R. J., Marcus, W. A., & Boardman, J. W. (2002). Considerations in collecting, processing, and analysing high spatial resolution hyperspectral data for environmental investigations. *Journal of Geographical Systems, 4*(1), 15-29.

Assesment, M. E. (2005). *Ecosystems and Human Well-being: Synthesis*. Washington: Island Press.

Baena, S., Moat, J., Whaley, O., & Boyd, D. S. (2017). Identifying species from the air: UAVs and the very high resolution challenge for plant conservation. *PLoS ONE, 12*(11), e0188714. doi:10.1371/journal.pone.0188714

Baldeck, C. A., & Asner, G. P. (2013). Estimating Vegetation Beta Diversity from Airborne Imaging Spectroscopy and Unsupervised Clustering. *Remote Sensing, 5*(5), 2057-2071. doi:10.3390/rs5052057

Barbosa, J. M., Sebastian-Gonzalez, E., Asner, G. P., Knapp, D. E., Anderson, C., Martin, R. E., & Dirzo, R. (2016). Hemiparasite-host plant interactions in a fragmented landscape assessed via imaging spectroscopy and LiDAR. *Ecological Applications, 26*(1), 55-66. doi:10.1890/14-2429

Barr, J. R., Green, M. C., DeMaso, S. J., & Hardy, T. B. (2018). Detectability and visibility biases associated with using a consumer-grade unmanned aircraft to survey nesting colonial waterbirds. *Journal of Field Ornithology, 89*(3), 242-257. doi:10.1111/jofo.12258

Bastos, A. P., Lira, C. P., Calvão, J., Catalão, J., Andrade, C., Pereira, A. J., . . . Correia, O. (2018). UAV Derived Information Applied to the Study of Slow-changing Morphology in Dune Systems. *Journal of Coastal Research, 85*(sp1), 226-230.

Baughman, C. A., Jones, B. M., Bodony, K. L., Mann, D. H., Larsen, C. F., Himelstoss, E., & Smith, J. (2018). Remotely Sensing the Morphometrics and Dynamics of a Cold Region Dune Field Using Historical Aerial Photography and Airborne LiDAR Data. *Remote Sensing, 10*(5). doi:10.3390/rs10050792

Bayer, D., Seifert, S., & Pretzsch, H. (2013). Structural crown properties of Norway spruce (Picea abies L. Karst.) and European beech (Fagus sylvatica L.) in mixed versus pure stands revealed by terrestrial laser scanning. *Trees-Structure and Function, 27*(4), 1035-1047. doi:10.1007/s00468-013-0854-4

Becker, R. H., Zmijewski, K. A., & Crail, T. (2013). Seeing the forest for the invasives: mapping buckthorn in the Oak Openings. *Biological Invasions, 15*(2), 315-326. doi:10.1007/s10530-012-0288-8

Benz, U. C., Hofmann, P., Willhauck, G., Lingenfelder, I., & Heynen, M. (2004). Multi-resolution, object-oriented fuzzy analysis of remote sensing data for GIS-ready information. *Isprs Journal of Photogrammetry and Remote Sensing, 58*(3-4), 239-258. doi:10.1016/j.isprsjprs.2003.10.002

Berg, P. J., & Smithies, C. W. (1973). Subsurface sowing of yellow lupin (Lupinus arboreus) for economical and rapid sand dune stabilization at Woodhill forest. *New Zealand Journal of Forestry, 18*(2), 285-293.

Bergstedt, J., Westerberg, L., & Milberg, P. (2009). In the eye of the beholder: bias and stochastic variation in cover estimates. *Plant Ecology, 204*(2), 271. doi:10.1007/s11258-009-9590-7

Borcard, D., Gillet, F., & Legendre, P. (2018). *Numerical Ecolgy with R* (2 ed.). Cham: Switzerland.

Bork, E. W., & Su, J. G. (2007). Integrating LIDAR data and multispectral imagery for enhanced classification of rangeland vegetation: A meta analysis. *Remote Sensing of Environment, 111*(1), 11-24. doi:https://doi.org/10.1016/j.rse.2007.03.011

Bradbury, R. B., Hill, R. A., Mason, D. C., Hinsley, S. A., Wilson, J. D., Balzter, H., . . . Bellamy, P. E. (2005). Modelling relationships between birds and vegetation structure using airborne LiDAR data: a review with case studies from agricultural and woodland environments. *Ibis, 147*(3), 443-452. doi:10.1111/j.1474-919x.2005.00438.x

Bradley, & Fleishman. (2008). Can Remote Sensing of Land Cover Improve Species Distribution Modelling? *Journal of Biogeography, 35*(7), 1158-1159. doi:10.2307/20143338

Bradley, A. V., Haughan, A. E., Al-Dughairi, A., & McLaren, S. J. (2019). Spatial variability in shrub vegetation across dune forms in central Saudi Arabia. *Journal of Arid Environments, 161*, 72-84. doi:https://doi.org/10.1016/j.jaridenv.2018.10.003

Breckenridge, R. P., Dakins, M., Bunting, S., Harbour, J. L., & Lee, R. D. (2012). Using Unmanned Helicopters to Assess Vegetation Cover in Sagebrush Steppe Ecosystems. *Rangeland Ecology & Management, 65*(4), 362-370. doi:10.2111/rem-d-10-00031.1

Breckenridge, R. P., Dakins, M., Bunting, S., Harbour, J. L., & White, S. (2011). Comparison of Unmanned Aerial Vehicle Platforms for Assessing Vegetation Cover in Sagebrush Steppe Ecosystems. *Rangeland Ecology & Management, 64*(5), 521-532. doi:10.2111/rem-d-10-00030.1

Brock, Pihur, Datta, & Datta. (2008). clValid: An R Package for Cluster Validation. *Journal of Statistical Software, 25*(4), 1-22.

Brownett, J. M., & Mills, R. S. (2017). The development and application of remote sensing to monitor sand dune habitats. *Journal of Coastal Conservation, 21*(5), 643-656. doi:10.1007/s11852-017-0504-x

Buermann, W., Saatchi, S., Smith, T. B., Zutta, B. R., Chaves, J. A., Mila, B., & Graham, C. H. (2008). Predicting species distributions across the Amazonian and Andean regions using remote sensing data. *Journal of Biogeography, 35*(7), 1160-1176. doi:10.1111/j.1365-2699.2007.01858.x

Burgheimer, J., Wilske, B., Maseyk, K., Karnieli, A., Zaady, E., Yakir, D., & Kesselmeier, J. (2006). Relationships between Normalized Difference Vegetation Index (NDVI) and carbon fluxes of

biologic soil crusts assessed by ground measurements. *Journal of Arid Environments, 64*(4), 651-669. doi:https://doi.org/10.1016/j.jaridenv.2005.06.025

CAA. (2018). Unmanned Aircraft.   Retrieved from https://www.caa.govt.nz/unmanned-aircraft

Cagney, J., Cox, S. E., & Booth, D. T. (2011). Comparison of Point Intercept and Image Analysis for Monitoring Rangeland Transects. *Rangeland Ecology & Management, 64*(3), 309-315. doi:https://doi.org/10.2111/REM-D-10-00090.1

Candiago, S., Remondino, F., De Giglio, M., Dubbini, M., & Gattelli, M. (2015). Evaluating Multispectral Images and Vegetation Indices for Precision Farming Applications from UAV Images. *Remote Sensing, 7*(4), 4026.

Carvalho, S., Schlerf, M., van der Putten, W. H., & Skidmore, A. K. (2013). Hyperspectral reflectance of leaves and flowers of an outbreak species discriminates season and successional stage of vegetation. *International Journal of Applied Earth Observation and Geoinformation, 24*, 32-41. doi:10.1016/j.jag.2013.01.005

Chabot, D., Dillon, C., Ahmed, O., & Shemrock, A. (2017). Object-based analysis of UAS imagery to map emergent and submerged invasive aquatic vegetation: a case study. *Journal of Unmanned Vehicle Systems, 5*(1), 27-33. doi:10.1139/juvs-2016-0009

Chabot, D., Dillon, C., Shemrock, A., Weissflog, N., & Sager, E. P. S. (2018). An Object-Based Image Analysis Workflow for Monitoring Shallow-Water Aquatic Vegetation in Multispectral Drone Imagery. *Isprs International Journal of Geo-Information, 7*(8). doi:10.3390/ijgi7080294

Charbonneau, B. R., Wootton, L. S., Wnek, J. P., Langley, J. A., & Posner, M. A. (2017). A species effect on storm erosion: Invasive sedge stabilized dunes more than native grass during Hurricane Sandy. *Journal of Applied Ecology, 54*(5), 1385-1394. doi:10.1111/1365-2664.12846

Chen, B., Yang, Y., Wen, H., Ruan, H., Zhou, Z., Luo, K., & Zhong, F. (2018). High-resolution monitoring of beach topography and its change using unmanned aerial vehicle imagery. *Ocean & Coastal Management, 160*, 103-116. doi:10.1016/j.ocecoaman.2018.04.007

Chen, G., Hay, G. J., Carvalho, L. M. T., & Wulder, M. A. (2012). Object-based change detection. *International Journal of Remote Sensing, 33*(14), 4434-4457. doi:10.1080/01431161.2011.648285

Chytry, M., Wild, J., Pysek, P., Jarosik, V., Dendoncker, N., Reginster, I., . . . Settele, J. (2012). Projecting trends in plant invasions in Europe under different scenarios of future land-use change. *Global Ecology and Biogeography, 21*(1), 75-87. doi:10.1111/j.1466-8238.2010.00573.x

Clark, M. L., Roberts, D. A., & Clark, D. B. (2005). Hyperspectral discrimination of tropical rain forest tree species at leaf to crown scales. *Remote Sensing of Environment, 96*(3-4), 375-398.

Clarke, K. R. (1993). Non-parametric multivariate analyses of changes in community structure. *Australian journal of ecology, 18*(1), 117-143.

Colomina, I., & Molina, P. (2014). Unmanned aerial systems for photogrammetry and remote sensing: A review. *Isprs Journal of Photogrammetry and Remote Sensing, 92*, 79-97. doi:http://dx.doi.org/10.1016/j.isprsjprs.2014.02.013

Congalton, R. G., & Green, K. (2008). *Assessing the accuracy of remotely sensed data: principles and practices*: CRC press.

Conlin, M., Cohn, N., & Ruggiero, P. (2018). A Quantitative Comparison of Low-Cost Structure from Motion (SfM) Data Collection Platforms on Beaches and Dunes. *Journal of Coastal Research, 34*(6), 1341-1357. doi:10.2112/jcoastres-d-17-00160.1

Cook, G. D., Meyer, C. P., Muepu, M., & Liedloff, A. C. (2016). Dead organic matter and the dynamics of carbon and greenhouse gas emissions in frequently burnt savannas. *International Journal of Wildland Fire, 25*(12), 1252-1263. doi:https://doi.org/10.1071/WF15218

Cook, K. L. (2017). An evaluation of the effectiveness of low-cost UAVs and structure from motion for geomorphic change detection. *Geomorphology, 278*, 195-208. doi:https://doi.org/10.1016/j.geomorph.2016.11.009

Corbane, C., Lang, S., Pipkins, K., Alleaume, S., Deshayes, M., García Millán, V. E., . . . Michael, F. (2015). Remote sensing for mapping natural habitats and their conservation status – New opportunities and challenges. *International Journal of Applied Earth Observation and Geoinformation, 37*, 7-16. doi:https://doi.org/10.1016/j.jag.2014.11.005

Corbi, H., Riquelme, A., Megias-Banos, C., & Abellan, A. (2018). 3-D Morphological Change Analysis of a Beach with Seagrass Berm Using a Terrestrial Laser Scanner. *Isprs International Journal of Geo-Information, 7*(7). doi:10.3390/ijgi7070234

Czerepowicz, L., Case, B. S., & Doscher, C. (2012). Using satellite image data to estimate aboveground shelterbelt carbon stocks across an agricultural landscape. *Agriculture Ecosystems & Environment, 156*, 142-150. doi:10.1016/j.agee.2012.05.014

Dash, J. P., Pearse, G. D., & Watt, M. S. (2018). UAV Multispectral Imagery Can Complement Satellite Data for Monitoring Forest Health. *Remote Sensing, 10*(8). doi:10.3390/rs10081216

Dassot, M., Constant, T., & Fournier, M. (2011). The use of terrestrial LiDAR technology in forest science: application fields, benefits and challenges. *Annals of Forest Science, 68*(5), 959-974. doi:10.1007/s13595-011-0102-2

Davis, M. (2002). *Kaitorete Spit resources and management report.* Retrieved from Christchurch, N.Z:

de Siqueira, M. F., Durigan, G., de Marco Júnior, P., & Peterson, A. T. (2009). Something from nothing: Using landscape similarity and ecological niche modeling to find rare plant species. *Journal for Nature Conservation, 17*(1), 25-32. doi:https://doi.org/10.1016/j.jnc.2008.11.001

Dick, M. A. (1994). Blight of Lupinus arboreus in New Zealand. *New Zealand Journal of Forestry Science, 24*(1), 51-68.

Dixon, P., Hilton, M., & Bannister, P. (2004). Desmoschoenus spiralis displacement by Ammophila arenaria: the role of drought. *New Zealand Journal of Ecology, 28*(2), 207-213.

Donager, J. J., Sankey, T. T., Sankey, J. B., Meador, A. J. S., Springer, A. E., & Bailey, J. D. (2018). Examining Forest Structure With Terrestrial Lidar: Suggestions and Novel Techniques Based on Comparisons Between Scanners and Forest Treatments. *Earth and Space Science, 5*(11), 753-776. doi:10.1029/2018ea000417

Dornhofer, K., & Oppelt, N. (2016). Remote sensing for lake research and monitoring - Recent advances. *Ecological Indicators, 64*, 105-122. doi:10.1016/j.ecolind.2015.12.009

Dubayah, R. O., & Drake, J. B. (2000). Lidar remote sensing for forestry. *Journal of Forestry, 98*(6), 44-46.

Duffy, J. P., Cunliffe, A. M., DeBell, L., Sandbrook, C., Wich, S. A., Shutler, J. D., . . . Anderson, K. (2018). Location, location, location: considerations when using lightweight drones in challenging environments. *Remote Sensing in Ecology and Conservation, 4*(1), 7-19. doi:doi:10.1002/rse2.58

Dufour, S., Bernez, I., Betbeder, J., Corgne, S., Hubert-Moy, L., Nabucet, J., . . . Trolle, C. (2013). Monitoring restored riparian vegetation: how can recent developments in remote sensing sciences help? *Knowledge and Management of Aquatic Ecosystems*(410). doi:10.1051/kmae/2013068

Dufrêne, M., & Legendre, P. (1997). Species assemblages and indicator species: the need for a flexible asymmetrical approach. *Ecological Monographs, 67*(3), 345-366.

Dulava, S., Bean, W. T., & Richmond, O. M. W. (2015). Applications of Unmanned Aircraft Systems (UAS) for Waterbird Surveys. *Environmental Practice, 17*(3), 201-210. doi:10.1017/s1466046615000186

Dymond, C. C., & Johnson, E. A. (2002). Mapping vegetation spatial patterns from modeled water, temperature and solar radiation gradients. *Isprs Journal of Photogrammetry and Remote Sensing, 57*(1–2), 69-85. doi:http://dx.doi.org/10.1016/S0924-2716(02)00110-7

E. Hunt, R., Hively, W., W. McCarty, G., Daughtry, C., Forrestal, P., J. Kratochvil, R., . . . D. Miller, C. (2011). *NIR-Green-Blue High-Resolution Digital Images for Assessment of Winter Cover Crop Biomass* (Vol. 48).

Eberhardt, L., & Thomas, J. (1991). Designing environmental field studies. *Ecological Monographs, 61*(1), 53-73.

Eisfelder, C., Kuenzer, C., & Dech, S. (2010). *A review on derivation of biomass information in semi-arid regions based on remote sensing data.* Paper presented at the Earth Resources and Environmental Remote Sensing/GIS Applications.

Eisfelder, C., Kuenzer, C., Dech, S., & Buchroithner, M. F. (2013). Comparison of Two Remote Sensing Based Models for Regional Net Primary Productivity Estimation-A Case Study in Semi-Arid

Central Kazakhstan. *Ieee Journal of Selected Topics in Applied Earth Observations and Remote Sensing, 6*(4), 1843-1856. doi:10.1109/jstars.2012.2226707

Elliott, S. E., & Jules, E. S. (2005). Small-scale community analyses of alpine ridge vegetation in the Central Sierra Nevada. *Madrono, 52*(1), 38-45. doi:10.3120/0024-9637(2005)52[38:scaoar]2.0.co;2

Elsherif, A., Gaulton, R., & Mills, J. (2018). Estimation of vegetation water content at leaf and canopy level using dual-wavelength commercial terrestrial laser scanners. *Interface Focus, 8*(2), 11. doi:10.1098/rsfs.2017.0041

Esler, A. E. (1970). Manawatu sand dune vegetation. *Proceedings of the New Zealand Ecological Society, 17*, 41-46.

ESRI. (2014). ArcGIS Desktop: Release 10.3. Redlands, CA: Environmental Systems Research Institute.

ESRI. (2018a). Convolution function. Retrieved from http://desktop.arcgis.com/en/arcmap/latest/manage-data/raster-and-images/convolution-function.htm

ESRI. (2018b). Segment Mean Shift. Retrieved from http://desktop.arcgis.com/en/arcmap/10.3/tools/spatial-analyst-toolbox/segment-mean-shift.htm

Evans, D. (2006). *The habitats of the European Union habitats directive.* Paper presented at the Biology and Environment: Proceedings of the Royal Irish Academy.

Farrell, M., Gili, A., & Noellemeyer, E. (2018). Spectral indices from aerial images and their relationship with properties of a corn crop. *Precision Agriculture, 19*(6), 1127-1137. doi:10.1007/s11119-018-9570-9

Fitzpatrick, M. C., Preisser, E. L., Ellison, A. M., & Elkinton, J. S. (2009). Observer bias and the detection of low-density populations. *Ecological Applications, 19*(7), 1673-1679. doi:doi:10.1890/09-0265.1

Foody. (1996). Fuzzy modelling of vegetation from remotely sensed imagery. *Ecological Modelling, 85*(1), 3-12. doi:https://doi.org/10.1016/0304-3800(95)00012-7

Foody, Mathur, Sanchez-Hernandez, & Boyd. (2006). Training set size requirements for the classification of a specific class. *Remote Sensing of Environment, 104*(1), 1-14. doi:http://dx.doi.org/10.1016/j.rse.2006.03.004

Foody, G. (2002). Hard and soft classifications by a neural network with a non-exhaustively defined set of classes. *International Journal of Remote Sensing, 23*(18), 3853-3864.

Foody, G. M. (2002). Status of land cover classification accuracy assessment. *Remote Sensing of Environment, 80*(1), 185-201. doi:http://dx.doi.org/10.1016/S0034-4257(01)00295-4

Foody, G. M., & Mathur, A. (2004). Toward intelligent training of supervised image classifications: directing training data acquisition for SVM classification. *Remote Sensing of Environment, 93*(1-2), 107-117.

Franke, J., Keuck, V., & Siegert, F. (2012). Assessment of grassland use intensity by remote sensing to support conservation schemes. *Journal for Nature Conservation, 20*(3), 125-134. doi:http://dx.doi.org/10.1016/j.jnc.2012.02.001

Fraser, R. H., Olthof, I., Lantz, T. C., & Schmitt, C. (2016). UAV photogrammetry for mapping vegetation in the low-Arctic. *Arctic Science, 2*(3), 79-102.

Frederick, P. C., Hylton, B., Heath, J. A., & Ruane, M. (2003). *Accuracy and variation in estimates of large numbers of birds by individual observers using an aerial survey simulator* (Vol. 74): SPIE.

Gadgil, R. L. (2002). Marram grass (Ammophila arenaria) and coastal sand stability in New Zealand. *New Zealand Journal of Forestry Science, 32*(2), 165-180.

Gadgil, R. L., & Ede, F. J. (1998). Application of scientific principles to sand dune stabilization in New Zealand: Past progress and future needs. *Land Degradation & Development, 9*(2), 131-142. doi:10.1002/(sici)1099-145x(199803/04)9:2<131::aid-ldr286>3.0.co;2-h

Gao, Z. G., & Zhang, L. Q. (2006). Multi-seasonal spectral characteristics analysis of coastal salt marsh vegetation in Shanghai, China. *Estuarine Coastal and Shelf Science, 69*(1-2), 217-224. doi:10.1016/j.ecss.2006.04.016

Garcia, M., Danson, F. M., Riano, D., Chuvieco, E., Ramirez, F. A., & Bandugula, V. (2011). Terrestrial laser scanning to estimate plot-level forest canopy fuel properties. *International Journal of*

Applied Earth Observation and Geoinformation, 13(4), 636-645. doi:10.1016/j.jag.2011.03.006

Getzin, S., Nuske, R. S., & Wiegand, K. (2014). Using Unmanned Aerial Vehicles (UAV) to Quantify Spatial Gap Patterns in Forests. *Remote Sensing, 6*(8), 6988-7004. doi:10.3390/rs6086988

Getzin, S., Wiegand, K., & Schoning, I. (2012). Assessing biodiversity in forests using very high-resolution images and unmanned aerial vehicles. *Methods in Ecology and Evolution, 3*(2), 397-404. doi:10.1111/j.2041-210X.2011.00158.x

Gilabert, M. A., González-Piqueras, J., García-Haro, F. J., & Meliá, J. (2002). A generalized soil-adjusted vegetation index. *Remote Sensing of Environment, 82*(2), 303-310. doi:https://doi.org/10.1016/S0034-4257(02)00048-2

Gitelson, A., Garbuzov, G., Szilagyi, F., Mittenzwey, K., Karnieli, A., & Kaiser, A. (1993). Quantitative remote sensing methods for real-time monitoring of inland waters quality. *International Journal of Remote Sensing, 14*(7), 1269-1295.

Gitelson, A. A., Kaufman, Y. J., & Merzlyak, M. N. (1996). Use of a green channel in remote sensing of global vegetation from EOS-MODIS. *Remote Sensing of Environment, 58*(3), 289-298.

Gitelson, A. A., Keydan, G. P., & Merzlyak, M. N. (2006). Three-band model for noninvasive estimation of chlorophyll, carotenoids, and anthocyanin contents in higher plant leaves. *Geophysical Research Letters, 33*(11). doi:doi:10.1029/2006GL026457

Gonçalves, J., Henriques, R., Alves, P., Sousa-Silva, R., Monteiro, A. T., Lomba, Â., . . . Honrado, J. (2016). Evaluating an unmanned aerial vehicle-based approach for assessing habitat extent and condition in fine-scale early successional mountain mosaics. *Applied Vegetation Science, 19*(1), 132-146. doi:doi:10.1111/avsc.12204

Goncalves, J. A., & Henriques, R. (2015). UAV photogrammetry for topographic monitoring of coastal areas. *Isprs Journal of Photogrammetry and Remote Sensing, 104*, 101-111. doi:10.1016/j.isprsjprs.2015.02.009

Gong, H. L., Jiao, C. C., Zhou, D. M., & Li, N. (2011). Scale issues of wetland classification and mapping using remote sensing images: A case of Honghe National Nature Reserve in Sanjiang Plain, Northeast China. *Chinese Geographical Science, 21*(2), 230-240. doi:10.1007/s11769-011-0461-5

Groom, G., Mücher, C., Ihse, M., & Wrbka, T. (2006). Remote sensing in landscape ecology: experiences and perspectives in a European context. *Landscape Ecology, 21*(3), 391-408.

Guerschman, J. P., Hill, M. J., Renzullo, L. J., Barrett, D. J., Marks, A. S., & Botha, E. J. (2009). Estimating fractional cover of photosynthetic vegetation, non-photosynthetic vegetation and bare soil in the Australian tropical savanna region upscaling the EO-1 Hyperion and MODIS sensors. *Remote Sensing of Environment, 113*(5), 928-945.

Guo, X. J., Shao, Q. Q., Li, Y. Z., Wang, Y. C., Wang, D. L., Liu, J. Y., . . . Yang, F. (2018). Application of UAV Remote Sensing for a Population Census of Large Wild Herbivores-Taking the Headwater Region of the Yellow River as an Example. *Remote Sensing, 10*(7). doi:10.3390/rs10071041

Hall, R. K., Watkins, R. L., Heggem, D. T., Jones, K. B., Kaufmann, P. R., Moore, S. B., & Gregory, S. J. (2009). Quantifying structural physical habitat attributes using LIDAR and hyperspectral imagery. *Environmental Monitoring and Assessment, 159*(1-4), 63-83. doi:10.1007/s10661-008-0613-y

Hancock, S., Gaulton, R., & Danson, F. M. (2017). Angular Reflectance of Leaves With a Dual-Wavelength Terrestrial Lidar and Its Implications for Leaf-Bark Separation and Leaf Moisture Estimation. *Ieee Transactions on Geoscience and Remote Sensing, 55*(6), 3084-3090. doi:10.1109/tgrs.2017.2652140

He, K. S., Rocchini, D., Neteler, M., & Nagendra, H. (2011). Benefits of hyperspectral remote sensing for tracking plant invasions. *Diversity and Distributions, 17*(3), 381-392. doi:10.1111/j.1472-4642.2011.00761.x

Heinzel, J., & Huber, M. O. (2017). Detecting Tree Stems from Volumetric TLS Data in Forest Environments with Rich Understory. *Remote Sensing, 9*(1), 17. doi:10.3390/rs9010009

Henning, J. G., & Radtke, P. J. (2006). Detailed stem measurements of standing trees from ground-based scanning lidar. *Forest Science, 52*(1), 67-80.

Hesp, P. (2002). Foredunes and blowouts: initiation, geomorphology and dynamics. *Geomorphology, 48*, 245-268.

Hill, M. (1979). 0.(1979): TWINSPAN—A FORTRAN program for arranging multivariate data in an ordered two-way table by classification of individuals and attributes. *Cornell University lthaca, NY*.

Hill, M. O., Bunce, R. G. H., & Shaw, M. W. (1975). Indicator species analysis, a divisive polythetic method of classification and its application to a survey of native pinewoods in Scotland. *Journal of Ecology, 63*, 597 - 613.

Hill, R. A., & Thomson, A. G. (2005). Mapping woodland species composition and structure using airborne spectral and LiDAR data. *International Journal of Remote Sensing, 26*(17), 3763-3779. doi:10.1080/01431160500114706

Hilton, M., Harvey, N., Hart, A., James, K., & Arbuckle, C. (2006). The impact of exotic dune grass species on foredune development in Australia and New Zealand: a case study of Ammophila arenaria and Thinopyrum junceiforme. *Australian Geographer, 37*(3), 313-334. doi:10.1080/00049180600954765

Hilton, M. J. (2006). The loss of New Zealand's active dunes and the spread of marram grass (Ammophila arenaria). *New Zealand Geographer, 62*(2), 105-120. doi:10.1111/j.1745-7939.2006.00054.x

Holmes, M. P. A. (1998). The geomorphology and radar facies of Kaitorete Spit, Canterbury, New Zealand.

Holyoak, M., Leibold, M. A., Mouquet, N., Holt, R. D., & Hoopes, M. (2005). A framework for large scale community ecology. *Metacommunities: spatial dynamics and ecological communities. The University of Chicago Press, Chicago*, 1-31.

Hooson, S. (2015). *Christchurch District Plan Site of Ecological Significance: Site Significance Statement*. Retrieved from Christchurch, N.Z.:

Hu, R. H., Bournez, E., Cheng, S. Y., Jiang, H. L., Nerry, F., Landes, T., . . . Yan, G. J. (2018). Estimating the leaf area of an individual tree in urban areas using terrestrial laser scanner and path length distribution model. *Isprs Journal of Photogrammetry and Remote Sensing, 144*, 357-368. doi:10.1016/j.isprsjprs.2018.07.015

Huang, C., Davis, L. S., & Townshend, J. R. G. (2002). An assessment of support vector machines for land cover classification. *International Journal of Remote Sensing, 23*(4), 725-749. doi:10.1080/01431160110040323

Hugenholtz, C. H., Levin, N., Barchyn, T. E., & Baddock, M. C. (2012). Remote sensing and spatial analysis of aeolian sand dunes: A review and outlook. *Earth-Science Reviews, 111*(3-4), 319-334. doi:10.1016/j.earscirev.2011.11.006

Husson, E., Ecke, F., & Reese, H. (2016). Comparison of Manual Mapping and Automated Object-Based Image Analysis of Non-Submerged Aquatic Vegetation from Very-High-Resolution UAS Images. *Remote Sensing, 8*(9), 724.

Husson, E., Hagner, O., & Ecke, F. (2014). Unmanned aircraft systems help to map aquatic vegetation. *Applied Vegetation Science, 17*(3), 567-577. doi:10.1111/avsc.12072

ICAO. (2012). Cir 328 AN/190 Unmanned Aircraft Systems (UAS) (Vol. 328). 999 University Street, Montréal, Quebec, Canada H3C 5H7: INTERNATIONAL CIVIL AVIATION ORGANIZATION.

Irisarri, J., Oesterheld, M., Verón, S., & Paruelo, J. (2009). Grass species differentiation through canopy hyperspectral reflectance. *International Journal of Remote Sensing, 30*(22), 5959-5975.

Jari Oksanen, F. Guillaume Blanchet, Michael Friendly, Roeland Kindt, Pierre Legendre, Dan McGlinn, . . . Wagner, H. (2018). *vegan: Community Ecology Package. R package version 2.5-3.* https://CRAN.R-project.org/package=vegan

Jeganathan, C., Dash, J., & Atkinson, P. M. (2014). Remotely sensed trends in the phenology of northern high latitude terrestrial vegetation, controlling for land cover change and vegetation type. *Remote Sensing of Environment, 143*(0), 154-170. doi:http://dx.doi.org/10.1016/j.rse.2013.11.020

Johnson, P. N. (1992). *The sand dune and beach vegetation inventory of New Zealand. II, South Island and Stewart Island / 1992*. Christchurch, NZ: DSIR Land Resources (N.Z.).

Jones, D., Pike, S., Thomas, M., & Murphy, D. (2011). Object-Based Image Analysis for Detection of Japanese Knotweed s.l. taxa (Polygonaceae) in Wales (UK). *Remote Sensing, 3*(2), 319-342. doi:10.3390/rs3020319

Jones, G. P., Pearlstine, L. G., & Percival, H. F. (2006). An assessment of small unmanned aerial vehicles for wildlife research. *Wildlife Society Bulletin, 34*(3), 750-758. doi:10.2193/0091-7648(2006)34[750:aaosua]2.0.co;2

Julian, J. T., Young, J. A., Jones, J. W., Snyder, C. D., & Wright, C. W. (2009). The use of local indicators of spatial association to improve LiDAR-derived predictions of potential amphibian breeding ponds. *Journal of Geographical Systems, 11*(1), 89-106. doi:10.1007/s10109-008-0074-4

Kaliraj, S., Chandrasekar, N., Ramachandran, K. K., Srinivas, Y., & Saravanan, S. (2017). Coastal landuse and land cover change and transformations of Kanyakumari coast, India using remote sensing and GIS. *Egyptian Journal of Remote Sensing and Space Sciences, 20*(2), 169-185. doi:10.1016/j.ejrs.2017.04.003

Karau, E. C., Sikkink, P. G., Keane, R. E., & Dillon, G. K. (2014). Integrating Satellite Imagery with Simulation Modeling to Improve Burn Severity Mapping. *Environmental Management, 54*(1), 98-111. doi:10.1007/s00267-014-0279-x

Kerr, J. T., & Ostrovsky, M. (2003). From space to species: ecological applications for remote sensing. *Trends in Ecology & Evolution, 18*(6), 299-305. doi:http://dx.doi.org/10.1016/S0169-5347(03)00071-5

Klosterman, S., Melaas, E., Wang, J. A., Martinez, A., Frederick, S., O'Keefe, J., . . . Richardson, A. D. (2018). Fine-scale perspectives on landscape phenology from unmanned aerial vehicle (UAV) photography. *Agricultural and Forest Meteorology, 248*, 397-407. doi:https://doi.org/10.1016/j.agrformet.2017.10.015

Knoth, C., Klein, B., Prinz, T., & Kleinebecker, T. (2013). Unmanned aerial vehicles as innovative remote sensing platforms for high-resolution infrared imagery to support restoration monitoring in cut-over bogs. *Applied Vegetation Science, 16*(3), 509-517. doi:10.1111/avsc.12024

Knox, N. M., Skidmore, A. K., van der Werff, H. M. A., Groen, T. A., de Boer, W. F., Prins, H. H. T., . . . Peel, M. (2013). Differentiation of plant age in grasses using remote sensing. *International Journal of Applied Earth Observation and Geoinformation, 24*(0), 54-62. doi:http://dx.doi.org/10.1016/j.jag.2013.02.004

Koedsin, W., & Vaiphasa, C. (2013). Discrimination of Tropical Mangroves at the Species Level with EO-1 Hyperion Data. *Remote Sensing, 5*(7), 3562-3582. doi:10.3390/rs5073562

Koh, L. P., & Wich, S. A. (2012). Dawn of drone ecology: low-cost autonomous aerial vehicles for conservation. *Tropical Conservation Science, 5*(2), 121-132.

Komarek, J., Kloucek, T., & Prosek, J. (2018). The potential of Unmanned Aerial Systems: A tool towards precision classification of hard-to-distinguish vegetation types? *International Journal of Applied Earth Observation and Geoinformation, 71*, 9-19. doi:10.1016/j.jag.2018.05.003

Kunin, W. E., & Gaston, K. J. (1993). The biology of rarity: patterns, causes and consequences. *Trends in Ecology & Evolution, 8*(8), 298-301.

Laba, M., Blair, B., Downs, R., Monger, B., Philpot, W., Smith, S., . . . Baveye, P. C. (2010). Use of textural measurements to map invasive wetland plants in the Hudson River National Estuarine Research Reserve with IKONOS satellite imagery. *Remote Sensing of Environment, 114*(4), 876-886. doi:10.1016/j.rse.2009.12.002

Landis, J. R., & Koch, G. G. (1977). The measurement of observer agreement for categorical data. *Biometrics*, 159-174.

Langley, S. K., Cheshire, H. M., & Humes, K. S. (2001). A comparison of single date and multitemporal satellite image classifications in a semi-arid grassland. *Journal of Arid Environments, 49*(2), 401-411.

Lantz, N. J., & Wang, J. (2013). Object-based classification of Worldview-2 imagery for mapping invasive common reed, Phragmites australis. *Canadian Journal of Remote Sensing, 39*(4), 328-340. doi:10.5589/m13-041

Lau, A., Bentley, L. P., Martius, C., Shenkin, A., Bartholomeus, H., Raumonen, P., . . . Herold, M. (2018). Quantifying branch architecture of tropical trees using terrestrial LiDAR and 3D modelling. *Trees-Structure and Function, 32*(5), 1219-1231. doi:10.1007/s00468-018-1704-1

Legendre, P., & Legendre, L. (2012a). Chapter 7 - Ecological resemblance. In L. Pierre & L. Louis (Eds.), *Developments in Environmental Modelling* (Vol. Volume 24, pp. 265-335): Elsevier.

Legendre, P., & Legendre, L. (2012b). Chapter 8 - Cluster analysis. In P. Legendre & L. Legendre (Eds.), *Developments in Environmental Modelling* (Vol. 24, pp. 337-424): Elsevier.

legendre, P., & legendre, L. (2012c). Chapter 9 - Ordination in reduced space. In L. Pierre & L. Louis (Eds.), *Developments in Environmental Modelling* (Vol. Volume 24, pp. 425-520): Elsevier.

Leibold, M. A., Holyoak, M., Mouquet, N., Amarasekare, P., Chase, J. M., Hoopes, M. F., . . . Gonzalez, A. (2004). The metacommunity concept: a framework for multi-scale community ecology. *Ecology Letters, 7*(7), 601-613. doi:doi:10.1111/j.1461-0248.2004.00608.x

Lettink, M. (2008). *Monitoring and restoration options for lizards on Kaitorete Spit, Canterbury* (Vol. 301). Wellington, N.Z.: Wellington, N.Z. : Dept. of Conservation.

Lisita, A., Sano, E. E., & Durieux, L. (2013). Identifying potential areas of Cannabis sativa plantations using object-based image analysis of SPOT-5 satellite data. *International Journal of Remote Sensing, 34*(15), 5409-5428. doi:10.1080/01431161.2013.790574

Lodge, D. M., Williams, S., MacIsaac, H. J., Hayes, K. R., Leung, B., Reichard, S., . . . McMichael, A. (2006). BIOLOGICAL INVASIONS: RECOMMENDATIONS FOR U.S. POLICY AND MANAGEMENT. *Ecological Applications, 16*(6), 2035-2054. doi:doi:10.1890/1051-0761(2006)016[2035:BIRFUP]2.0.CO;2

Lu, & Weng, Q. (2007). A survey of image classification methods and techniques for improving classification performance. *International Journal of Remote Sensing, 28*(5), 823-870. doi:10.1080/01431160600746456

Lu, M. L., Huang, J. Y., Chung, Y. L., & Huang, C. Y. (2013). Modelling the invasion of a Central American Mimosoid tree species (Leucaena leucocephala) in a tropical coastal region of Taiwan. *Remote Sensing Letters, 4*(5), 485-493. doi:10.1080/2150704x.2012.755274

Lunetta, R. S., & Lyon, J. G. (2004). *Remote sensing and GIS accuracy assessment*: CRC press.

Magiera, A., Feilhauer, H., Otte, A., Waldhardt, R., & Simmering, D. (2013). Relating canopy reflectance to the vegetation composition of mountainous grasslands in the Greater Caucasus. *Agriculture Ecosystems & Environment, 177*, 101-112. doi:10.1016/j.agee.2013.05.017

Manfreda, S., McCabe, M. E., Miller, P. E., Lucas, R., Madrigal, V. P., Mallinis, G., . . . Toth, B. (2018). On the Use of Unmanned Aerial Systems for Environmental Monitoring. *Remote Sensing, 10*(4). doi:10.3390/rs10040641

Mantero, P., Moser, G., & Serpico, S. B. (2005). Partially supervised classification of remote sensing images through SVM-based probability density estimation. *Ieee Transactions on Geoscience and Remote Sensing, 43*(3), 559-570.

Marceau, D. J., Howarth, P. J., & Gratton, D. J. (1994). Remote sensing and the measurement of geographical entities in a forested environment. 1. The scale and spatial aggregation problem. *Remote Sensing of Environment, 49*(2), 93-104. doi:https://doi.org/10.1016/0034-4257(94)90046-9

Maron, J. L., & Connors, P. G. (1996). A Native Nitrogen-Fixing Shrub Facilitates Weed Invasion. *Oecologia, 105*(3), 302-312. doi:10.2307/4221187

Martinez-Carricondo, P., Aguera-Vega, F., Carvajal-Ramirez, F., Mesas-Carrascosa, F. J., Garcia-Ferrer, A., & Perez-Porras, F. J. (2018). Assessment of UAV-photogrammetric mapping accuracy based on variation of ground control points. *International Journal of Applied Earth Observation and Geoinformation, 72*, 1-10. doi:10.1016/j.jag.2018.05.015

Matese, A., Toscano, P., Di Gennaro, S., Genesio, L., Vaccari, F., Primicerio, J., . . . Gioli, B. (2015). Intercomparison of UAV, Aircraft and Satellite Remote Sensing Platforms for Precision Viticulture. *Remote Sensing, 7*(3), 2971.

Mathieu, R., Aryal, J., & Chong, A. K. (2007). Object-based classification of ikonos imagery for mapping large-scale vegetation communities in urban areas. *Sensors, 7*(11), 2860-2880. doi:10.3390/s7112860

Mayr, M. J., Malss, S., Ofner, E., & Samimi, C. (2018). Disturbance feedbacks on the height of woody vegetation in a savannah: a multi-plot assessment using an unmanned aerial vehicle (UAV). *International Journal of Remote Sensing, 39*(14), 4761-4785. doi:10.1080/01431161.2017.1362132

Molloy, B. P. J., Partridge, T. R., & Thomas, W. P. (1991). Decline of tree lupin (lupinus-arboreus) on kaitorete spit, canterbury, new-zealand, 1984-1990. *New Zealand Journal of Botany, 29*(3), 349-352.

Morrison, J., Higginbottom, T. P., Symeonakis, E., Jones, M. J., Omengo, F., Walker, S. L., & Cain, B. (2018). Detecting Vegetation Change in Response to Confining Elephants in Forests Using MODIS Time-Series and BFAST. *Remote Sensing, 10*(7). doi:10.3390/rs10071075

Motohka, T., Nasahara, K. N., Oguma, H., & Tsuchida, S. (2010). Applicability of Green-Red Vegetation Index for Remote Sensing of Vegetation Phenology. *Remote Sensing, 2*(10), 2369.

Mountrakis, G., Im, J., & Ogole, C. (2011). Support vector machines in remote sensing: A review. *Isprs Journal of Photogrammetry and Remote Sensing, 66*(3), 247-259. doi:https://doi.org/10.1016/j.isprsjprs.2010.11.001

Mucher, C. A., Kooistra, L., Vermeulen, M., Vanden Borre, J., Haest, B., & Haveman, R. (2013). Quantifying structure of Natura 2000 heathland habitats using spectral mixture analysis and segmentation techniques on hyperspectral imagery. *Ecological Indicators, 33*, 71-81. doi:10.1016/j.ecolind.2012.09.013

Muellerova, J., Pergl, J., & Pysek, P. (2013). Remote sensing as a tool for monitoring plant invasions: Testing the effects of data resolution and image classification approach on the detection of a model plant species Heracleum mantegazzianum (giant hogweed). *International Journal of Applied Earth Observation and Geoinformation, 25*, 55-65. doi:10.1016/j.jag.2013.03.004

Mullerova, J., Pergl, J., & Pysek, P. (2013). Remote sensing as a tool for monitoring plant invasions: Testing the effects of data resolution and image classification approach on the detection of a model plant species Heracleum mantegazzianum (giant hogweed). *International Journal of Applied Earth Observation and Geoinformation, 25*, 55-65. doi:10.1016/j.jag.2013.03.004

Nagendra, H., Lucas, R., Honrado, J. P., Jongman, R. H. G., Tarantino, C., Adamo, M., & Mairota, P. (2013). Remote sensing for conservation monitoring: Assessing protected areas, habitat extent, habitat condition, species diversity, and threats. *Ecological Indicators, 33*, 45-59. doi:10.1016/j.ecolind.2012.09.014

Nagler, P. L., Daughtry, C. S. T., & Goward, S. N. (2000). Plant Litter and Soil Reflectance. *Remote Sensing of Environment, 71*(2), 207-215. doi:https://doi.org/10.1016/S0034-4257(99)00082-6

Navratil, P., & Wilps, H. (2013). Object-based locust habitat mapping using high-resolution multispectral satellite data in the southern Aral Sea basin. *Journal of Applied Remote Sensing, 7*. doi:10.1117/1.jrs.7.075097

Neumann, C., Itzerott, S., Weiss, G., Kleinschmit, B., & Schmidtlein, S. (2016). Mapping multiple plant species abundance patterns - A multiobjective optimization procedure for combining reflectance spectroscopy and species ordination. *Ecological Informatics, 36*, 61-76. doi:https://doi.org/10.1016/j.ecoinf.2016.10.002

Nevalainen, O., Hakala, T., Suomalainen, J., Mäkipää, R., Peltoniemi, M., Krooks, A., & Kaasalainen, S. (2014). Fast and nondestructive method for leaf level chlorophyll estimation using hyperspectral LiDAR. *Agricultural and Forest Meteorology, 198-199*, 250-258. doi:https://doi.org/10.1016/j.agrformet.2014.08.018

Newnham, G. J., Armston, J. D., Calders, K., Disney, M. I., Lovell, J. L., Schaaf, C. B., . . . Danson, F. M. (2015). Terrestrial Laser Scanning for Plot-Scale Forest Measurement. *Current Forestry Reports, 1*(4), 239-251. doi:10.1007/s40725-015-0025-5

Newsome, P. (1987). *The vegetation cover of New Zealand*. Retrieved from Wellington, New Zealand:

Norton, D. A. (1991). *Scientific basis for the conservation and management of New Zealand plant communities*. Oxford, England: Blackwell Scientific Press.

Okin, G. S., Roberts, D. A., Murray, B., & Okin, W. J. (2001). Practical limits on hyperspectral vegetation discrimination in arid and semiarid environments. *Remote Sensing of Environment, 77*(2), 212-225.

Oloo, O. J. (2017). ASSESSING THE ACCURACY OF REMOTE SENSING TECHNIQUES IN VEGETATION FRACTIONS ESTIMATION. *South African Journal of Geomatics, 6*(1), 106-129. doi:10.4314/sajg.v6i1.7

Olsoy, P. J., Shipley, L. A., Rachlow, J. L., Forbey, J. S., Glenn, N. F., Burgess, M. A., & Thornton, D. H. (2018). Unmanned aerial systems measure structural habitat features for wildlife across multiple scales. *Methods in Ecology and Evolution, 9*(3), 594-604. doi:10.1111/2041-210x.12919

Orwig, D. A., Boucher, P., Paynter, I., Saenz, E., Li, Z., & Schaaf, C. (2018). The potential to characterize ecological data with terrestrial laser scanning in Harvard Forest, MA. *Interface Focus, 8*(2), 9. doi:10.1098/rsfs.2017.0044

Otukei, J. R., & Blaschke, T. (2010). Land cover change assessment using decision trees, support vector machines and maximum likelihood classification algorithms. *International Journal of Applied Earth Observation and Geoinformation, 12*, S27-S31. doi:https://doi.org/10.1016/j.jag.2009.11.002

Ouyang, Z. T., Gao, Y., Xie, X., Guo, H. Q., Zhang, T. T., & Zhao, B. (2013). Spectral Discrimination of the Invasive Plant Spartina alterniflora at Multiple Phenological Stages in a Saltmarsh Wetland. *PLoS ONE, 8*(6). doi:10.1371/journal.pone.0067315

Pajares, G. (2015). Overview and Current Status of Remote Sensing Applications Based on Unmanned Aerial Vehicles (UAVs). *Photogrammetric Engineering & Remote Sensing, 81*(4), 281-329. doi:https://doi.org/10.14358/PERS.81.4.281

Paneque-Galvez, J., McCall, M. K., Napoletano, B. M., Wich, S. A., & Koh, L. P. (2014). Small Drones for Community-Based Forest Monitoring: An Assessment of Their Feasibility and Potential in Tropical Areas. *Forests, 5*(6), 1481-1507. doi:10.3390/f5061481

Partridge, T. R. (1992). Vegetation recovery following sand mining on coastal dunes at kaitorete spit, canterbury, new-zealand. *Biological Conservation, 61*(1), 59-71. doi:10.1016/0006-3207(92)91208-a

Patrick, B. (1994). Lepidoptera of Kaitorete Spit, Canterbury. *New Zealand Entomologist, 17*, 52-63.

Peace, M. (1975). *The Plant Ecology of the Dune System on Kaitorete Spit: A Thesis Presented for the Degree of M. Sc. in Botany in the University of Canterbury, Christchurch, New Zealand.* University of Canterbury.

Pearson, R. L., & Miller, L. D. (1972). *Remote Mapping of Standing Crop Biomass for Estimation of the Productivity of the Shortgrass Prairie.* Paper presented at the Proceedings of the Eighth International Symposium on Remote Sensing of Environment, Pawnee National Grasslands, Colorado.

Pegman, A. P. M., & Rapson, G. L. (2005). Plant succession and dune dynamics on actively prograding dunes, Whatipu Beach, northern New Zealand. *New Zealand Journal of Botany, 43*(1), 223-244.

Pettorelli, N., Safi, K., & Turner, W. (2014). Satellite remote sensing, biodiversity research and conservation of the future: The Royal Society.

Pettorelli, N., Vik, J. O., Mysterud, A., Gaillard, J.-M., Tucker, C. J., & Stenseth, N. C. (2005). Using the satellite-derived NDVI to assess ecological responses to environmental change. *Trends in Ecology & Evolution, 20*(9), 503-510. doi:https://doi.org/10.1016/j.tree.2005.05.011

Pickart, A. J. (2004). *Introduced yellow bush lupin (L. arboreus) in coastal dunes of Northern California*.

Pihur, Datta, & Datta. (2018). RankAggreg: Weighted Rank Aggregation (Version R package version 0.6.5). Retrieved from https://CRAN.R-project.org/package=RankAggreg

Platt, R. V. (2014). Wildfire hazard in the home ignition zone: An object-oriented analysis integrating LiDAR and VHR satellite imagery. *Applied Geography, 51*, 108-117. doi:10.1016/j.apgeog.2014.03.011

Price, K. P., Guo, X., & Stiles, J. M. (2002). Optimal Landsat TM band combinations and vegetation indices for discrimination of six grassland types in eastern Kansas. *International Journal of Remote Sensing, 23*(23), 5031-5042.

Pu, R., Landry, S., & Yu, Q. (2011). Object-based urban detailed land cover classification with high spatial resolution IKONOS imagery. *International Journal of Remote Sensing, 32*(12), 3285-3308. doi:10.1080/01431161003745657

Pudji, W. (1997). *Floristic variation and environmental relationships of sand dune communities at Kaitorete Spit Scientific Reserve.* Lincoln University.

Pullanagari, R. R., Kereszturi, G., & Yule, I. J. (2017). Quantification of dead vegetation fraction in mixed pastures using AisaFENIX imaging spectroscopy data. *International Journal of Applied Earth Observation and Geoinformation, 58*, 26-35. doi:https://doi.org/10.1016/j.jag.2017.01.004

Pyorala, J., Liang, X. L., Vastaranta, M., Saarinen, N., Kankare, V., Wang, Y. S., . . . Hyyppa, J. (2018). Quantitative Assessment of Scots Pine (Pinus Sylvestris L.) Whorl Structure in a Forest Environment Using Terrestrial Laser Scanning. *Ieee Journal of Selected Topics in Applied Earth Observations and Remote Sensing, 11*(10), 3598-3607. doi:10.1109/jstars.2018.2819598

Pysek, P., & Richardson, D. M. (2010). Invasive Species, Environmental Change and Management, and Health. In A. Gadgil & D. M. Liverman (Eds.), *Annual Review of Environment and Resources, Vol 35* (Vol. 35, pp. 25-55). Palo Alto: Annual Reviews.

Qi, J., & Wallace, O. (2002). *Biophysical attributes estimation from satellite images in arid regions.* Paper presented at the Geoscience and Remote Sensing Symposium, 2002. IGARSS'02. 2002 IEEE International.

R Core Team. (2018). R: A language and environment for statistical computing. Vienna, Austria. Retrieved from URL https://www.R-project.org/.

Ramírez-García, P., López-Blanco, J., & Ocaña, D. (1998). Mangrove vegetation assessment in the Santiago River Mouth, Mexico, by means of supervised classification using LandsatTM imagery. *Forest Ecology and Management, 105*(1–3), 217-229. doi:http://dx.doi.org/10.1016/S0378-1127(97)00289-2

Rapinel, S., Rossignol, N., Hubert-Moy, L., Bouzille, J. B., & Bonis, A. (2018). Mapping grassland plant communities using a fuzzy approach to address floristic and spectral uncertainty. *Applied Vegetation Science, 21*(4), 678-693. doi:10.1111/avsc.12396

Rastmanesh, F., Moore, F., Kharrati-Kopaei, M., & Behrouz, M. (2010). Monitoring deterioration of vegetation cover in the vicinity of smelting industry, using statistical methods and TM and ETM+ imageries, Sarcheshmeh copper complex, Central Iran. *Environmental Monitoring and Assessment, 163*(1), 397-410. doi:10.1007/s10661-009-0843-7

Reif, M. K., & Theel, H. J. (2017). Remote sensing for restoration ecology: Application for restoring degraded, damaged, transformed, or destroyed ecosystems. *Integrated Environmental Assessment and Management, 13*(4), 614-630. doi:10.1002/ieam.1847

Ren, H., & Zhou, G. (2012). Estimating senesced biomass of desert steppe in Inner Mongolia using field spectrometric data. *Agricultural and Forest Meteorology, 161*, 66-71.

Ricotta, C., & Podani, J. (2017). On some properties of the Bray-Curtis dissimilarity and their ecological meaning. *Ecological Complexity, 31*, 201-205. doi:https://doi.org/10.1016/j.ecocom.2017.07.003

Roberts. (2016). labdsv: Ordination and Multivariate Analysis for Ecology (Version R package version 1.8-0). Retrieved from https://CRAN.R-project.org/package=labdsv

Rolecek, J., Tichy, L., Zeleny, D., & Chytry, M. (2009). Modified TWINSPAN classification in which the hierarchy respects cluster heterogeneity. *Journal of Vegetation Science, 20*(4), 596-602. doi:10.1111/j.1654-1103.2009.01062.x

Rollins, M. G., Keane, R. E., & Parsons, R. A. (2004). Mapping fuels and fire regimes using remote sensing, ecosystem simulation, and gradient modeling. *Ecological Applications, 14*(1), 75-95.

Rondeaux, G., Steven, M., & Baret, F. (1996). Optimization of soil-adjusted vegetation indices. *Remote Sensing of Environment, 55*(2), 95-107. doi:https://doi.org/10.1016/0034-4257(95)00186-7

Roth, K. L., Roberts, D. A., Dennison, P. E., Peterson, S. H., & Alonzo, M. (2015). The impact of spatial resolution on the classification of plant species and functional types within imaging

spectrometer data. *Remote Sensing of Environment, 171*, 45-57. doi:https://doi.org/10.1016/j.rse.2015.10.004

Rouse Jr, J. W., Haas, R., Schell, J., & Deering, D. (1974). Monitoring vegetation systems in the Great Plains with ERTS.

Sarda-Palomera, F., Bota, G., Vinolo, C., Pallares, O., Sazatornil, V., Brotons, L., . . . Sarda, F. (2012). Fine-scale bird monitoring from light unmanned aircraft systems. *Ibis, 154*(1), 177-183. doi:10.1111/j.1474-919X.2011.01177.x

Schaaf, A. N., Dennison, P. E., Fryer, G. K., Roth, K. L., & Roberts, D. A. (2011). Mapping plant functional types at multiple spatial resolutions using imaging spectrometer data. *GIScience & Remote Sensing, 48*(3), 324-344.

Schalles, J. F., Hladik, C. M., Lynes, A. A., & Pennings, S. C. (2013). Landscape Estimates of Habitat Types, Plant Biomass, and Invertebrate Densities in a Georgia Salt Marsh. *Oceanography, 26*(3), 88-97.

Şerban, G., Rus, I., Vele, D., Breţcan, P., Alexe, M., & Petrea, D. (2016). Flood-prone area delimitation using UAV technology, in the areas hard-to-reach for classic aircrafts: case study in the north-east of Apuseni Mountains, Transylvania. *Natural Hazards, 82*(3), 1817-1832. doi:10.1007/s11069-016-2266-4

Shin, P., Sankey, T., Moore, M. M., & Thode, A. E. (2018). Evaluating Unmanned Aerial Vehicle Images for Estimating Forest Canopy Fuels in a Ponderosa Pine Stand. *Remote Sensing, 10*(8). doi:10.3390/rs10081266

Shirley, S. M., Yang, Z., Hutchinson, R. A., Alexander, J. D., McGarigal, K., & Betts, M. G. (2013). Species distribution modelling for the people: unclassified landsat TM imagery predicts bird occurrence at fine resolutions. *Diversity and Distributions, 19*(7), 855-866. doi:10.1111/ddi.12093

Shumack, S., Hesse, P., & Turner, L. (2017). The impact of fire on sand dune stability: Surface coverage and biomass recovery after fires on Western Australian coastal dune systems from 1988 to 2016. *Geomorphology, 299*, 39-53. doi:https://doi.org/10.1016/j.geomorph.2017.10.001

Skole, D., & Tucker, C. (1993). Tropical deforestation and habitat fragmentation in the amazon - satellite data from 1978 to 1988. *Science, 260*(5116), 1905-1910. doi:10.1126/science.260.5116.1905

Skowronek, S., Ewald, M., Isermann, M., Van de Kerchove, R., Lenoir, J., Aerts, R., . . . Feilhauer, H. (2017). Mapping an invasive bryophyte species using hyperspectral remote sensing data. *Biological Invasions, 19*(1), 239-254. doi:10.1007/s10530-016-1276-1

Smith, A. M. S., Strand, E. K., Steele, C. M., Hann, D. B., Garrity, S. R., Falkowski, M. J., & Evans, J. S. (2008). Production of vegetation spatial-structure maps by per-object analysis of juniper encroachment in multitemporal aerial photographs. *Canadian Journal of Remote Sensing, 34*, S268-S285.

Soons, J. M., Shulmeister, J., & Holt, S. (1997). The Holocene evolution of a well nourished gravelly barrier and lagoon complex, Kaitorete ''Spit'', Canterbury, New Zealand. *Marine Geology, 138*(1-2), 69-90. doi:10.1016/s0025-3227(97)00003-0

Spanhove, T., Vanden Borre, J., Delalieux, S., Haest, B., & Paelinckx, D. (2012). Can remote sensing estimate fine-scale quality indicators of natural habitats? *Ecological Indicators, 18*(0), 403-412. doi:http://dx.doi.org/10.1016/j.ecolind.2012.01.025

Sripada, R. P., Heiniger, R. W., White, J. G., & Meijer, A. D. (2006). Aerial Color Infrared Photography for Determining Early In-Season Nitrogen Requirements in Corn This project was supported in part by Initiative for Future Agriculture and Food Systems Grant no. 00-52103-9644 from the USDA Cooperative State Research, Education, and Extension Service. *Agronomy Journal, 98*(4), 968-977. doi:10.2134/agronj2005.0200

Story, M., & Congalton, R. G. (1986). Accuracy assessment: a user's perspective. *Photogrammetric Engineering and Remote Sensing, 52*(3), 397-399.

Stovall, A. E. L., Anderson-Teixeira, K. J., & Shugart, H. H. (2018). Assessing terrestrial laser scanning for developing non-destructive biomass allometry. *Forest Ecology and Management, 427*, 217-229. doi:https://doi.org/10.1016/j.foreco.2018.06.004

Su, L., & Gibeaut, J. (2017). Using UAS Hyperspatial RGB Imagery for Identifying Beach Zones along the South Texas Coast. *Remote Sensing, 9*(2), 159.

Sun, C., Fagherazzi, S., & Liu, Y. (2018). Classification mapping of salt marsh vegetation by flexible monthly NDVI time-series using Landsat imagery. *Estuarine, Coastal and Shelf Science, 213*, 61-80. doi:https://doi.org/10.1016/j.ecss.2018.08.007

Suo, C., McGovern, E., & Gilmer, A. (2018). VEGETATION MAPPING OF A COASTAL DUNE COMPLEX USING MULTISPECTRAL IMAGERY ACQUIRED FROM AN UNMANNED AERIAL SYSTEM. *International Archives of the Photogrammetry, Remote Sensing & Spatial Information Sciences*.

Trevithick, R., Muir, J., & Denham, R. (2012). The effect of observer experience levels on the variability of fractional ground cover reference data. *Proceeding of the 16th Annual ARSPC, Melbourne, Australia, August*.

Turner, W., Spector, S., Gardiner, N., Fladeland, M., Sterling, E., & Steininger, M. (2003). Remote sensing for biodiversity science and conservation. *Trends in Ecology & Evolution, 18*(6), 306-314. doi:10.1016/s0169-5347(03)00070-3

Underwood, E. C., Ustin, S. L., & Ramirez, C. M. (2007). A comparison of spatial and spectral image resolution for mapping invasive plants in coastal California. *Environmental Management, 39*(1), 63-83. doi:10.1007/s00267-005-0228-9

Ustin, S. L., & Gamon, J. A. (2010). Remote sensing of plant functional types. *New Phytologist, 186*(4), 795-816. doi:10.1111/j.1469-8137.2010.03284.x

Vanden Borre, J., Paelinckx, D., Mücher, C. A., Kooistra, L., Haest, B., De Blust, G., & Schmidt, A. M. (2011). Integrating remote sensing in Natura 2000 habitat monitoring: Prospects on the way forward. *Journal for Nature Conservation, 19*(2), 116-125. doi:https://doi.org/10.1016/j.jnc.2010.07.003

Varela, R. D., Rego, P. R., Iglesias, S. C., & Sobrino, C. M. (2008). Automatic habitat classification methods based on satellite images: A practical assessment in the NW Iberia coastal mountains. *Environmental Monitoring and Assessment, 144*(1-3), 229-250.

Verbesselt, J., Zeileis, A., & Herold, M. (2012). Near real-time disturbance detection using satellite image time series. *Remote Sensing of Environment, 123*, 98-108.

Vittoz, P., & Guisan, A. (2007). How reliable is the monitoring of permanent vegetation plots? A test with multiple observers. *Journal of Vegetation Science, 18*(3), 413-422.

Wang. (1990). Fuzzy supervised classification of remote sensing images. *Ieee Transactions on Geoscience and Remote Sensing, 28*(2), 194-201.

Wang, F.-m., Huang, J.-f., Tang, Y.-L., & Wang, X.-z. (2007). *New Vegetation Index and Its Application in Estimating Leaf Area Index of Rice* (Vol. 14).

Wang, K., Franklin, S. E., Guo, X., & Cattet, M. (2010). Remote Sensing of Ecology, Biodiversity and Conservation: A Review from the Perspective of Remote Sensing Specialists. *Sensors, 10*(11), 9647-9667. doi:10.3390/s101109647

Wang, K., Franklin, S. E., Guo, X., He, Y., & McDermid, G. J. (2009). Problems in remote sensing of landscapes and habitats. *Progress in Physical Geography, 33*(6), 747-768. doi:10.1177/0309133309350121

Wardle, P. (1991). *Vegetation of New Zealand*. Cambridge, England: Cambridge University Press.

Watts, A. C., Perry, J. H., Smith, S. E., Burgess, M. A., Wilkinson, B. E., Szantoi, Z., . . . Percival, H. F. (2010). Small Unmanned Aircraft Systems for Low-Altitude Aerial Surveys. *Journal of Wildlife Management, 74*(7), 1614-1619. doi:10.2193/2009-425

Weber, D., Schaepman-Strub, G., & Ecker, K. (2018). Predicting habitat quality of protected dry grasslands using Landsat NDVI phenology. *Ecological Indicators, 91*, 447-460. doi:https://doi.org/10.1016/j.ecolind.2018.03.081

Westman, W. E., & Price, C. V. (1988). Detecting air pollution stress in southern California vegetation using Landsat Thematic Mapper band data.

Westoby, M. J., Brasington, J., Glasser, N. F., Hambrey, M. J., & Reynolds, J. M. (2012). 'Structure-from-Motion' photogrammetry: A low-cost, effective tool for geoscience applications. *Geomorphology, 179*, 300-314. doi:https://doi.org/10.1016/j.geomorph.2012.08.021

Whitaker, A. H. (1987). The roles of lizards in New Zealand plant reproductive strategies. *New Zealand Journal of Botany, 25*(2), 315-328. doi:10.1080/0028825X.1987.10410078

Williams, A. P., & Hunt, E. R. (2002). Estimation of leafy spurge cover from hyperspectral imagery using mixture tuned matched filtering. *Remote Sensing of Environment, 82*(2-3), 446-456.

Williams, D., Thorne, J. H., Sumba, D., Muruthi, P., & Gregory-Michelman, N. (2018). Evaluating outcomes of community-based conservation on Kenyan group ranches with remote sensing. *Environmental Conservation, 45*(2), 173-182. doi:10.1017/s0376892917000418

Xie, Y., Sha, Z., & Yu, M. (2008). Remote sensing imagery in vegetation mapping: a review. *Journal of Plant Ecology, 1*(1), 9-23. doi:10.1093/jpe/rtm005

Xu, D., Guo, X., Li, Z., Yang, X., & Yin, H. (2014). Measuring the dead component of mixed grassland with Landsat imagery. *Remote Sensing of Environment, 142*(0), 33-43. doi:http://dx.doi.org/10.1016/j.rse.2013.11.017

Xue, J., & Su, B. (2017). Significant Remote Sensing Vegetation Indices: A Review of Developments and Applications. *Journal of Sensors, 2017*, 17. doi:10.1155/2017/1353691

Young, K. E., Abbott, L. B., Caldwell, C. A., & Schrader, T. S. (2013). Estimating suitable environments for invasive plant species across large landscapes: a remote sensing strategy using Landsat 7 ETM+. *International Journal of Biodiversity and Conservation, 5*(3), 122-134.

Yu, Q., Gong, P., Clinton, N., Biging, N., Kelly, M., & Schirokauer, D. (2006). Object-Based Detailed Vegetation Classification with Airborne High Spatial Resolution Aerial Imagery. *Photogrammetric Engineering and Remote Sensing, 72*(7), 799-811.

Zadeh, L. A. (1965). Fuzzy sets. *Information and control, 8*(3), 338-353.

Zahawi, R. A., Dandois, J. P., Holl, K. D., Nadwodny, D., Reid, J. L., & Ellis, E. C. (2015). Using lightweight unmanned aerial vehicles to monitor tropical forest recovery. *Biological Conservation, 186*, 287-295. doi:10.1016/j.biocon.2015.03.031

Zeleny, Smilauer, Hennekens, & Hill, O. (2016). twinspanR: TWo-way INdicator SPecies ANalysis (and its modified version) in R (Version R package version 0.16).

Zhang, P., Lv, Z., & Shi, W. (2013). Object-Based Spatial Feature for Classification of Very High Resolution Remote Sensing Images. *Ieee Geoscience and Remote Sensing Letters, 10*(6), 1572-1576. doi:10.1109/lgrs.2013.2262132

Zhang, X., Friedl, M. A., Schaaf, C. B., Strahler, A. H., Hodges, J. C., Gao, F., . . . Huete, A. (2003). Monitoring vegetation phenology using MODIS. *Remote Sensing of Environment, 84*(3), 471-475.

Zhumanova, M., Mönnig, C., Hergarten, C., Darr, D., & Wrage-Mönnig, N. (2018). Assessment of vegetation degradation in mountainous pastures of the Western Tien-Shan, Kyrgyzstan, using eMODIS NDVI. *Ecological Indicators, 95*, 527-543. doi:https://doi.org/10.1016/j.ecolind.2018.07.060

Zweig, C. L., Burgess, M. A., Percival, H. F., & Kitchens, W. M. (2015). Use of Unmanned Aircraft Systems to Delineate Fine-Scale Wetland Vegetation Communities. *Wetlands, 35*(2), 303-309. doi:10.1007/s13157-014-0612-4